

# WHY THAUMASITE IS FORMING IN CONCRETE STRUCTURES

A DISSERTATION SUBMITTED  
TO THE DOCTORAL SCHOOL OF GEOSCIENCES  
OF GRAZ UNIVERSITY OF TECHNOLOGY  
IN PARTIAL FULFILLMENT  
OF THE REQUIREMENTS  
FOR THE DEGREE

Doktor der Naturwissenschaften

Florian Mittermayr

October 2012

Supervisors:

Dietmar Klammer · Martin Dietzel · Stephan Köhler

Reviewer committee:

Martin Dietzel · Per Hagelia



# Abstract

Sulfate attack involving thaumasite formation leads to serious damage of concrete structures. Even though the destructive nature of sulfate attack is well known, reaction paths and mechanisms responsible for the deterioration of concrete are still debated and not well resolved. The aim of this thesis is to contribute to a deeper understanding by introducing methods that are novel and promising for investigating concrete damage.

Methods commonly used in environmental and climatological studies were applied to comprehend the interactions in the system concrete – water – atmosphere. The methodology comprises advanced mineralogical and hydro-geochemical methods as well as stable isotope signals. Investigations were performed on various field concrete structures and experimental setups.

Sulfur and carbon isotopic ratios were successfully applied to decipher the origin of compounds in secondary formed minerals. For the investigated tunnel case studies the primary source of C and S for e.g. thaumasite formation was found to be provided by the local ground water. Despite the fact that ground water was classified as slightly aggressive in accordance to e.g. DIN EN 206-1, intensive concrete damage by sulfate attack was found. Expressed interstitial solutions from damaged concrete material were extremely enriched in  $\text{SO}_4$ . Stable hydrogen and oxygen isotope were feasible of verifying evaporation for the enrichment in  $\text{SO}_4$  and other dissolved, potential harmful ions such as Cl. Furthermore the enormous accumulation of incompatible trace elements (e.g. Rb and Li) clearly indicates that numerous wetting and drying cycles had occurred. Such a highly dynamic system is known to have severe destructive effects on concrete. The isotope ratios of water molecules which are trapped in the crystal structure of thaumasite further proof evaporation to be a driving force for its formation. Additionally thermodynamic modeling of the interstitial solutions results in supersaturated solutions with respect to thaumasite and gypsum. As a “by-product” of sulfate attack, dolomite aggregates have shown to be incongruently dissolved via the neof ormation of calcite and brucite. Thus the utilization of dolomite fillers or aggregates should be critically discussed when sulfate attack is expected.

The present thesis clearly shows that complex reaction mechanisms of sulfate attack are best discovered by using a multi proxy approach. More detailed knowledge on individual reactions responsible for concrete damage in field structures and from experiments will help us to find specific and tailored counter measures for already affected buildings and to develop proper concrete recipes, applications and constructive measures for future projects.

# Table of Contents

Abstract ..... 2

## Chapter 1

**The Problem of Thaumasite  
Formation in Underground Structures ..... 5**

1.1 Introduction..... 5

1.2 Abbreviations ..... 6

1.3 Concrete damage in underground structures ..... 7

1.4 References ..... 16

## Chapter 2

**Sulfur sources for sulfate attack ..... 19**

2.1 Introduction..... 19

2.2 Concrete under Sulfate Attack: An Isotope Study on Sulfur Sources ..... 19

2.3 Remarks and Outlook ..... 31

2.4 References ..... 33

2.5 Appendix ..... 39

## Chapter 3

**Why concrete disintegrates  
completely and thaumasite remains? ..... 43**

3.1 Introduction..... 43

3.2 Evaporation – A Key Mechanism for the Thaumasite Form of Sulfate Attack.... 44

3.3 Are environmental conditions during thaumasite and gypsum  
formation traced by crystal water?..... 64

3.4 Conclusive Remarks ..... 65

3.5 References ..... 66

3.6 Appendix ..... 71

## Chapter 4

<b>The Sources of Carbon for Thaumasite .....</b>	<b>75</b>
4.1 Introduction.....	75
4.2 A Carbon Isotope Study of Thaumasite and Calcite Sinter Formation in Underground Constructions .....	76
4.3. Remarks and Outlook.....	87
4.4 References .....	89
4.5 Appendix .....	94

## Chapter 5

<b>Is Dolomite in Concrete affected by Sulfate Attack? .....</b>	<b>97</b>
5.1 Introduction.....	97
5.2 Dissolution of Dolomite in Alkaline Cementitious Media .....	98
5.3 Remarks and Outlook .....	104
5.4 References .....	105

## Chapter 6

<b>Perspectives.....</b>	<b>109</b>
6.1 Introduction .....	109
6.2 Thaumasite Dissolution and Syntheses .....	109
6.3 Studies on Natural Thaumasite.....	110
6.4 Critical Level of Sulfate in Concrete .....	110
6.5 Accelerated Sulfate Attack Test .....	112
6.6 References .....	112

## Chapter 7

<b>Afterword .....</b>	<b>115</b>
7.1 Acknowledgement.....	115
7.2 Curriculum Vitae .....	115
7.3 References .....	116

# CHAPTER 1

## The Problem of Thaumasite Formation in Underground Structures

### 1.1 Introduction

The primary aim of this study is to contribute to the task “Why Thaumasite is forming in Concrete Structures?” In order to prevent concrete damaging processes such as sulfate attack and thaumasite formation it is highly required getting an advanced understanding about the valid reactions. Thus the main focus of this thesis is to decipher the causes and the reaction mechanisms that lead to concrete deterioration. This is done by using combined and sophisticated methods in addition to those most commonly used for concrete research. Accordingly the focus is given on the whole system of concrete interacting with solids, solutions and the atmosphere. Applied methods besides mineralogical analyses are – in analogy to environmental studies - minor and trace element distributions and stable isotope ratios of  $^{34}\text{S}/^{32}\text{S}$ ,  $^{13}\text{C}/^{12}\text{C}$ ,  $^{18}\text{O}/^{16}\text{O}$  and  $^2\text{H}/\text{H}$  of the interacting components and phases within a multi proxy approach.

This thesis is compiled by individual chapters that contain published articles and one submitted manuscript. Articles are printed in this thesis as published with the exception of a conformed format throughout the work. In this first chapter the paper “Concrete Damage in Underground Structures” should give a short but comprehensive overview of the studies that have been carried out [1]. The second chapter contains the paper “Concrete under Sulfate Attack: An Isotope Study on Sulfur Sources”. The article is dealing with stable sulfur isotope ratios to reveal the sulfur sources for secondary sulfate minerals such as thaumasite, ettringite and gypsum [2]. It is clearly shown that the application of  $\delta^{34}\text{S}$  values is an excellent tool to decipher potential sulfur sources. The third chapter contains important findings to understand how consolidated concrete can be transformed to a mush. Within the latter chapter the manuscript “Evaporation – A Key Mechanism for the Thaumasite Form of Sulfate Attack” is placed [3]. The further two sections of the chapter give first insights about extracting,

measuring and interpretation of the crystal water and its isotopic composition which is stored in thaumasite and gypsum. A model to reconstruct drying and wetting cycles is developed. In the fourth chapter new data and results on the hotly debated topic on the sources of carbon for thaumasite are discussed. This chapter contains the paper “A Carbon Isotope Study of Thaumasite and Calcite Sinter Formation in Underground Construction” [4]. Subsequently chapter five deals with the finding that whenever thaumasite is found and dolomite is used as aggregate the latter is incongruently dissolved. The paper “Dissolution of Dolomite in Alkaline Cementitious Media” gives a summary and conclusions of field concrete samples and experimental approaches [5]. The following sixth chapter contains an outlook and topics of currently running and promising future projects.

## 1.2 Abbreviations

*Table 1. The following table comprises some frequently used abbreviations used in the theses. Other abbreviations will be specified in the text; those for minerals are in accordance with Whitney and Evans [6].*

AAR.....	Alkali aggregate reaction
ACR.....	Alkali carbonate reaction
Anh.....	Anhydrite
Arg.....	Aragonite
ASR.....	Alkali silicon reaction
Bas.....	Bassanite
Brc.....	Brucite
Cal.....	Calcite
DIC.....	Dissolved inorganic carbon
Dol.....	Dolomite
DrW.....	Drip water
DW.....	Drainage water
EDS.....	Energy dispersive spectroscopy
Eff.....	Efflorescence
EPMA.....	Electron probe micro analyzer
Ett.....	Ettringite
FTIR.....	Fourier transform infrared spectroscopy
Gp.....	Gypsum
GW.....	Ground water
IC.....	Ion chromatography
ICP MS.....	Inductively coupled plasma mass spectrometry

IRMS .....	Isotope-ratio mass spectrometry
IS .....	Interstitial solution
LMWL .....	Local meteoritic water line
Mb.....	Mirabilite
Qz.....	Quartz
Raman .....	Laser Micro Raman spectroscopy
SEM .....	Scanning electron microscopy
TDS .....	Total dissolved solids
TF.....	Thaumasite formation
Th.....	Thenardite
Tha.....	Thaumasite
TOC .....	Total organic carbon
TSA.....	Thaumasite form of sulfate attack
VCDT .....	Vienna canon diablo meteorite
VPDB.....	Vienna pee dee belemnite
VSMOW .....	Vienna standard mean ocean water
WDS .....	Wavelength dispersive spectroscopy
WS-CRDS.....	Wavelength-scanned cavity ring-down spectroscopy
XRD .....	X-ray Diffraction

## 1.3 Concrete damage in underground structures

Florian Mittermayr<sup>1</sup>, Dietmar Klammer<sup>1</sup>, Daniel Höllen<sup>1</sup>, Christoph Kurta<sup>2</sup>, Albrecht Leis<sup>3</sup>, Michael E. Böttcher<sup>4</sup> and Martin Dietzel<sup>1</sup>

<sup>1</sup>*Institute of Applied Geosciences, Graz University of Technology, Graz, Austria*

<sup>2</sup>*Institute of Chemistry - Analytical Chemistry, University of Graz, Graz, Austria*

<sup>3</sup>*RESOURCES – Institute for Water, Energy and Sustainability, Joanneum Research, Graz, Austria*

<sup>4</sup>*Leibniz Institute for Baltic Sea Research, IOW, Rostock, Germany*

### 1.3.1 Abstract

In this paper we present an overview about our findings concerning the damage of underground concrete structures. Case studies were performed in Austrian highway and railroad tunnels and associated structures for drainage and ventilation. In several cases severe damage of the concrete was found owing to sulfate attack, alkali aggregate reactions, leaching and drainage clogging. The focus of this study is to demonstrate by some

selected examples how to decipher the causes and reaction mechanisms of damaging reactions. Thus besides conventional mineralogical and hydro-geochemical methods, we apply stable isotope and trace element signals within multi proxy approaches. For instance stable isotope results indicate that  $\text{SO}_4$  and  $\text{CO}_3$  from local ground water are mostly responsible for thaumasite formation. More detailed knowledge on individual reactions responsible for concrete damage in underground structures will help to find specific counter measures for already affected buildings and to develop proper concrete recipes, applications and constructive measures for future projects.

### 1.3.2 Introduction

Especially the invention of shotcrete and the New Austrian tunnel method (NATM) have led to a major advance for tunneling since 1950 [7]. Tunnels can be constructed much faster, saver and longer lasting. Estimates for tunnels - recently built and currently build - predict a lifespan of at least 100 years. However, these long term performance calculations do not precisely encounter potential locally appearing threats caused by physicochemical reactions between the concrete and the environment of the underground. Glasser et al. [8] have pointed out such reactions that may take place in the concrete – water – atmosphere system. In consequence remediation of concrete structures in the underground caused by the interaction with the local environments is highly cost intensive and has to be reduced at all means. Therefore it is important to provide detailed knowledge on potential negative sustainability aspects.

In the present study sulfate attack and consequently thaumasite formation are highlighted. Simply saying sulfate attack is leading to a reduction of the stability which can cause in extreme cases even the failure of the concrete structure. In spite of enormous research effort there still persist many uncertainties in regard to causes and reaction mechanisms. Thus, the understanding has to be brought to the next level [9, 10].

Due to the environmental conditions, like geology, temperature and ground water chemistry, underground structures are frequently affected by sulfate attack as shown in various studies [11-14]. When damage is appearing it is important to find out why it happened and where it is originating from. A powerful tool to approach such matter is the application of stable isotopes [15, 16]. With this study we demonstrate that multi proxy approaches including isotopic signatures and trace element contents will lead to a deeper understanding of concrete damage.



### 1.3.3 Materials and Methods

For our investigations we sampled solids and liquids from Austrian highway and railroad tunnels. Additional samples were taken from associated structures for the drainage of ground water and concrete from a separate ventilation tunnel for a highway tunnel. In Figures 1 and 2 two sampling sites of heavily deteriorated concrete are displayed.

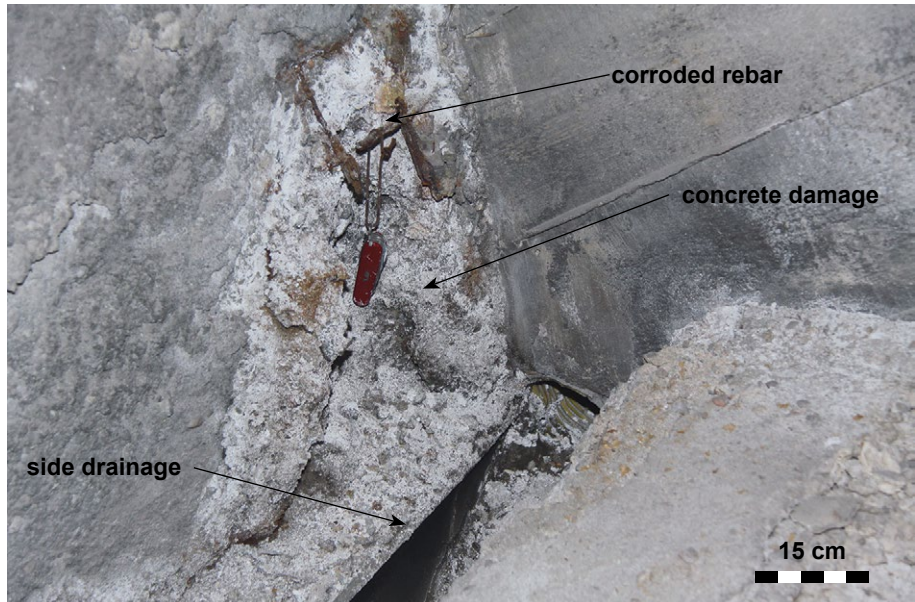


*Figure 1. Heavily damaged side drainage. White alteration products consist mostly of thaumasite and calcite. Corrosion of reinforcements is caused by high Cl contents in the ground water stemming from salt host rocks.*

#### Solids

In general solid samples comprise shotcrete and concrete (unaltered and deteriorated) and secondary solids such as mushy concrete, efflorescences and sinter. Completely disintegrated mushy material was shoveled in plastic bags, whereas consolidated concrete and shotcrete samples were excavated by drilling cores. Furthermore natural host rock was investigated. In a railroad tunnel soot relicts were removed from the tunnel walls. Solid samples were dried at 40 °C, grounded and analyzed with a PANalytical X'Pert PRO X-ray powder diffractometer (XRD). Mineralogical phase identification was carried out with a PANalytical X'Pert HighScore (version 2.2e). Secondary electron images (SEI)

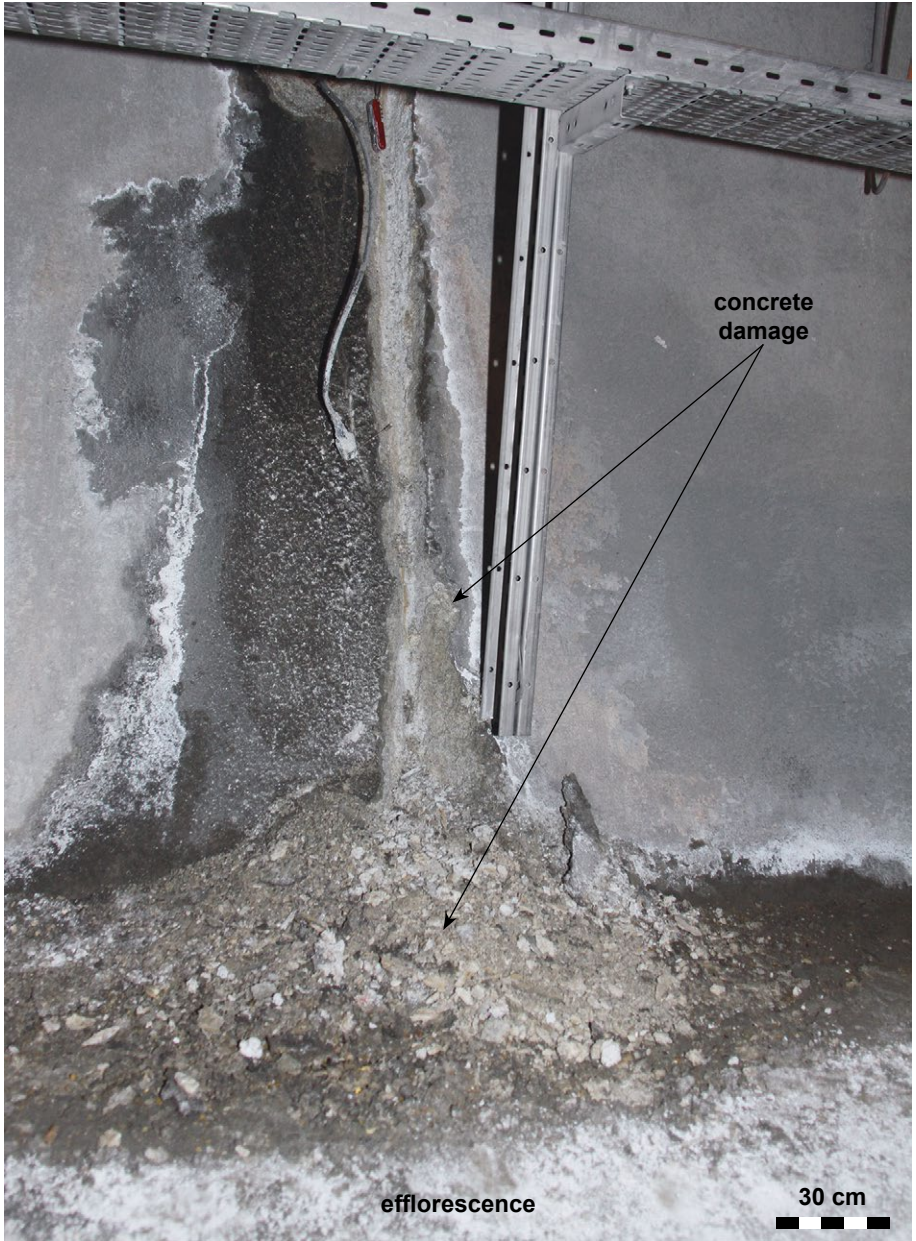


Figure 2. Severe concrete damage due to sulfate attack is also affecting the inner lining of this ventilation tunnel.

were acquired using a Zeiss DSM 982 Gemini scanning electron microscopy (SEM) with AuPd sputtered samples at 10 kV. Back scattered images (BSE) and spot analyses were acquired from C-coated samples using a JEOL JXA-8200 Superprobe (EPMA).

## Liquids

Liquid samples comprise drainage solutions, local ground water and interstitial solutions that were expressed from damaged concrete materials by a specially adapted hydraulic press in accordance to the setup described in Barneyback and Diamond [17]. In the field temperature and pH of the sampled ground, spring and drainage water were measured. Subsequently alkalinity was determined by potentiometric titration with 0.005 M HCl in the lab. Concentrations of dissolved ions were analyzed by a Dionex ICS-3000 ion chromatograph (IC) and by an Agilent 7500cx inductively coupled plasma mass spectrometer (ICP-MS).

## Isotope Measurements

To obtain sufficient thaumasite material for isotopic analyses the deteriorated concrete samples were pretreated to increase the thaumasite content. The removal of consolidated concrete fragments and aggregates is based on a modified separation technique by sedimentation in accordance to Mittermayr et al. [2]. Note that both sulfur and carbon isotope analyses were performed for solid and liquid samples.  $^{18}\text{O}/^{16}\text{O}$  and  $^2\text{H}/\text{H}$  ratios were measured only in liquid samples. Stable sulfur isotope ratios ( $^{34}\text{S}/^{32}\text{S}$ ) were analyzed by combustion of barium sulfate ( $\text{BaSO}_4$ ) and soot samples using a Thermo Finnigan 253 mass spectrometer [18]. Results are given in the  $\delta^{34}\text{S}$  -notation in ‰ relative to the Vienna Canyon Diablo Troilite standard (VCDT). Stable carbon isotope ratios are given as  $\delta^{13}\text{C}$  values in ‰ relative to the Vienna Pee Dee Belemnite standard (VPDB). Isotopic composition of dissolved inorganic carbon (DIC) and solid carbonate was analyzed using a fully automated peripheral continuous-flow gas preparation device (Gasbench II), which was connected to a Finnigan DELTAplus XP Mass Spectrometer. The analytical setup is comparable to previous studies [19]. The isotopes of hydrogen ( $^2\text{H}/\text{H}$ ) were analyzed similar to the setup described by Morrison et al. (2001) using a high-temperature oven and chromium reduction. The  $^{18}\text{O}/^{16}\text{O}$  ratios of  $\text{H}_2\text{O}$  molecules were measured by the classic  $\text{CO}_2 - \text{H}_2\text{O}$  equilibrium technique [20]. Hydrogen and oxygen isotopic ratios were both measured by a Finnigan DELTAplus XP mass spectrometer and results are given as  $\delta^{18}\text{O}$  and  $\delta^2\text{H}$  in ‰ relative to the Vienna Standard Mean Ocean Water (VSMOW).

### 1.3.4 Results and Discussions

XRD pattern of sound concrete and shotcrete display poorly crystalline CSH-phases, portlandite ( $\text{Ca}(\text{OH})_2$ ) as well as silicate and carbonate aggregates like quartz, feldspar, dolomite and calcite. Mineralogical investigations (XRD, EPMA, SEM) clearly show that severe concrete deterioration is caused by sulfate attack. Complete disintegrated materials consist mainly of thaumasite, calcite, gypsum and silicate aggregates (Figure 3). In some tunnels gypsum was not found at all or only in small quantities and ettringite could not be identified unambiguously due to the structural similarity and the overwhelming presents of thaumasite [21]. Furthermore a significant reduction and even total lacking of dolomite aggregates were detected by comparing sound and deteriorated material.

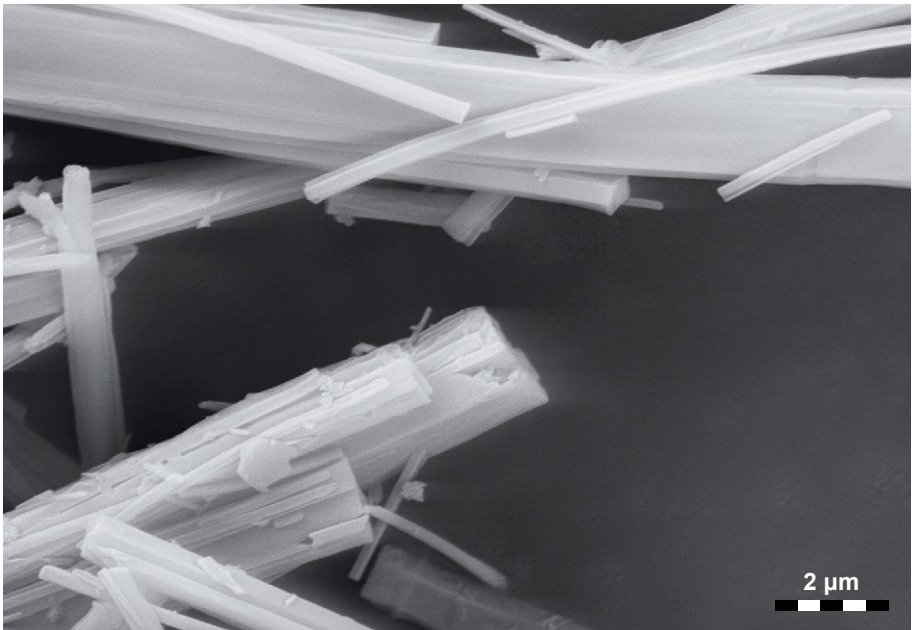


*Figure 3. SEI of thaumasite needles from a purified sample used for isotopic measurements.*

Thus without any doubt concrete damage is owing to intensive sulfate attack and thaumasite formation. The next step was to investigate the sources of sulfur for the attack. Surprisingly ground water and drainage water analyses generally showed only low

to moderately enriched  $\text{SO}_4$  content with values ranging from about 3 to 500  $\text{mg L}^{-1}$ . Chemical compositions of typical solutions are given in Table 2. In rare cases slowly running and dripping waters were found being saturated with respect to gypsum by containing up to 1300  $\text{mg L}^{-1}$  of  $\text{SO}_4$ . As sulfate attack appears also in areas with lower  $\text{SO}_4$  concentrations of ground water, the following question arises: Is dissolved sulfate of ground water the only source or are we facing other S sources coming from e.g. internal sulfate from concrete/shotcrete, oxidation of sulfides (like pyrite in associated solids and rocks), atmospheric contribution, or organic matter as for instance soot particles [22]. The latter source was the most likely candidate for a more than 100 years old railroad tunnel which was not properly cleaned before shotcrete was applied about 50 years ago. In spite of rather low  $\text{SO}_4$  content in the ground water S-isotope measurements clearly indicate that S in thaumasite is stemming from infiltrating ground water implicating the dissolution of local occurring gypsum and anhydrite rocks.  $\delta^{34}\text{S}$  values of thaumasite, ground water sulfate and host rock are mostly within the range of +14 to +27 ‰ [2]. In a few locations significantly lower  $\delta^{34}\text{S}$  signals were detected in thaumasite resulting from pyrite oxidation. Interestingly internal sulfate attack, contributions from soot or the Earth's atmosphere can be ruled out by the given  $\delta^{34}\text{S}$  ranges which opens up a new subject: How does ground water with about 500  $\text{mg L}^{-1}$  of sulfate or even less may cause intensive sulfate attack?

Therefore we analyzed the chemical and isotopic composition of interstitial solutions extracted from heavily damaged concrete samples by using a hydraulic press. Proportions of extracted solutions correspond to about 5 up to 20 wt. % of the solid material and extreme accumulation of Na and  $\text{SO}_4$  is observed compared to the locally occurring ground water (see values given in Table 2). Considering the dramatic increase of univalent cations compared to the local ground water and the rather conservative behavior of e.g. K and Rb (or uncharged species  $\text{B}(\text{OH})_3$ ) suggests evaporation of water to be responsible for extreme  $\text{SO}_4$  concentrations of up to 30000  $\text{mg L}^{-1}$  [23]. Proof is gained from analyses of  $\delta^2\text{H}$  and  $\delta^{18}\text{O}$  values of  $\text{H}_2\text{O}$  molecules which display a strong enrichment of the heavy stable isotopes. The respective kind of isotopic evolution clearly indicates evaporation of  $\text{H}_2\text{O}$  from the local ground water.

A further curiosity with a high need to be verified was the incongruent dissolution of dolomite aggregates. In spite of being a well known reaction for deteriorating concrete, it has not gained much attention in scientific research. The so-called alkali carbonate reaction (ACR) comprises the dissolution of dolomite at alkaline conditions in concrete [24]. Previously we have suggested that dolomite aggregates are preferentially



dissolving incongruently governed by high Ca vs. Mg ratio in the interacting aqueous solution. Calcite becomes more stable versus dolomite. As long as the pH remains above 10.5 the continuous removal of dissolved Mg from the solution is leading to brucite ( $\text{Mg}(\text{OH})_2$ ) formation [5]. Surprisingly in all cases where sulfate attack in combination with dolomite aggregates was found a partial dissolution of the latter and precipitation of secondary calcite and brucite were found. A typical example is illustrated in Figure 4. Thus we assumed carbonate released by dolomite dissolution to have contributed to thaumasite formation.

*Table 2. Characteristic composition and isotopic signatures of ground water (GW-1 and GW-2), drainage water (DW) and interstitial solution (IS).  $\delta^2\text{H}$  and  $\delta^{18}\text{O}$  values of  $\text{H}_2\text{O}$  are given in ‰ (VSMOW). Ion content (Na, K, Mg, Ca, Cl,  $\text{HCO}_3^-$ ,  $\text{NO}_3^-$ ,  $\text{SO}_4^{2-}$ ) is given in  $\text{mg L}^{-1}$  and trace elemental content (Rb and B) in  $\mu\text{g L}^{-1}$ .*

Sample	pH	Na	K	Mg	Ca	Cl	$\text{NO}_3^-$
GW_1	8.35	0.41	0.40	7.59	25.0	0.40	3.26
GW_2	7.60	3.77	0.92	32.9	206	4.85	0.96
DW	7.78	9.52	1.32	35.5	206	12.9	1.50
IS	8.79	7239	307	942	636	2930	69.8
Sample	$\text{SO}_4^{2-}$	$\text{HCO}_3^-$	TDS	Rb	B	$\delta^{18}\text{O}$	$\delta^2\text{H}$
GW_1	2.95	112	152	0.45	2.20	-83.1	-12.0
GW_2	505	165	919	0.86	14.8	-82.8	-12.0
DW	502	167	935	0.90	14.6	-85.9	-12.4
IS	15953	188	28265	616	1656	-50.0	-6.6

Various studies suggest that the carbonate can be stemming from the absorption of atmospheric  $\text{CO}_2$ , carbonate aggregates or DIC of ground water [25]. To investigate the carbon source in thaumasite we applied stable carbon isotopes. In contrary to our assumption that carbonate is originating from dolomite aggregates we found the carbon in thaumasite to be related to DIC uptake from ground water.  $\delta^{13}\text{C}$  values from thaumasite and DIC are mostly in the same range from -11 to -5 ‰ [4]. Marine carbonates (limestone and dolomite) used as aggregates are usually much heavier in isotopic values and are plotting at  $0 \pm 2$  ‰. In contrary Dietzel [26] has pointed out that the formation of calcium carbonate related to the absorption of atmospheric  $\text{CO}_2$  is leading to a strong depletion of  $^{13}\text{C}$  versus  $^{12}\text{C}$ . The latter reaction occurs at high pH and is governed by a kinetic isotope fractionation leading to  $\delta^{13}\text{C}$  values of  $-25 \pm 3$  ‰.

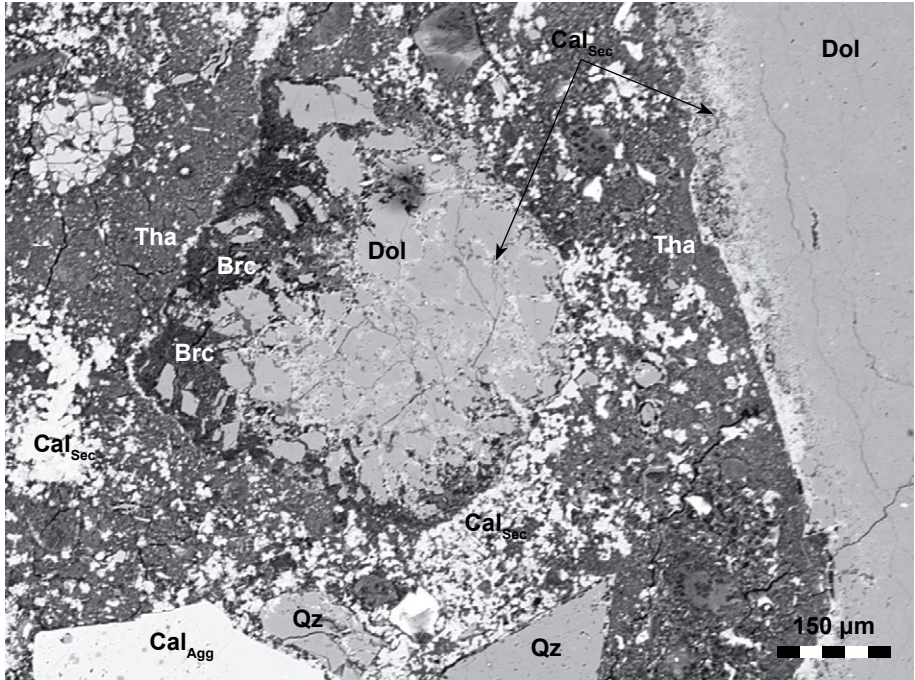


Figure 4. BSE image of concrete that has suffered severe sulfate attack displaying partially dissolved dolomite grains. The reaction products of the incongruent dolomite (Dol) dissolution are calcite ( $Cal_{Sec}$ ) and brucite (Brc). The cement matrix is completely altered and mainly consists of thaumasite (Tha). Furthermore calcite ( $Cal_{Agg}$ ) and quartz (Qz) aggregates are displayed.

### 1.3.5 Conclusions

Applications of multi proxy approaches including stable isotope distributions and trace element contents have shown to be very powerful tools for a deeper and sophisticated understanding of concrete deteriorating processes. Complex reaction paths can be reconstructed and individual causes for the damage can be revealed. Thus repair and remediation measures can be focused and potential threats to the concrete structure should be assessed in the forefront of future projects.

### 1.3.6 Acknowledgement

Financial support of the present study by NAWI Graz (Graz Advanced School of Science, GASS) and Österreichische Forschungsförderungsgesellschaft (FFG, 828476) is greatly appreciated. The authors also want thank Josef Tritthart for helpful comments and discussions.

## 1.4 References

1. Mittermayr, F., D. Klammer, D. Höllen, M. Dietzel, C. Kurta, A. Leis, and M.E. Böttcher, Concrete damage in underground structures, in *Concrete Repair, Rehabilitation and Retrofitting III*, M.G. Alexander, et al., Editors. 2012, Taylor & Francis Group: London,UK. p. 580-584.
2. Mittermayr, F., C. Bauer, D. Klammer, M.E. Böttcher, A. Leis, P. Escher, and M. Dietzel, Concrete under Sulfate Attack: An Isotope Study on Sulfur Sources Isotopes in *Environmental & Health Studies*, 2012. 48(1): p. 105-117.
3. Mittermayr, F., A. Baldermann, C. Kurta, T. Rinder, D. Klammer, A. Leis, J. Tritthart, and M. Dietzel, Evaporation – A Key Mechanism for the Thaumasite Form of Sulfate Attack. *Cement and Concrete Research*, submitted.
4. Mittermayr, F., T. Rinder, D. Klammer, A. Leis, and M. Dietzel, A Carbon Isotope Study of Thaumasite and Calcite Sinter Formation in Underground Construction, in *1<sup>st</sup> International Congress on Durability of Concrete*, H. Justnes and S. Jacobsen, Editors. 2012, NTNU: Trondheim. p. No. C6-1: 1-14.
5. Mittermayr, F., D. Klammer, S. Köhler, A. Leis, D. Höllen, and M. Dietzel, Dissolution of Dolomite in alkaline cementitious media, in *Cementing a sustainable future 13<sup>th</sup> International Congress on the Chemistry of Cement*, Á. Palomo, A. Zaragoza, and J. C. López Agüí, Editors. 2011, CSIC: Madrid. p. No. 278: 1-6
6. Whitney, D.L. and B.W. Evans, Abbreviations for names of rock-forming minerals. *American Mineralogist*, 2010. 95(1): p. 185-187.
7. Rabcewicz, L. and J. Gosler, Application of the NATM to the underground works at Tarbela. Part 1. *International Journal of Rock Mechanics and Mining Science & Geomechanics Abstracts*, 1974. 11(11): p. 225.



8. Glasser, F.P., J. Marchand, and E. Samson, Durability of concrete — Degradation phenomena involving detrimental chemical reactions. *Cement and Concrete Research*, 2008. 38(2): p. 226-246.
9. Neville, A., The confused world of sulfate attack on concrete. *Cement and Concrete Research*, 2004. 34(8): p. 1275-1296.
10. Santhanam, M., M.D. Cohen, and J. Olek, Sulfate attack research — whither now? *Cement and Concrete Research*, 2001. 31(6): p. 845-851.
11. Bellmann, F., W. Erfurt, and H.M. Ludwig, Field performance of concrete exposed to sulphate and low pH conditions from natural and industrial sources. *Cement and Concrete Composites*, 2012. 34(1): p. 86-93.
12. Leemann, A. and R. Loser, Analysis of concrete in a vertical ventilation shaft exposed to sulfate-containing groundwater for 45 years. *Cement and Concrete Composites*, 2011. 33(1): p. 74-83.
13. Long, G.C., Y.J. Xie, D.H. Deng, and X.K. Li, Deterioration of concrete in railway tunnel suffering from sulfate attack. *Journal of Central South University of Technology*, 2011. 18(3): p. 881-888.
14. Romer, M., L. Holzer, and M. Pfiffner, Swiss tunnel structures: concrete damage by formation of thaumasite. *Cement and Concrete Composites*, 2003. 25(8): p. 1111-1117.
15. Iden, I.K. and P. Hagelia, C, O and S isotopic signatures in concrete which have suffered thaumasite formation and limited thaumasite form of sulfate attack. *Cement and Concrete Composites*, 2003. 25(8): p. 839-846.
16. Pye, K. and N. Schiavon, Cause of Sulfate Attack on Concrete, Render and Stone indicated by Sulfur Isotope Ratios. *Nature*, 1989. 342(6250): p. 663-664.
17. Barneyback, J., R. S. and S. Diamond, Expression and analysis of pore fluids from hardened cement pastes and mortars. *Cement and Concrete Research*, 1981. 11(2): p. 279-285.
18. Mann, J.L., R.D. Vocke, and W.R. Kelly, Revised  $\delta^{34}\text{S}$  reference values for IAEA sulfur isotope reference materials S-2 and S-3. *Rapid Communications in Mass Spectrometry*, 2009. 23(8): p. 1116-1124.

19. Spötl, C., A robust and fast method of sampling and analysis of  $\delta^{13}\text{C}$  of dissolved inorganic carbon in ground waters. *Isotopes in Environmental and Health Studies*, 2005. 41(3): p. 217-221.
20. Epstein, S. and T. Mayeda, Variation of  $^{18}\text{O}$  content of waters from natural sources. *Geochimica Et Cosmochimica Acta*, 1953. 4(5): p. 213-224.
21. Stark, D.C., Occurrence of thaumasite in deteriorated concrete. *Cement and Concrete Composites*, 2003. 25(8): p. 1119-1121.
22. Suput, J.S., A. Mladenovic, L. Cernilogar, and V. Olensek, Deterioration of mortar caused by the formation of thaumasite on the limestone cladding of some Slovenian railway tunnels. *Cement and Concrete Composites*, 2003. 25(8): p. 1141-1145.
23. Mittermayr, F., D. Klammer, D. Höllen, S. Köhler, M. Böttcher, A. Leis, and M. Dietzel, Deterioration of Concrete: Application of Stable Isotopes, in *Proceedings of the 10<sup>th</sup> International Congress for Applied Mineralogy (ICAM)*, M.A.T.M. Broekmans, Editor. 2012, Springer Berlin Heidelberg. p. 435-443.
24. Katayama, T., The so-called alkali-carbonate reaction (ACR) -- Its mineralogical and geochemical details, with special reference to ASR. *Cement and Concrete Research*, 2010. 40(4): p. 643-675.
25. Justnes, H., Thaumasite formed by sulfate attack on mortar with limestone filler. *Cement and Concrete Composites*, 2003. 25(8): p. 955-959.
26. Dietzel, M.,  $^{13}\text{C}/^{12}\text{C}$  Signatures and  $^{18}\text{O}/^{16}\text{O}$  signatures of calcite precipitations in drainage systems. *Acta Hydrochimica Et Hydrobiologica*, 1995. 23(4): p. 180-184.

## CHAPTER 2

# Sulfur sources for sulfate attack

## 2.1 Introduction

This chapter is mainly dealing with the sources of sulfur for delirious secondary sulfate minerals such as thaumasite, ettringite and gypsum involving sulfate attack. This topic is approached by the usage of stable sulfur isotopes and the main part herein is presented in the following section. The section Remarks and Outlook contains some further discussion and continuative recommendations.

## 2.2 Concrete under Sulfate Attack: An Isotope Study on Sulfur Sources

Florian Mittermayr<sup>1</sup> Christoph Bauer<sup>1,2</sup>, Dietmar Klammer<sup>1</sup>, Michael E. Böttcher<sup>3</sup>, Albrecht Leis<sup>4</sup>, Peter Escher<sup>3</sup> and Martin Dietzel<sup>1</sup>

<sup>1</sup>*Institute of Applied Geosciences, Graz University of Technology, Graz, Austria*

<sup>2</sup>*The RHI Technology Center, Leoben, Austria;*

<sup>3</sup>*Leibniz Institute for Baltic Sea Research, IOW, Rostock, Germany*

<sup>3</sup>*RESOURCES – Institute for Water, Energy and Sustainability, Joanneum Research, Graz, Austria*

### 2.2.1 Abstract

The formation of secondary sulfate minerals, as thaumasite, ettringite and gypsum is a process causing severe damage to concrete constructions. A major key to understand the complex reactions involving concrete deterioration is to decipher the cause of its appearance, including the sources of the involved elements. In the present study, sulfate attack on concrete of two Austrian tunnels is investigated.

The distribution of stable sulfur isotopes is successfully applied to decipher the source(s) of sulfur in the deteriorating sulfate-bearing minerals. Interestingly,  $\delta^{34}\text{S}$  values (VCDT) of sulfate in local ground water and in the deteriorating minerals are mostly in the range from +14 to +27 ‰. These  $\delta^{34}\text{S}$  values match the isotope patterns of regional Permian and Triassic marine evaporites. Soot relicts from steam and diesel driven trains found in one of the tunnels show  $\delta^{34}\text{S}$  values from -3 to +5 ‰ and are therefore assumed to be of minor importance for sulfate attack on the concretes. In areas of pyrite containing sedimentary rocks the  $\delta^{34}\text{S}$  values of sulfate from damaged concrete range between -1 and +11 ‰. The latter range reflects the impact of sulfide oxidation on local ground water sulfate.

## 2.2.2 Introduction

Sulfate attack on cementitious materials may lead to the formation of new minerals that have negative effects on the stability, sustainability and life span of concrete constructions. Secondary formation of sulfate minerals like thaumasite ( $\text{Ca}_3\text{Si}(\text{OH})_6(\text{CO}_3)(\text{SO}_4)\cdot 12\text{H}_2\text{O}$ ), ettringite ( $\text{Ca}_6\text{Al}_2(\text{SO}_4)_3(\text{OH})_{12}\cdot 26\text{H}_2\text{O}$ ) and gypsum ( $\text{CaSO}_4\cdot 2\text{H}_2\text{O}$ ) can result in softening, cracking, spalling and complete disintegration of the concrete. Numerous studies display the challenge to decipher the causes of sulfate attack on concrete [1-5]. Besides changing the material characteristics, sulfate attack on concrete has strong economic consequences, e.g. for renovation costs. Although the occurrence of sulfate attack on concrete is well known and documented from case studies, the reactions that lead to the formation of damaging sulfate minerals as well as the origin of the involved ions such as carbonate and sulfate are poorly understood. For sulfate ions numerous origins are assumed such as cement phases, the dissolution of aggregates, the Earth's atmosphere, fertilizers, and sulfate in ground water that may originate from the dissolution of sulfate minerals or the oxidation of metal sulfide [6-9].

Analysis of stable sulfur isotope distribution is a powerful tool to investigate the sources and potential transformations of sulfur within a wide field of applications including hydrogeochemistry, sedimentology, (paleo-)environmental studies including the impact of acid mine drainage and acid rain, the genesis of ores, petrol, and coal [10-19]. In the field of conservation and reconstruction it is inevitable to have detailed knowledge of the basic causes of the damaging mechanisms. Considering ancient buildings most serious is the formation of Na, Mg, Ca related sulfate salts

mostly gained from atmospheric  $\text{SO}_2$  due to air pollution. Additional sulfur sources like sulfate from reservation material, rising ground water, soils, sea water spray, and reconstruction materials were verified by stable sulfur isotope analysis [20-30]. In the case of sulfate attack on concrete, a huge range of locally occurring sulfur sources are discussed [6, 31, 32]. However the application of stable isotopes is rather challenging. Pye and Schiavon [33], Iden and Hagelia [34] and Vallet et al. [35] successfully applied stable sulfur isotope signatures to distinguish sulfate types for respective concrete attack but could not provide well-defined individual sources of sulfate for the investigated damaged concrete. Thus upon characterization of all relevant sources in terms of isotopic composition this should be possible. In the present study, sulfur isotope ( $^{34}\text{S}/^{32}\text{S}$ ) data for concrete damaged by sulfate attack from distinct areas of two Austrian tunnels are presented to decipher the source of sulfate involved in concrete deterioration. This will help to gain further insights into reaction mechanisms for sulfate attack.

### 2.2.3 Study area

Two major tunnels of the North-South traverse through the eastern Alps were selected for the present study. Both tunnels are passing through tectonically altered horizons containing sedimentary and metamorphous rocks. Sulfur is mostly present in marine evaporites (e.g. gypsum, anhydrite) of Upper Permian to Lower Triassic age and as disulfide pyrite in Cretaceous black shales.

Tunnel 1 is a railroad tunnel constructed in the beginning of the 20<sup>th</sup> century (1901 - 1906) with a length of 4.8 km. Originally the tunnel was mostly lined with granite bricks. As the surrounding rocks were considered to be stable no brick wall was installed. For remediation measures shotcrete was first applied throughout the entire tunnel in the 1960s. Since then, the shotcrete lining had to be frequently renewed at several locations due to decomposition and spalling. As initial damaging is localized at the transition between shotcrete lining and old tunnel wall or rock, the suspected origin for the damage was insufficiently removed soot from steam and diesel trains. A similar scenario was described in previous studies [31, 32]. Tunnel 1 intersects different geological units including marine evaporites (gypsum, anhydrite and rock salt), dominantly clastic sediments containing small amounts of sulfates and pyrite as well as massive carbonates with low pyrite content. The northern part cuts through upper Permian

to Skythian evaporites known as ‚Haselgebirge‘. Within this sequence lower Triassic units of the Werfen formation are present that are tectonically interlayered with the evaporites. The central part of the tunnel is running through massive limestones and dolomites with Middle to Upper Triassic ages. The southern part of the tunnel is dominated by the Werfen formation with intercalated younger units (Dolomite-anhydrite facies with ‚Rhät Buntsandstein‘ age and ‚Anisian Rauhwaacke‘). Furthermore Permian evaporitic rocks are also found in small quantities. The main water inflows are located in the vicinity of the borders to the carbonate rock horizons. Through the evaporitic rock horizons minor inflow of water into the drainage system is observed.

Tunnel 2 is a 6.3 km long highway tunnel that was constructed in the 70s of the last century by conventional tunnel driving using the New Austrian Tunneling Method (NATM) [36]. During the construction of a second tube the existing rescue tunnels were partly used for the new construction. Due to the larger cross section of the new construction the concrete was removed from those areas leaving a unique view behind the old rescue tunnel walls. Intensive deterioration of the concrete was found in some places hidden behind the inner concrete lining. Furthermore damages were revealed during renovation by drilling cores. In some areas, the concrete of the drainage system was also damaged. Tunnel 2 is passing several geological units containing marine evaporites (gypsum, anhydrite) as well as black, green and grey shales grey shales with various amounts of pyrite. Marine evaporates are of Triassic, whereas black shales are of Cretaceous age. Both were accumulated in an accretionary wedge, overprinted tectonically and by metamorphism during the Alpine orogeny. Inside the tunnel, low amounts of highly mineralized ground water are found.

## 2.2.4 Materials and Methods

Solid samples comprise both unaltered and deteriorated shotcrete and concrete from the tunnel buildings, soot from the tunnel wall as well as natural host rocks. The damaged mushy concrete material was easily removed by hand and was shovelled into plastic bags. Furthermore concrete with stable appearing surfaces next to damaged areas was sampled by drilling cores. Figure 1 shows a 100 mm  $\varnothing$  drilling core from Tunnel 1 with concrete damage at the transition between the rock and shotcrete. Black crusts on the former tunnel walls are soot relicts from steam and diesel driven engines. Soot samples throughout Tunnel 1 were carefully scratched off for further investigation. Rock samples were acquired from drilling cores of a nearby highway tunnel project. The highway tunnel

is located a few hundred meters apart from Tunnel 1 passing through the same lithologies. In Tunnel 2 rock samples were taken during the driving of a second tube.



Figure 1: 100 mm  $\varnothing$  drill core from a shotcrete with damage due to sulfate attack.

Damaged material was treated to increase the concentration of thaumasite for further mineralogical characterization and isotope analyses. To remove aggregates and consolidated concrete the fraction  $> 500 \mu\text{m}$  was separated by sieving. The remaining material was placed in containers filled with ethanol and treated in an ultrasonic bath. Due to differences in specific density small aggregates or fragments of e.g. quartz sand, calcite and dolomite were accumulated on the bottom of the container while thaumasite is staying in suspension. Almost pure thaumasite was obtained by subsequent decantation of the suspension. The final suspensions were filtered through  $2 \mu\text{m}$  membranes and the remaining material was dried at  $40 \text{ }^\circ\text{C}$ .

All samples were dried at  $40 \text{ }^\circ\text{C}$  before being grounded and analyzed by X-ray powder diffraction (XRD). X-ray patterns were collected with a PANalytical X'Pert PRO diffractometer with an X'Celerator detector ( $\text{CoK}\alpha$  radiation, 45 kV and 40 mA). The angular range reached from  $4 - 120^\circ$  per  $2\theta$  with a step size of  $0.008^\circ$  and counting time of 40 s per step. Qualitative phase identification was carried out with PANalytical X'Pert HighScore (version 2.2.e). Concentrations of mineral phases were obtained by Rietveld

refinement by PANalytical X'Pert HighScore plus software. Secondary electron images (SEI) were acquired using a scanning electron microscopy (SEM) Zeiss DSM 982 Gemini from AuPd sputtered samples at 10 kV.

Temperature, pH, and oxygen concentration of the sampled ground, spring and drainage waters were measured in-situ. Subsequently alkalinity was determined by potentiometric titration with 0.005 M HCl in the lab. Concentrations of dissolved ions were analyzed by ion chromatography (Dionex ICS-3000). For hydrogeochemical modeling the computer code PHREEQC (version 2.17.01) was used to calculate saturation indices with respect to relevant minerals [37].

For sulphur isotope analysis, solid samples were crushed and dissolved in diluted double distilled  $\text{HNO}_3$ . The digestion was filtrated and the dissolved sulfate ions were quantitatively precipitated as barium sulfate ( $\text{BaSO}_4$ ) by the addition of  $\text{BaCl}_2$ . In analogy, dissolved sulfate from collected water samples was precipitated as  $\text{BaSO}_4$  by  $\text{BaCl}_2$  addition. Barium sulfate precipitates were carefully washed with de-ionized water and dried at 60 °C in a drying oven. Sulfur isotope ( $^{34}\text{S}/^{32}\text{S}$ ) measurements at IOW were carried out on  $\text{BaSO}_4$  and soot samples. Sample powders were placed in Sn cups with added p.a. grade  $\text{V}_2\text{O}_5$ , and combusted in a Thermo Scientific FLASH 2000 elemental analyzer coupled to a Thermo Finnigan 253 gass mass spectrometer via a Thermo Scientific ConFlo IV split interface. Silver sulfide isotope reference materials (IAEA-S-1, IAEA-S-2 and IAEA-S-3) were used to link the mass spectrometric results towards the V-CDT scale [38]. Isotope measurements are given in the conventional  $\delta$ -notation, and replicate measurements agreed within better than  $\pm 0.3$  ‰.

## 2.2.5 Results and Discussion

### Composition of damaged concrete material

Results from XRD and SEM indicate neof ormation of thaumasite as the main reason for the concrete damage. Gypsum is of minor importance. A typical mineralogical composition of seriously damaged concrete measured by XRD and quantified by Rietveld refinement is given in Table 1. The purified sample consists of thaumasite with up to 95 wt. % (see SEM image in Figure 2). Cement phases (e.g. CSH-phases, portlandite ( $\text{Ca}(\text{OH})_2$ ) are completely missing and replaced by the sulfate containing material. Due to the dominance of thaumasite and the structural similarities of ettringite and



thaumasite, it was not possible to identify ettringite unambiguously in the presence of thaumasite as main solid phase [39, 40].

*Table 1: Typical mineralogical composition of damaged concrete material in the < 500  $\mu\text{m}$  fraction and separated thaumasite obtained by Rietveld refinement. Values are given in wt. %. Tha: thaumasite; Gp: gypsum; Qz: quartz; Cal: calcite; Dol: dolomite; n.d.: not detected.*

Sample	Tha	Gp	Qz	Cal	Dol
Damaged Concrete	45	<2	41	15	<2
Purified Thaumasite	95	n.d.	3	2	n.d.

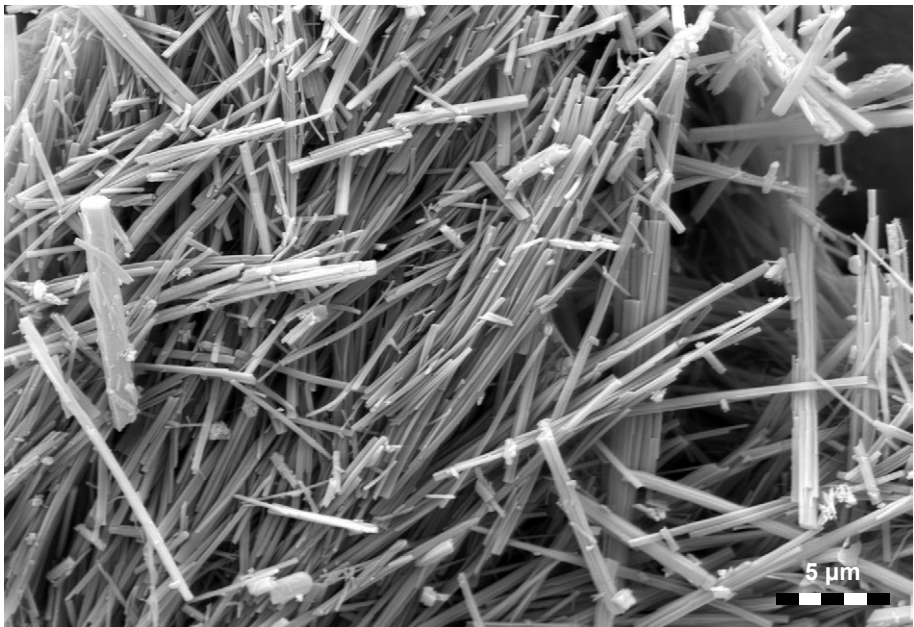


*Figure 2: SEM image of a purified thaumasite sample*

## Hydrogeochemical characterization of sampled solutions

Analytical results from ground, spring, and drainage water are given in Table 2 (see appendix). The overall discharge of drainage water from Tunnel 1 is about  $300 \text{ L s}^{-1}$ . The  $\text{SO}_4$  concentration of individual drainage solutions range from 12 to  $500 \text{ mg L}^{-1}$ . Low  $\text{SO}_4$  concentrations are especially present at high inflow rates. However in several areas with intensive concrete damage it was not possible to analyze the composi-

tion of the respective water due to extreme low drop rates. As molar ratios regarding Ca and  $\text{SO}_4$  are close to 1 the origin of sulfate is assumed to be mostly related to the dissolution of anhydrite or gypsum from the host rocks. The natural waters are under-saturated with respect to gypsum. The highest saturation index with respect to gypsum (SI Gp; Table 2 see appendix) is -0.6 in the drainage water leaving the tunnel in the south. The origin of Na is not only contributed by rock salt as molar ratios of Na and Cl are not balanced. The excess of Na can be explained by water-concrete interaction. Elevated K concentrations are also interpreted to stem from concrete. Because of the elevated time span for concrete alteration (leaching of hydroxyl ions) and high water flow rates it was not possible to find typically high pH drainage solutions [41, 42]. Solution T1\_45 (Tables 2 and 3) was sampled in a nearby highway tunnel where a spring is located inside the limestone horizon and thus represents Ca-Mg- $\text{HCO}_3$  dominated water with low  $\text{SO}_4$  concentrations.

The water from the drainage of Tunnel 2 displays a low overall discharge of about  $0.3 \text{ L s}^{-1}$ . In the drainage water and several ground waters the concentration of  $\text{SO}_4$  is high and saturation with respect to gypsum is reached (SI  $\approx 0$ ; Table 2 see appendix). High Na and K concentrations in samples T2\_5 and T2\_20 can be related to intensive water-concrete interaction. These water samples were collected during construction from solutions dripping through only a few months old shotcrete linings. Sample T2\_12 denotes water running out of an iron tube that was installed for deep drilling about 40 years ago and located 550 m above the tunnel in middle of the tunnel length. This water is saturated with respect to gypsum and did not interact with concrete.

## Sulfur Isotopes

In total, 51 and 24 solid and liquid samples were measured for  $\delta^{34}\text{S}$  in Tunnels 1 and 2, respectively (Table 3 see appendix). Figure 3 gives an overview of the  $\delta^{34}\text{S}$  variability in Tunnel 1. The southernmost part of the tunnel (SI) is located in a lower Triassic dolomite-anhydrite series and Skythian Werfen formation with  $\delta^{34}\text{S}$  values for the sulfates of  $28.4 \pm 1.7$  and  $19.9 \pm 1.0$  ‰, respectively. Additional values from nearby studies in the same geological units are included in Table 3 (see appendix) for comparison. Samples from Niedermayr and Pak [43] were taken from the same tunnel. Samples analyzed by Spötl and Pak [44] are collected from nearby quarries located 4 and 9 km away from the tunnel. Damaged concrete and investigated ground water show comparable isotope signatures with  $\delta^{34}\text{S}$  values from +13.5 to +28.7 ‰ and an average value of  $+22.4 \pm 6.0$  ‰ (n=10). In the northernmost area (NI), a tectonic mélange of

upper Permian salt rocks and lower Triassic Skythian sedimentary formation is located. Ground water inside the tunnel and the drainage water outlet resemble values of  $+15.3 \pm 0.4$  ‰ displaying a mixture of local Permian sulfates ( $+10.2$  to  $+12.9$  ‰, average  $+11.3 \pm 0.9$  ‰;  $n=8$ ) and sulfates from Skythian rocks ( $19.9 \pm 1.0$ ). Concrete damage in the area NI is displaying very similar  $\delta^{34}\text{S}$  values from  $+12.2$  to  $+20.8$  ‰ (average  $+15.3 \pm 2.2$  ‰;  $n=15$ ), again indicating a sulfur supply from ground water in this area. The location SII is located further inside the tunnel compared to SI. In this area  $\delta^{34}\text{S}$  values of deteriorated concrete are significantly lower than in the tunnel display values from  $-0.3$  to  $+7.9$  ‰ (average  $+2.7 \pm 3.2$  ‰;  $n=6$ ). Damage is by far not as intensive as in NI and SI. In location SII it was not possible to sample neither ground water nor are rocks matching this sulfur isotope signature. According to the local geology, Skythian to Anisian sedimentary rocks are found in this area but without any  $\delta^{34}\text{S}$  values available. The geological units comprise colored and dark shales containing pyrite. Isotopically lighter  $\delta^{34}\text{S}$  values in concrete damage may be related to the oxidation of pyrite and the corresponding release of  $\text{SO}_4$  to the ground waters. In the central part of the tunnel (NII) no obvious concrete damage was found. In this area the tunnel is rather dry except for the transition from evaporite bearing rocks to massive limestones where high water discharge is found. Massive upper Triassic carbonate rocks with pyrite content of  $< 5$  wt. % are located in the latter area. Isotope analyses of limestone and dolomite horizons and spring water located in a rescue tunnel from a nearby highway rescue tunnel yield in  $\delta^{34}\text{S}$  values of  $+3.0$ ,  $-2.3$  and  $-8.6$  ‰, respectively.

Soot as black crusts on the old tunnel walls results in  $\delta^{34}\text{S}$  values from  $-3.2$  to  $+5.0$  ‰ (average  $+1.5 \pm 2.8$  ‰;  $n=5$ ). The soot has been deposited on the tunnel wall for approximately 60 years (time span between finalization of the tunnel building and shotcrete application), thus stemming from different kinds of fossil fuels. From literature it is known that combustion of fossil fuel can have a wide range of  $\delta^{34}\text{S}$  values from  $-30$  to  $+30$  ‰ [45]. High regional differences with respect to  $\delta^{34}\text{S}$  range can be obtained due to different parental material [46-49]. However most common values are in the range from  $-1$  to  $+10$  ‰ [50]. This  $\delta^{34}\text{S}$  range is reflecting the results for soot in the investigated Tunnel 1.

From studies conducted on the role of soot in sulfate attack of a railroad tunnels, Romer [32] concluded that soot was not the main source for concrete deterioration. In contrast, soot and fumes of modern diesel engines were considered responsible in case studies regarding Slovenian railroad tunnels [31]. In both studies stable isotope char-

acterization was not included. Based on our new sulfur isotope data, we conclude that soot will have no significant influence on concrete deterioration and can be excluded as major potential sulfur source. Although  $\delta^{34}\text{S}$  values of deteriorated concrete in area SII seem to match the isotopic composition of soot, it is more likely that in this area sulfate gained from pyrite oxidation is contributing to the concrete damage.

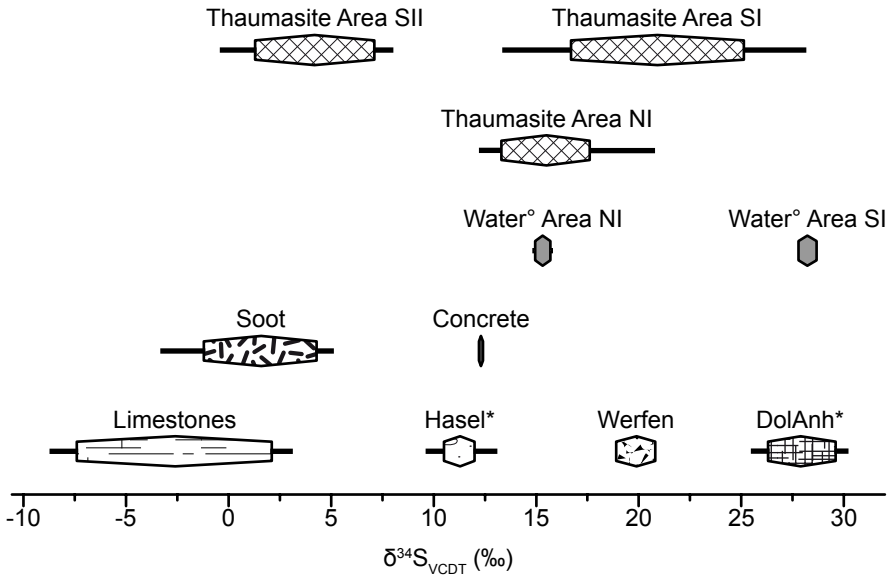


Figure 3: Range of  $\delta^{34}\text{S}_{\text{VCDT}}$  values associated with Tunnel 1. °denotes  $\delta^{34}\text{S}_{\text{VCDT}}$  values for ground, spring, and drainage water. \*denotes  $\delta^{34}\text{S}_{\text{VCDT}}$  values of solids from this study; others are obtained from the literature [44, 57].

Figure 4 is showing the range of  $\delta^{34}\text{S}$  values associated with Tunnel 2. Samples of non-altered concrete and shotcrete display  $\delta^{34}\text{S}$  values of +7.6, +10.6 and +10.7 ‰. In contrast to this, thaumasite and directly corresponding ground water with high sulfate concentrations yield  $\delta^{34}\text{S}$  values from +14.1 to +19.0 ‰ (average +18.0±2.2 ‰; n=13). Analysis of local calcium sulfate rocks (anhydrite and gypsum) results in  $\delta^{34}\text{S}$  values from +17.1 to +19.9 ‰ (average +17.9±1.0 ‰; n=5). Three thaumasite samples in a designated area are giving  $\delta^{34}\text{S}$  values of +11.8, +3.8, and -1.2 ‰. In Tunnel 2 the sulfur isotope signature of concrete damage matches nearby that of ground water, except for T2\_7 to T2\_9 with isotopically lighter  $\delta^{34}\text{S}$  values. Latter values are caused by pyrite oxidation in the surrounding black shales of Cretaceous ages [51].

$\delta^{34}\text{S}$  values from analogous units of other localities display average values of about  $-15 \pm 7 \text{‰}$  [52, 53]. Even  $\delta^{34}\text{S}$  values down to  $-42 \text{‰}$  have been found for Cretaceous black shales at a North-Italian site [54]. This range is also close to results reported for pyrite in sediments of upper Permian and lower Triassic age [55, 56]. Although a rather wide range of S-isotope composition of individual occurring pyrite in the local black shales is possible, the above given range can be easily distinguished from the local marine evaporitic sulfates with  $\delta^{34}\text{S}$  values from  $+14$  to  $+27 \text{‰}$ . Accordingly, in the present study pyrite oxidation from black shales is a valid sulfur source for the formation of thaumasite creating isotopically lighter S-signatures. The oxidation of sulfides is facilitated by the observed dissolved oxygen content of the ground water thus contributing to dissolved sulfate for sulfate attack (Table 2 see appendix).

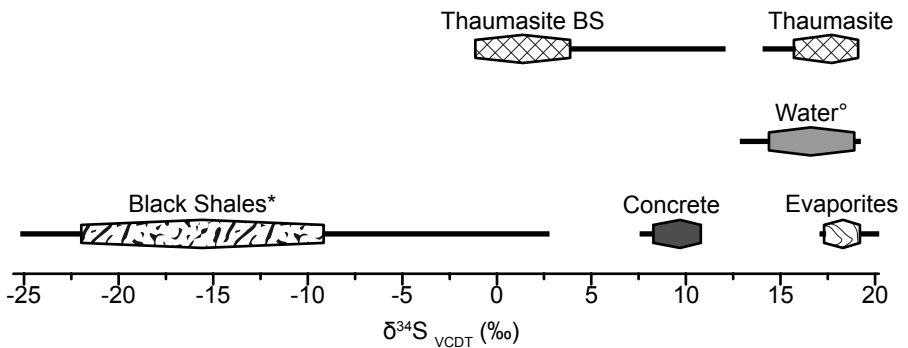


Figure 4: Range of  $\delta^{34}\text{S}_{\text{VCDT}}$  values associated with Tunnel 2. °denotes  $\delta^{34}\text{S}_{\text{VCDT}}$  values for ground, spring, and drainage water. \*denotes  $\delta^{34}\text{S}_{\text{VCDT}}$  values from [52].

The present study clearly indicates a good correlation between  $\delta^{34}\text{S}$  signatures of sulfate from deteriorated concrete and adjacent ground water. From samples e.g. 11 to 13 and 15 to 17 of Tunnel 2, where it was possible to sample damaged concrete and associated rocks and ground water, no sulfur isotope fractionation during thaumasite formation is observed. Slightly lower  $\delta^{34}\text{S}$  values of sulfate from damaged concrete compared to those of sulfate from local ground water can be explained by the minor impact of the internal concrete sulfate with generally lower  $\delta^{34}\text{S}$  values versus those of the local evaporites. Internal concrete sulfate is mostly related to gypsum which is added in low quantities to the cement to improve its processability. All  $\delta^{34}\text{S}$  values for samples of non-alternated concrete from both tunnels are in the range from  $+10.6$  to  $+12.3 \text{‰}$ . This displays the application of Permian gypsum for cement production

[44, 57]. In Tunnel 1 shotcrete was first applied in 1964 and was renewed several times up to present days due to sulfate attack. Expected values for internal sulfate (gypsum) are in the range from +10.0 to +15.0 ‰, stemming from marine evaporites. However, other internal sulfate sources in concrete are possible like gypsum with non Permo Skythian to lower Triassic ages or gypsum that was produced from desulfurization from power plants with  $\delta^{34}\text{S}$  values from +14 to +18 ‰ [47].

Contribution from atmospheric  $\text{SO}_2$  to the neoformation of thaumasite seems unlikely in this study. Sulfur isotopes of air borne sulfur are usually much more depleted compared to the  $\delta^{34}\text{S}$  values found for concrete damage in Tunnels 1 and 2 [58]. Thus the impact of  $\text{SO}_2$  due to air pollution on sulfate attack on concrete assumed by various studies is not valid for concrete alteration in the present tunnel buildings [33, 59, 60]. Moreover, the amount of  $\text{SO}_2$  may be not sufficient for the observed intensive thaumasite formation.

To the authors knowledge, the only study using sulfur isotopes in relation to thaumasite formation was performed by Iden and Hagelia [34]. They commented on their use of laser ablation techniques that it might not be suitable for very fine grained material such as (deteriorated) concretes due to micro-scale inhomogeneity. In the present study we have followed the authors' recommendation to use small bulk amounts of degraded material (purified thaumasite in our case).

## 2.2.6 Conclusions

Our results from two tunnels indicate that the distribution of sulfur isotopes can be applied as an excellent tool to decipher the origin of sulfate for chemical attack on concrete.  $\delta^{34}\text{S}$  values of thaumasite perfectly match with the sulfur isotopic composition of sulfate from associated ground water. Thus the newly formed sulfate mineral thaumasite reflects the isotopic signatures of gypsum and anhydrite from local host rocks. Isotopically lighter  $\delta^{34}\text{S}$  values of solids from concrete damage are assumed to be influenced by pyrite oxidation from the local rocks. Accordingly pyrite has been proven to be a potential sulfur sources for sulfate attack via mobilisation and transport of sulfate within the local ground water. No indications are found for a significant contribution from sulfur sources like atmospheric  $\text{SO}_2$ , internal sulfate of the cement, and organic relicts (soot from combustion). A successful application of sulfur isotope distribution for the investigation of sulfate attack on concrete requires consistent isotope data of potential sulfur sources, sulfate in aqueous solutions, and secondary minerals in concrete.

## 2.2.7 Acknowledgment

The present study was funded by NAWI Graz (Graz Advanced School of Science, GASS), Österreichische Forschungsförderungsgesellschaft (FFG, 828476) and further supporting companies. Sulfur isotope measurements were supported by Leibniz Society. We particularly want to thank Josef Tritthart (TU Graz) and Walter Kurz (KFU Graz) for their suggestions and advice, Andreas Mayer (bf:gh) organizing sampling and providing additional data, Thomas Rinder (TU Graz) for the assistance during sampling and Patrick Grunert (KFU Graz) supervising SEM imaging.

## 2.3 Remarks and Outlook

In the given previous section it was clearly shown that analyses of sulfur isotopes provides powerful tools in order to decipher possible sulfur sources for sulfate attack. However some limitations and further promising research topics should be discussed: The major outcome of this chapter is based on the principle that during the formation of secondary sulfate minerals such as thaumasite, ettringite and gypsum in concrete none or negligible small fractionation between the sulfur isotopes  $^{34}\text{S}$  and  $^{32}\text{S}$  is occurring. In field studies, presented in the previous section, this approach was well demonstrated to be valid. Furthermore studies concerning the formation of gypsum under laboratory conditions confirm this finding [18]. However no data on possible sulfur isotope fractionation with respect to ettringite and thaumasite is available neither from synthesized pure phases nor from concrete or mortar bars that have degraded in experimental setups.

The stable sulfur isotopes methodology presented in this study is referred to small bulk samples. However for concrete deterioration one of the crucial questions is "What is the initiation of concrete deterioration?". Thus ideally in-situ measurement at the micro scale or even nano scale should be performed. In case of whether thaumasite and ettringite are forming as end member phases or thaumasite is forming as a consequence of a solid solution with ettringite cannot sufficiently be solved at the micro scale [39]. Unfortunately methods to provide sulfur isotope measurements at the nano scale are not provided yet. Iden and Hagelia [34] have presented  $\delta^{34}\text{S}$  micro scale results from concrete that had been degraded by sulfate attack. These measurements were acquired by a laser ablation probe coupled to an IRMS. The results are somewhat difficult to interpret and it is still doubtful that no isotope fractionation

occurs during the ablation of high water containing phases such as Tha, Ett, and Gp. Furthermore (deteriorated) concrete is a very inhomogeneous fine grained material. Suitable matrix matched standards are not available. Challenging for future studies is therefore to compare and improve laser methods and combustion techniques e.g. by using self-made matrix matched standards such as pure thaumasite.

A perfect complement to the samples described in previous section would be to measure  $\delta^{34}\text{S}$  values of sulfate in the interstitial solutions that have been expressed from deteriorated samples (for more details see Chapter 3). These solutions represent the fluids that are directly responsible for the formation of secondary sulfate minerals. Solids and liquids should be measured in the same area.

Ground water which dissolves gypsum and anhydrite from the local host rock is a main cause for sulfate attack of concrete in underground structures as  $\delta^{34}\text{S}$  values of ground water sulfate and deteriorated concrete lie in the same range. In some areas, however, Tha was found in the vicinity of e.g. black shale which resembles much lower  $\delta^{34}\text{S}$  values. This is accounted to the oxidation of metal sulfides, mainly pyrite, and the liberation of  $\text{SO}_4$  to the ground water. It is quite clear that the lower  $\delta^{34}\text{S}$  values are due to pyrite dissolution but isotopic ratios have not been measured for the host rock except for one example. A large idiomorphic pyrite grain that was taken from a matrix of talc, dolomite and quartz yields a  $\delta^{34}\text{S}$  value of + 8.7 ‰. Presumably the pyrite origin is linked to post-digenetic highly enriched sulfides and or interaction with late migrating solutions. The signal is secondary but not a primary digenetic one [61]. Consequently a promising extension to this study is to measure  $\delta^{34}\text{S}$  values of the local host rock in areas where concrete damage was found near black and green shales of the Penninic units and colored and dark shales from Skythian to Anisian sedimentary rocks from the Bosruck massif.

Besides sulfur isotopes the additional use of stable oxygen isotopes from sulfates will provide a deeper understanding of the reaction mechanisms. For instance  $\delta^{18}\text{O}$  values from thaumasite that was formed due to iron sulfide oxidation would greatly differ from thaumasite that has derived its sulfate from marine gypsum and anhydrite. Isotope fractionation between  $^{18}\text{O}$  and  $^{16}\text{O}$  is also sensitive to potential bioactivity or atmospheric impact (e.g.  $\text{SO}_2$ ) as reported by Iden and Hagelia [34].



## 2.4 References

1. Mittermayr, F., D. Klammer, D. Höllen, S. Köhler, M. Böttcher, A. Leis, and M. Dietzel, Deterioration of Concrete: Application of Stable Isotopes, in Proceedings of the 10<sup>th</sup> International Congress for Applied Mineralogy (ICAM), M.A.T.M. Broekmans, Editor. 2012, Springer Berlin Heidelberg. p. 435-443.
2. Bellmann, F. and J. Stark, The role of calcium hydroxide in the formation of thaumasite. *Cement and Concrete Research*, 2008. 38(10): p. 1154-1161.
3. Hagelia, P. and R.G. Sibbick, Thaumasite Sulfate Attack, Popcorn Calcite Deposition and acid attack in concrete stored at the "Blindtarmen" test site Oslo, from 1952 to 1982. *Materials Characterization*, 2009. 60(7): p. 686-699.
4. Romer, M., L. Holzer, and M. Pfiffner, Swiss tunnel structures: concrete damage by formation of thaumasite. *Cement and Concrete Composites*, 2003. 25(8): p. 1111-1117.
5. Tritthart, J., D. Klammer, F. Mittermayr, and A. Brunnsteiner, A Casestudy of Thaumasite Formation in an Austrian Tunnel, in Cementing a sustainable future 13<sup>th</sup> International Congress on the Chemistry of Cement, Á. Palomo, A. Zaragoza, and J. C. López Agüí, Editors. 2011, CSIC: Madrid. p. No. 126: 1-6
6. Lee, H., R.D. Cody, A.M. Cody, and P.G. Spry, The formation and role of ettringite in Iowa highway concrete deterioration. *Cement and Concrete Research*, 2005. 35(2): p. 332-343.
7. Czerewko, M.A., J.C. Cripps, J.M. Reid, and C.G. Duffell, Sulfur species in geological materials--sources and quantification. *Cement and Concrete Composites*, 2003. 25(7): p. 657-671.
8. Blanco-Varela, M.T., J. Aguilera, S. Martinez-Ramirez, F. Puertas, A. Palomo, C. Sabbioni, G. Zappia, C. Riontino, K. Van Balen, and E.E. Toumbakari, Thaumasite formation due to atmospheric SO<sub>2</sub>-hydraulic mortar interaction. *Cement and Concrete Composites*, 2003. 25(8): p. 983-990.
9. Stark, J. and B. Wicht, Sulfatwiderstandsfähigkeit von Beton, in Dauerhaftigkeit Von Beton: Der Baustoff Als Werkstoff, F.A. Finger-Institut-f.-Baustoffkunde-d.-Bauhaus-Universität-Weimar, Editor. 2001, Birkhäuser: Basel. p. 120-132.
10. Bottomley, D.J., J. Veizer, H. Nielsen, and M. Moczydlowska, Isotopic composition

- of disseminated sulfur in Precambrian sedimentary rocks. *Geochimica et Cosmochimica Acta*, 1992. 56(8): p. 3311-3322.
11. Cook, N.J. and J. Hoefs, Sulphur isotope characteristics of metamorphosed Cu-(Zn) volcanogenic massive sulphide deposits in the Norwegian Caledonides. *Chemical Geology*, 1997. 135(3-4): p. 307-324.
  12. Dill, H. and H. Nielsen, Carbon-Sulfur-Iron-Variations and Sulfur Isotope Patterns of Silurian Graptolite Shales. *Sedimentology*, 1986. 33(5): p. 745-755.
  13. Knöller, K. and M. Schubert, Interaction of dissolved and sedimentary sulfur compounds in contaminated aquifers. *Chemical Geology*, 2010. 276(3-4): p. 284-293.
  14. Nielsen, H. and W. Rieke, Schwefelisotopen Verhältnisse von Evaporiten aus Deutschland; Ein Beitrag zur Kenntnis von  $\delta^{34}\text{S}$  im Meerwasser-Sulfat. *Geochimica et Cosmochimica Acta*, 1964. 28(5): p. 577-591.
  15. Nriagu, J.O., R.D. Coker, and L.A. Barrie, Origin of sulphur in Canadian Arctic haze from isotope measurements. *Nature*, 1991. 349(6305): p. 142-145.
  16. Tichomirowa, M., F. Haubrich, W. Klemm, and J. Matschullat, Regional and temporal (1992-2004) evolution of air-borne sulphur isotope composition in Saxony, southeastern Germany, central Europe. *Isotopes in Environmental and Health Studies*, 2007. 43(4): p. 295-305.
  17. Wakshal, E. and H. Nielsen, Variations of  $\delta^{34}\text{S}$  ( $\text{SO}_4$ ),  $\delta^{18}\text{O}$  ( $\text{H}_2\text{O}$ ) and  $\text{Cl}/\text{SO}_4$  ratio in rainwater over northern Israel, from the Mediterranean Coast to Jordan Rift Valley and Golan Heights. *Earth and Planetary Science Letters*, 1982. 61(2): p. 272-282.
  18. Faure, G. and T. Mensing, *Isotopes Principles and Applications*. 3<sup>rd</sup> ed. 2005, Hoboken: John Wiley & Sons. 897.
  19. Hoefs, J., *Stable Isotope Geochemistry*. 6<sup>th</sup> ed. 2008, Berlin: Springer. 288.
  20. Hosono, T., E. Uchida, C. Suda, A. Ueno, and T. Nakagawa, Salt weathering of sandstone at the Angkor monuments, Cambodia: identification of the origins of salts using sulfur and strontium isotopes. *Journal of Archaeological Science*, 2006. 33(11): p. 1541-1551.
  21. Klemm, W., Die Isotopensignatur von Sulfaten an Bauwerken. *Zeitschrift der Deutschen Gesellschaft für Geowissenschaften*, 2005. 156(1): p. 51-58.

22. Nord, A.G. and K. Holenyi, Sulphur deposition and damage on limestone and sandstone in Stockholm city buildings. *Water Air and Soil Pollution*, 1999. 109(1-4): p. 147-162.
23. Prikryl, R., J. Svobodova, K. Zak, and D. Hradil, Anthropogenic origin of salt crusts on sandstone sculptures of Prague's Charles Bridge (Czech Republic): Evidence of mineralogy and stable isotope geochemistry. *European Journal of Mineralogy*, 2004. 16(4): p. 609-617.
24. Roesch, H. and H.J. Schwarz, Damage to Frescoes Caused by Sulphate-Bearing Salts: Where Does the Sulphur Come from? *Studies in Conservation*, 1993. 38(4): p. 224-230.
25. Schleicher, N. and C.R. Hernandez, Source identification of sulphate forming salts on sandstones from monuments in Salamanca, Spain-a stable isotope approach. *Environmental Science and Pollution Research*, 2010. 17(3): p. 770-778.
26. Sanchez, J.S., C.A.S. Alves, J.R.V. Romani, and D.F. Mosquera, Origin of Gypsum-rich Coatings on Historic Buildings. *Water Air and Soil Pollution*, 2009. 204(1-4): p. 53-68.
27. Böttcher, M.E., The stable isotopic geochemistry of the sulfur and carbon cycles in a modern karst environment. *Isotopes in Environmental and Health Studies*, 1999. 35(1-2): p. 39-61.
28. Ohmoto, H., Y. Watanabe, H. Ikemi, S.R. Poulson, and B.E. Taylor, Sulphur isotope evidence for an oxic Archaean atmosphere. *Nature*, 2006. 442(7105): p. 908-911.
29. Siedel, H., W. Klemm, and F. Vasco. Evaluation of the environmental influence on sulphate salt formation at monuments in Dresden (Germany) by sulphur isotope measurements. in *Proceedings of the 9<sup>th</sup> International Congress on Deterioration and Conservation of Stone*. 2000. Amsterdam: Elsevier Science B.V.
30. Clark, I. and P. Fritz, *Environmental Isotopes in Hydrogeology*. 1997, Boca Raton: Lewis Publishers. 328.
31. Suput, J.S., A. Mladenovic, L. Cernilogar, and V. Olensek, Deterioration of mortar caused by the formation of thaumasite on the limestone cladding of some Slovenian railway tunnels. *Cement and Concrete Composites*, 2003. 25(8): p. 1141-1145.

32. Romer, M., Steam locomotive soot and the formation of thaumasite in shotcrete. *Cement and Concrete Composites*, 2003. 25(8): p. 1173-1176.
33. Pye, K. and N. Schiavon, Cause of Sulfate Attack on Concrete, Render and Stone indicated by Sulfur Isotope Ratios. *Nature*, 1989. 342(6250): p. 663-664.
34. Iden, I.K. and P. Hagelia, C, O and S isotopic signatures in concrete which have suffered thaumasite formation and limited thaumasite form of sulfate attack. *Cement and Concrete Composites*, 2003. 25(8): p. 839-846.
35. Vallet, J.M., C. Gosselin, P. Bromblet, O. Rolland, V. Verges-Belmin, and W. Kloppmann, Origin of salts in stone monument degradation using sulphur and oxygen isotopes: First results of the Bourges cathedral (France). *Journal of Geochemical Exploration*, 2006. 88(1-3): p. 358-362.
36. Rabcewicz, L. and J. Gosler, Application of the NATM to the underground works at Tarbela. Part 1. *International Journal of Rock Mechanics and Mining Science & Geomechanics Abstracts*, 1974. 11(11): p. 225.
37. Parkhurst, D.L. and C.A.J. Apello, User's guide to PHREEQC (V2). U.S. Geol. Sur, 1999. 312.
38. Mann, J.L., R.D. Vocke, and W.R. Kelly, Revised  $\delta^{34}\text{S}$  reference values for IAEA sulfur isotope reference materials S-2 and S-3. *Rapid Communications in Mass Spectrometry*, 2009. 23(8): p. 1116-1124.
39. Kohler, S., D. Heinz, and L. Urbonas, Effect of ettringite on thaumasite formation. *Cement and Concrete Research*, 2006. 36(4): p. 697-706.
40. Macphee, D.E. and S.J. Barnett, Solution properties of solids in the ettringite-thaumasite solid solution series. *Cement and Concrete Research*, 2004. 34(9): p. 1591-1598.
41. Dietzel, M., Measurement of the stable carbon isotopes in calcite sinters on concrete. *ZKG International*, 2000. 53(9): p. 544-548.
42. Dietzel, M., T. Rinder, A. Niedermayr, F. Mittermayr, A. Leis, D. Klammer, S. Köhler, and P. Reichl, Mechanisms of Sinter Formation in Drainage Systems. *BHM Berg- und Hüttenmännische Monatshefte*, 2008. 153(10): p. 369-372.
43. Niedermayr, G. and E. Pak, *Archiv für Lagerstätten Forschung*, ed. L. Weber. Vol. 19. 1997, Wien: Geologische Bundesanstalt. 607.

44. Spötl, C. and E. Pak, A strontium and sulfur isotopic study of Permo-Triassic evaporites in the Northern Calcareous Alps, Austria. *Chemical Geology*, 1996. 131(1-4): p. 219-234.
45. Nielsen, H., Isotopic Composition of Major Contributors to Atmospheric Sulfur. *Tellus*, 1974. 26(1-2): p. 213-221.
46. Grey, D.C. and M.L. Jensen, Bacteriogenic Sulfur in Air Pollution. *Science*, 1972. 177(4054): p. 1099-1100.
47. Klemm, W., R. Kleeberg, M. Tichomirowa, and H. Siedel, Mineralogische und isotopengeochemische Untersuchungen von Sulfatausblühungen an historischen Bauwerken. *Zeitschrift der Deutschen Gesellschaft für Geowissenschaften*, 1999. 27(5): p. 455-460.
48. Torfs, K.M., R.E. vanGrieken, and F. Buzek, Use of stable isotope measurements to evaluate the origin of sulfur in gypsum layers on limestone buildings. *Environmental Science & Technology*, 1997. 31(9): p. 2650-2655.
49. H. R. Krouse, L.N. Grinenko, V.A. Grinenko, L. Newman, J. Forrest, N. Nakai, Y. Tsuji, T. Yatsumimi, V. Takeuchi, B.W. Robinson, M.K. Stewart, A. Gunatilaka, L.A. (Chambers) Plumb, J.W. Smith, F. Buzek, J. Cerny, J. Sramek, A.G. Menon, G.V.A. Iyer, V.S., Venkatasubramanian, B.E.C. Egboka, M.M. Irogbenachi, and C.A. Eligwe, Case Studies and Potential Applications, in *Stable Isotopes, Natural and Anthropogenic Sulphur in the Environment*, H.R. Krouse and V.A. Grinenko, Editors. 1991, John Wiley & Sons: Chichester. p. 307-423.
50. Nielsen, H., J. Pilot, L.N. Grinenko, V.A. Grinenko, A.Y. Lein, J.W. Smith, and R.G. Pankina, Lithospheric Sources of Sulphur, in *Stable Isotopes, Natural and Anthropogenic Sulphur in the Environment*, H.R. Krouse and V.A. Grinenko, Editors. 1991, John Wiley & Sons: Chichester. p. 65-133.
51. Demmer, W., C. Exner, H. Häusler, and A. Tollmann, Blatt 156 Muhr, ed. H. Häusler. 1995, Wien: Geologische Bundesanstalt.
52. Hetzel, A., M.E. Böttcher, U.G. Wortmann, and H.J. Brumsack, Paleo-redox conditions during OAE 2 reflected in Demerara Rise sediment geochemistry (ODP Leg 207). *Palaeogeography Palaeoclimatology Palaeoecology*, 2009. 273(3-4): p. 302-328.

53. Kolonic, S., J.S.S. Damste, M.E. Böttcher, M.M.M. Kuypers, W. Kuhnt, B. Beckmann, G. Scheeder, and T. Wagner, Geochemical characterization of Cenomanian/Turonian black shales from the Tarfaya Basin (SW Morocco) - Relationships between palaeoenvironmental conditions and early sulphurization of sedimentary organic matter. *Journal of Petroleum Geology*, 2002. 25(3): p. 325-350.
54. Böttcher, M.E., M.M.M. Kuypers, and M. Gehre. unpublished.
55. Grice, K., C.Q. Cao, G.D. Love, M.E. Böttcher, R.J. Twitchett, E. Grosjean, R.E. Summons, S.C. Turgeon, W. Dunning, and Y.G. Jin, Photic zone euxinia during the Permian-Triassic superanoxic event. *Science*, 2005. 307(5710): p. 706-709.
56. Nabbefeld, B., K. Grice, A. Schimmelmann, P.E. Sauer, M.E. Böttcher, and R. Twitchett, Significance of dDkerogen,  $\delta^{13}\text{C}$  kerogen and  $\delta^{34}\text{S}$  pyrite from several Permian/Triassic (P/Tr) sections. *Earth and Planetary Science Letters*, 2010. 295(1-2): p. 21-29.
57. Schroll, E., Geochemische und geochronologische Daten und Erläuterungen, in *Archiv für Lagerstätten Forschung*, L. Weber, Editor. 1997, Geologische Bundesanstalt: Wien. p. 395-537.
58. Newman, L., H.R. Krouse, and V.A. Grinenko, Sulphur Isotope Variations in the Atmosphere, in *Stable Isotopes, Natural and Anthropogenic Sulphur in the Environment*, H.R. Krouse and V.A. Grinenko, Editors. 1991, John Wiley & Sons: Chichester. p. 133-177.
59. Kloppmann, W., P. Bromblet, J.M. Vallet, V. Vergès-Belmin, O. Rolland, C. Guerrot, and C. Gosselin, Building materials as intrinsic sources of sulphate: A hidden face of salt weathering of historical monuments investigated through multi-isotope tracing (B, O, S). *Science of The Total Environment*, 2011. 409(9): p. 1658-1669.
60. Schweigstillova, J., R. Prikryl, and M. Novotna, Isotopic composition of salt efflorescence from the sandstone castellated rocks of the Bohemian Cretaceous Basin (Czech Republic). *Environmental Geology*, 2009. 58(1): p. 217-225.
61. Böttcher, M.E. pers. comm.

## 2.5 Appendix

Table 2: Typical chemical composition of aqueous solutions from Tunnels 1 and 2. Concentrations are given in  $\text{mg L}^{-1}$ . Note: TDS: total dissolved solids; SI Gp: saturation index with respect to gypsum; DW: drainage water; GW: ground water; HWT: ground water from a nearby highway rescue tunnel; n.a.: not analyzed; n.d.: not detected.

Sample	Type	Position [m]	Discharge [L s <sup>-1</sup> ]	pH	T [°C]	Na	K	Mg
<b>Tunnel 1</b>								
T1_1	DW	0	100	8.34	6.3	6.70	0.32	10.0
T1_14	GW	1196	3.00	8.32	8.5	0.60	0.25	10.6
T1_15	GW	1620	5.00	8.15	6.3	0.62	0.24	10.1
T1_31	GW	4206	n.a.	7.54	7.8	3.52	0.94	31.6
T1_36	DW	4766	200	7.78	7.7	9.52	1.32	35.5
T1_45	GW	HWT	10.0	8.35	6.7	0.41	0.40	7.59
<b>Tunnel 2</b>								
T2_1	DW	0	0.50	8.26	9.1	650	33.8	18.7
T2_4	GW	800	n.a.	8.04	5.2	0.19	0.12	9.07
T2_5	GW	1731	0.0003	8.53	14.3	281	8.99	83.7
T2_12	GW	3117	0.028	7.53	4.3	1.61	1.84	32.6
T2_20	GW	5911	0.002	7.66	12.8	41.3	2.64	30.9
T2_24	Spring	6341	n.a.	7.97	4.9	0.58	0.29	21.5
Sample	Ca	Cl	NO <sub>3</sub>	SO <sub>4</sub>	HCO <sub>3</sub>	TDS	O <sub>2</sub>	SI <sub>Gp</sub>
<b>Tunnel 1</b>								
T1_1	37.6	7.37	3.00	22.1	139	226	11.4	-2.4
T1_14	40.2	1.03	3.69	13.9	150	220	10.5	-2.5
T1_15	36.5	0.82	4.00	12.4	142	207	11.3	-2.6
T1_31	193	3.80	1.91	464	162	861	6.10	-0.7
T1_36	206	12.9	1.50	502	167	935	n.a.	-0.6
T1_45	25.0	0.40	3.26	2.95	107	147	n.a.	-3.3
<b>Tunnel 2</b>								
T2_1	145	655	12.7	817	126	2457	10.9	-0.7
T2_4	24.6	0.57	1.04	5.96	113	155	10.5	-3.0
T2_5	468	12.4	n.d.	2026	92.8	2973	n.a.	0.0
T2_12	550	1.53	0.22	1353	153	2094	0.28	0.0
T2_20	564	9.20	1.46	1339	274	2263	n.a.	0.0
T2_24	66.8	0.55	2.48	143	122	357	10.8	-1.4

Table 3: Sulfur content and  $\delta^{34}\text{S}_{\text{VCDT}}$  values in ‰ of natural rocks, dissolved sulfate of sampled solutions and of sulfate containing damaged concrete from Tunnels 1 and 2. Tha: thaumasite; DW: drainage water; GW: ground water; TS: tunnel surface; LS: limestone; Anh: anhydrite; Gp: gypsum; Dol: dolomite; DrW: drip water; HWT: ground water from a nearby highway rescue tunnel; n.a.: not analyzed

Sample	Position	Area	$\delta^{34}\text{S}$	$\text{SO}_4$	$\text{SO}_4$	Type	Geol. Unit	Comment
	[m]		[‰]	[mg L <sup>-1</sup> ]	[wt. %]			
Tunnel 1								
T1_1	0	NI 000	14.8	22.1		DW	Haselgebirge & Werfen	North outlet
T1_2	211	NI 027	12.2		8.40	Tha		
T1_3	211	NI 027	19.7		12.2	Tha		
T1_4	211	NI 027	20.8		n.a.	TS		Gp + breaking dust
T1_5	243	NI 031	15.6		11.6	Tha		
T1_6	243	NI 031	15.3		14.6	Tha		
T1_7	259	NI 033	15.7		2.36	Shotcrete		
T1_8	259	NI 033	15.5		n.a.	Shotcrete		
T1_9	259	NI 033	15.1		n.a.	Shotcrete		
T1_10	307	NI 039	12.3		1.20	Shotcrete		No damage
T1_11	420	NI 053	14.7		n.a.	Shotcrete		
T1_12	420	NI 053	14.9		20.5	Tha		
T1_13	420	NI 053	14.6		n.a.	Shotcrete		
T1_14	1196	NI 025	15.7	13.9		GW	Wetterstein LS	Well fast flowing
T1_15	1620	NI 078	15.3	12.4		GW		Well fast flowing
T1_16	2397	SIII 047	3.4		n.a.	Soot	Werfen	
T1_17	2981	SII 099	7.9		1.00	Shotcrete		
T1_18	3173	SII 075	7.7		1.87	Shotcrete		
T1_19	3173	SII 075	4.7		10.8	Shotcrete		
T1_20	3269	SII 057	2.7		4.64	Tha		
T1_21	3269	SII 057	2.7		5.93	Shotcrete		
T1_22	3510	SII 033	-0.3		1.62	Shotcrete		LS & Rauhacke
T1_23	4132	SI 080	28.1		21.2	Tha	Anh & Dol	
T1_24	4156	SI 078	21.0	13.6		Tha		
T1_25	4156	SI 078	13.5	10.2		Tha		
T1_26	4156	SI 078	1.1		n.a.	Soot		
T1_27	4156	SI 078	1.5		n.a.	Soot		



Table 3: Continued

Sample	Position [m]	Area	$\delta^{34}\text{S}$ [‰]	$\text{SO}_4$ [mg L <sup>-1</sup> ]	$\text{SO}_4$ [wt. %]	Type	Geol. Unit	Comment
T1_28	4183	SI 073	15.6	3.31		Tha	Werfen & Rauhacke	
T1_29	4183	SI 073	5.0		n.a.	Soot		
T1_30	4183	SI 073	-3.2		n.a.	Soot		
T1_31	4206	SI 070	28.7	464		GW	Anh & Dol	Well filling reservoir
T1_32	4280	SI 061	22.4		4.74	Shotcrete	Werfen	
T1_33	4279	SI 061	22.7		n.a.	Shotcrete		
T1_34	4279	SI 061	21.3		n.a.	Shotcrete		
T1_35	4279	SI 061	22.4		n.a.	TS		Gp + breaking dust
T1_36	4766	SI 000	27.8	502		DW		South outlet
T1_37	-	-	3.0		0.03	Drillcore	Reichenhaller LS	
T1_38	-	-	-2.3		0.02	Drillcore	Guttensteiner Dol	
T1_39	-	-	18.9		0.63	Drillcore	Werfen	
T1_40	-	-	20.8		0.77	Drillcore		
T1_41	-	-	12.8		7.55	Drillcore	Hasegebirge	
T1_42	-	-	11.3		3.71	Drillcore		
T1_43	-	-	10.2	1955		Brine		
T1_44	-	-	11.2	7933		Brine		
T1_45	-	-	12.9	1223		Spring		
T1_46	-	-	11.9		58.4	Salt rock		
T1_47	-	-	10.9		55.1	Salt rock		
T1_48	-	-	11.1		5.30	Salt rock		
T1_49	-	-	30.1		56.3	Drillcore	Anha & Dol	
T1_50	-	-	30.1		51.7	Drillcore		
T1_51	-	HWT	-8.6	2.95		GW	Wetterstein LS	

Table 3: Continued

Sample	Position	Area	$\delta^{34}\text{S}$	$\text{SO}_4$	$\text{SO}_4$	Type	Geol. Unit	Comment
	[m]		[‰]	[mg L <sup>-1</sup> ]	[wt. %]			
Tunnel 2								
T2_1	0		14.7	817		DW	Debris of Triassic Carbonates	North outlet
T2_2	0		14.1		6.95	Tha		No damage
T2_3	345		7.6		n.a.	Shotcrete		No damage
T2_4	800		12.9	5.96		GW	Penninic units of the Tauern window	Slow flowing
T2_5	1731		18.8	2026		GW		DrW
T2_6	1800		10.6		1.04	Shotcrete		No damage
T2_7	1841		11.8		14.1	Tha		Black shale area
T2_8	1841		3.8		10.6	Tha		
T2_9	1860		-1.2		7.79	Tha		
T2_10	2055		17.6		17.9	Rock		Green phyllite + Anh
T2_11	3117		18.8	1298		GW		550 m above tunnel
T2_12	3117		19.0	1353		GW		
T2_13	3117		18.6		13.7	Tha		
T2_14	3316		10.7		0.50	Concrete		No damage
T2_15	3316		19.9		3.09	Rock		Anh
T2_16	3316		19.0		11.5	Tha		
T2_17	3316		18.6		12.5	Tha		
T2_18	3525		17.9		28.5	Rock		Anh
T2_19	5906		14.4	1373		GW		DrW
T2_20	5911		14.4	1339		GW		
T2_21	5921		18.4		37.0	Rock		Anh
T2_22	5933		17.1		43.3	Rock		Gp
T2_23	6341		17.6	142		Spring		Close to south portal
T2_24	6341		18.0	143		Spring		

## CHAPTER 3

# Why concrete disintegrates completely and thaumasite remains?

### 3.1 Introduction

In this chapter the reactions that may lead to transform consolidated concrete to a mush of thaumasite, calcite and aggregate relics are discussed (see Figure 1).



*Figure 1: Completely disintegrated concrete found in a ventilation tube of a highway tunnel. The side drainage tube underneath this area is not working properly and water is leaking into the concrete. White mushy material has no cohesion and is sampled by a garden shovel. The mineralogical composition and the corresponding expressed interstitial solution are referred to sample HW\_IS01 in Tables 1 to 3 in the following section 3.2. and in the appendix.*

In the following section analytical data and results to verify the impact of evaporating and wetting cycles on concrete deterioration by sulfate attack are presented. Supplementary aspects and perspectives for ongoing and future studies in particular regarding the use of crystal water as elemental proxy are given in the section 3.3.

## 3.2 Evaporation – A Key Mechanism for the Thaumasite Form of Sulfate Attack

Florian Mittermayr<sup>1</sup>, Andre Baldermann<sup>1</sup>, Christoph Kurta<sup>2</sup>, Thomas Rinder<sup>1,3</sup>, Dietmar Klammer<sup>1</sup>, Albrecht Leis<sup>4</sup>, Josef Tritthart<sup>5</sup>, Martin Dietzel<sup>1</sup>

<sup>1</sup>*Institute of Applied Geosciences, Graz University of Technology, Graz, Austria*

<sup>2</sup>*Institute of Chemistry - Analytical Chemistry, University of Graz, Graz, Austria*

<sup>3</sup>*Laboratoire Géosciences Environnement, Observatoire Midi-Pyrénées, Toulouse, France*

<sup>4</sup>*RESOURCES – Institute for Water, Energy and Sustainability, Joanneum Research, Graz, Austria*

<sup>5</sup>*Institute of Technology and Testing of Building Materials, Graz University of Technology, Graz, Austria*

### 3.2.1 Abstract

Mechanisms leading to chemical attack on concrete are crucial to be understood in order to prevent damage of concrete structures. Nevertheless, most studies on sulfate attack and thaumasite formation are based on empirical approaches, as the identification of reaction mechanisms and paths is known to be highly complex. In this study, sulfate damaged concrete from Austrian tunnels is investigated by mineralogical, chemical and isotope methods to discover the reactions which caused intense concrete alteration. Therefore, major, minor and trace elemental contents as well as isotope ratios of local ground water (GW), drainage water (DW) and interstitial solutions (IS) extracted from damaged concrete material are analyzed.

Locally occurring GW contains 3-545 mg L<sup>-1</sup> of SO<sub>4</sub> and is thus regarded as slightly aggressive to concrete in accordance to standard specifications (e.g. DIN EN 206-1). The concrete linings and drainage systems of the studied tunnels, however, have partly suffered from intensive sulfate attack. Heavily damaged concrete consists mainly of thaumasite, secondary calcite, gypsum, and relicts of aggregates. Surprisingly, the

concentrations of dissolved ions are extremely enriched in the IS with up to 30000 and 12000 mg L<sup>-1</sup> of SO<sub>4</sub> and Cl, respectively. Analyses of aqueous ions with a highly conservative behavior, e.g. K, Rb and Li, as well as <sup>2</sup>H/H and <sup>18</sup>O/<sup>16</sup>O isotope ratios of H<sub>2</sub>O of the IS show an intensive accumulation of ions and discrimination of the light isotopes vs. the GW. These isotope signals of the IS clearly discover evaporation at distinct relative humidities. From ion accumulation and isotope fractionation individual total and current evaporation degrees are estimated. Our combined elemental and isotopic approach verifies and assesses wetting-drying cycles within a highly dynamic concrete-solution-atmosphere system. Based on these boundary conditions, key factors controlling thaumasite formation are discussed with respect to the development of sulfate-resistant concrete.

### 3.2.2 Introduction

Despite a couple of decades of intensive work on sulfate attack and in particular on the related thaumasite form of sulfate attack (TSA), many uncertainties still persist concerning the mechanisms which trigger concrete damage [1-3]. Reports about TSA affected concrete structures are increasing steadily in numbers where environments for potential TSA are particularly provided in underground buildings and tunnels ([4-10] and references therein). In such settings, cool and wet conditions may induce rapid and intensive TSA. However, characterizing the (micro) environmental conditions and reaction paths that have caused the damage is highly challenging. For instance, in former studies on concrete damage in tunnels the importance of wick action and evaporation was already proposed [11-13], but the individual impact of both on deterioration of concrete is still not verified and by far not quantified.

A common approach to prevent potential sulfate attack is to improve the chemical resistance of the concrete. Therefore, specimens with different concrete admixtures are typically tested by submersion in Na and Mg sulfate solutions at different temperatures, pH, and concentration levels. E.g. changes in mechanical properties are used to determine the resistance of the concrete against sulfate attack. But drawn results are often not persuasive and are regarded as not practical to evaluate alteration of concrete in the field [14, 15]. According to Bellmann et al. [16] results and interpretations from experiments were not confirmed in the aspect of field performing concrete. In several experimental setups natural environmental conditions are approached by using partially immersed concrete, but authors are reporting diverging results. Haynes et al. [17], for

example, criticized that the aspect of physical attack from crystallization pressure of sulfate salts is potentially far more harmful and was overlooked by past researchers, who focused mainly on chemical sulfate attack. In contrast, Liu et al. [18] reported that the damage is mostly accounted to chemical sulfate rather than to physical attack. Consequently, it is inevitable to investigate concrete that has been subjected to sulfate attack in field studies in order to decipher the individual causes for the damage. Significant gaps of knowledge about reaction processes of TSA still exist and further advanced and sophisticated tools are needed to prevent concrete damage more effectively.

To provide a better understanding of concrete deterioration, pore fluids or interstitial solutions can be expressed from damaged concrete to consider their individual composition for damaging aspects. Longuet et al. [19] and Barneyback and Diamond [20] were among the first who successfully extracted pore fluids with a hydraulic press. This technique is widely used at present in concrete research (Cyr et al. [21] and references therein). Although the extraction of pore fluids of concrete is a well-known procedure, it was rarely used in studies dealing with sulfate attack [18, 22]. In this study we present for the first time chemical and isotopic composition of interstitial solutions (IS) which were extracted from concrete that has suffered TSA. Besides investigating the deteriorated concrete itself the novel approach of this study is to determine the impact of all involved solutions such as ground water (GW), drainage water (DW), and IS for a given case. Trace elemental signals and isotope ratios can be used to provide an advanced understanding of the concrete-solution-atmosphere system. Up to now e.g. stable sulfur and carbon isotopes were successfully applied in a few studies dealing with sulfate attack [23-26]. Herein, we introduce the distribution of stable hydrogen and oxygen isotopes of the extracted water to reveal actual causes for TSA on field concrete. Both isotope proxies are frequently used in environmental and climatological studies and have extensively led to an advanced understanding of water cycle on Earth [27, 28].  $^2\text{H}/\text{H}$  and  $^{18}\text{O}/^{16}\text{O}$  ratios represent the only reliable proxy for the solvent itself and to verify evaporation. Complementary main and in particular trace element concentrations in IS can provide information about reaction mechanisms and paths as well as about overall ion depletion or accumulation degrees.

### 3.2.3 Study sites

A railroad tunnel (RR) and a ventilation tube for a highway tunnel (HW) with respective lengths of 5425 and 4766 m were investigated for sulfate damaged concrete. Both

tunnels are passing parallel through the same mountain ridge about 100 m apart from each other. The HW and its ventilation tube which is situated a few meters underneath the highway pavement were constructed in 1983 by using the New Austrian Tunneling Method. Besides ventilating the highway tunnel with fresh air the ventilation tube is used as rescue tube and water drainage. The RR was built in the beginning of the 20<sup>th</sup> century. At the time of construction the rock excavation was left unsupported at mechanically stable heading horizons. Alternatively, a granitic brick wall lining was installed. Starting in 1964, shotcrete was applied throughout the entire length as a renovation measure.

The geological situation is rather delicate for tunnel engineering. Besides massive lime- and dolostone units in the center of the transverse section, low grade metamorphic rock sequences with embedded evaporitic rocks consisting of anhydrite and gypsum horizons have been encountered during tunnel heading. The latter geological units are located mainly in the northern and southern areas of both tunnels, where the most intensive concrete damage to occurs. More detailed informations about the geology of the study area and the spatial correlations between the adjoining geological units and respective concrete damages in respect to RR is given in [25]. Ground water encroachment in the tunnels is generally low in the areas with surrounding anhydrite and gypsum horizons, whereas at threshold regions to the lime- and dolostone units the discharge of water is high with runoffs of up to 100 L s<sup>-1</sup>.

### 3.2.4 Sampling and methodology

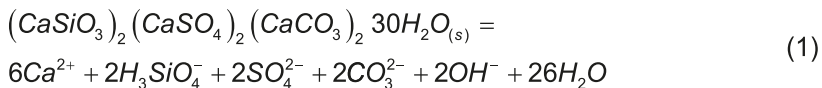
#### Solids

Heavily damaged concrete and shotcrete with white mushy appearance as well as white soft efflorescences which were found on tunnel linings were sampled and placed into air tight plastic containers. All samples collected inside the tunnel were stored in a cooler at about 10 °C. Damaged concrete samples were dried at 40 °C in the lab and subsequently ground for X-ray powder diffraction (XRD) analyses, while the white efflorescences were analyzed by XRD without drying. XRD patterns were collected using a PANalytical (Almelo, Netherlands) X'Pert PRO diffractometer equipped with a Co-tube (45 kV and 40 mA), 0.5° divergence and antiscattering slit, a rotating sample stage and an X'Celerator detector. The  $2\theta$  angle ranged from 4 to 100 ° with a step size of 0.016 °s<sup>-1</sup>

and a counting time of 40 s per step. Phase identification and quantification by Rietveld refinement were obtained using the PANalytical X'Pert HighScore software.

## Aqueous solutions

The IS of the damaged concrete were expressed from untreated (non-dried) material within 6 hours after sampling. Therefore, about 300 – 1100 g of concrete material was filled into the steel cylinder of a special adapted hydraulic press which squeezes the sample with a maximum load of 1300 kN/mm<sup>2</sup>. The expressed IS was sucked up with a syringe and filtered through a 0.45 µm cellulose acetate membrane. In order to monitor changes in the solution composition related to an increasing hydraulic pressure, multiple containers were filled during the expression experiments. The alkalinity and the pH were determined instantly after the expression at 20 °C. In analogy to the IS, the GW and DW samples were also filtered and analyzed for temperature, alkalinity and pH, but directly in the field. The chemical composition of the solutions (Na, K, Mg, Ca, Cl, SO<sub>4</sub>, NO<sub>3</sub>) was analyzed using a Dionex ICS-3000 ion chromatograph (IC) with an accuracy of ± 3 %. Dissolved trace elements were analyzed in 10 % HNO<sub>3</sub> by an Agilent 7500ce inductively coupled plasma mass spectrometer (ICP-MS with an accuracy of ±5 %). Calibration was performed using Merck CertiPUR® ICP multi-element standard VI for ICP-MS. Signal and drift correction was performed by online-addition of internal standards (Ge, In, Lu). The detection limit for Li, Si, Rb and Sr is 0.05 µg L<sup>-1</sup>. For hydro-geochemical modeling, the computer code PHREEQC and the minteq database were used [29] in order to calculate aqueous complex formation, charge balance and saturation indices with respect to the relevant solid phases (e.g. SI<sub>Calcite</sub>). The minteq database was modified for concrete phases in accordance to Schmidt et al. [22] including the theoretically calculated solubility constant for thaumasite according to the overall reaction



whereby the used value of  $K_{Thaumasite}$  ( $10^{-49.4}$  at 25 °C) was recently approved by Damidot et al. [30].

## Stable isotope ratios

Stable hydrogen and oxygen isotope ratios of the water molecules from the IS, GW and DW samples were analyzed by wavelength-scanned cavity ring-down spectroscopy



(WS-CRDS). The WS-CRDS analyzer was a model L1102-i system for liquid water isotopic analysis from Picarro [31]. The water samples were injected into a pre-heated evaporator unit, kept at 110°C using a PAL autosampler for liquid samples. The procedure used for the isotopic measurements is very similar to that described by Brand et al. [32]. From each water sample six consecutive injections were performed, of which the last three  $\delta$ -values were used for averaging. Results are given as  $\delta^2\text{H}$  and  $\delta^{18}\text{O}$  values in ‰ relative to the Vienna Standard Mean Ocean Water (VSMOW). Replicate measurements for  $\delta^2\text{H}$  and  $\delta^{18}\text{O}$  values result in an analytical precision  $< \pm 0.8$  and  $\pm 0.1$  ‰, respectively. Normalization of the raw results versus the VSMOW-SLAP scale was achieved by using a four-point calibration of in-house water standards that have been calibrated against the international reference materials VSMOW, GISP and VSLAP.

### 3.2.5. Results

#### Concrete damage

Quantitative XRD results (see Table 1 and Figure 2) of the samples taken in the HW indicate that the concrete mush material consists mainly of thaumasite (3-33 wt. %), gypsum (2-8 wt. %), calcite (20-39 wt. %) and dolomite (27-71 wt. %) and traces of quartz. Figure 3 illustrates an example of intensive sulfate attack on concrete found in the RR tunnel. In this tunnel heavily damaged concrete shows a similar mineralogy, consisting of thaumasite (5-17 wt. %) and gypsum (3-21 wt. %) among high contents of calcite (9-66 wt. %) and dolomite (20-61 wt. %) and minor proportions of quartz, muscovite, bassanite, and aragonite. In spite of a similar visual appearance sample RR\_I06, did not contain thaumasite or gypsum, but is consisting predominantly of quartz (53 wt. %), feldspar (30 wt. %), calcite (9 wt. %), and aragonite (7 wt. %). The latter material was scratched from joints between granitic bricks that were primarily installed more than a hundred of years ago. The white efflorescences found on the linings of both tunnels were identified as the highly soluble salt mineral mirabilite ( $\text{Na}_2\text{SO}_4 \cdot 10\text{H}_2\text{O}$ ).

The water content that was separated by squeezing from the concrete mush ranged from 5 up to 23 wt. %. Subsequent drying at 40 °C - until a constant weight was reached - allows to calculate the efficiency rate of water extraction to be about 36 - 78 %, in accordance to Cry et al. [21] (see Table 1).

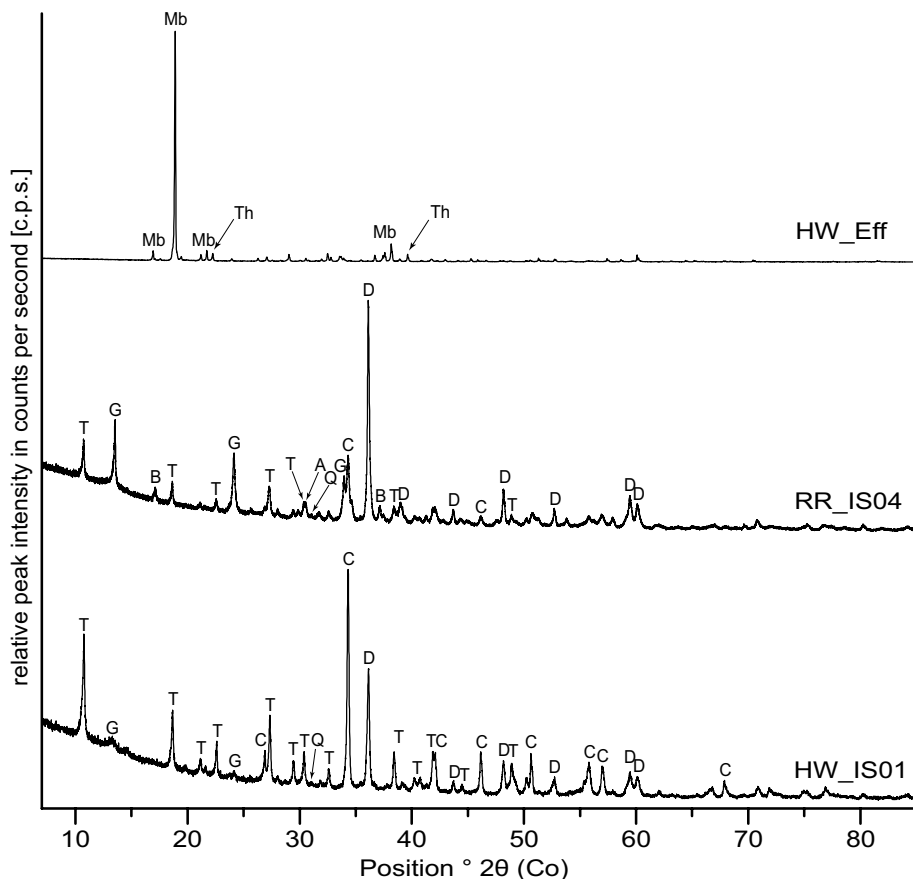


Figure 2. The lower two XRD patterns are showing typical reflexes for highly altered concrete and shotcrete containing (D): dolomite, (C): calcite, (G): gypsum, (T): thaumasite, (Q): quartz, (B): bassanite, (A): aragonite, while the upper pattern indicates (Mb) mirabilite and (Th): thenardite. Quantifications of the corresponding samples are given in Table 1.

### Solution chemistry

Chemical compositions of all extracted interstitial solutions, ground and drainage waters are displayed in the appendix. In general, two types of ground water were found. The first type is dominated by Ca-Mg-HCO<sub>3</sub> with total dissolved solids (TDS) and low SO<sub>4</sub> content of 150 – 230 mg L<sup>-1</sup> and 3 – 14 mg L<sup>-1</sup>, respectively. This low ion content of type 1 GW is found in the catchment areas of lime- and dolostone units (HW\_GW01, 02, 03, 04,

RR\_GW02, 03, 05, and 06). The second type is a Ca-SO<sub>4</sub> dominated GW (RR\_GW01, 04) with a TDS of approximately 900 mg L<sup>-1</sup>. Interestingly, the molar concentrations of Ca and SO<sub>4</sub> are 1:1 balanced at a maximum level of 545 mg L<sup>-1</sup> of SO<sub>4</sub>. This type 2 GW is typically and significantly enriched in dissolved components such as Ca, Mg, SO<sub>4</sub>, Si(OH)<sub>4</sub> and Sr versus the GW of type 1. Both GW types display molar Na versus Cl ratios of about 1. Although IS have obviously reacted with the (deteriorated) concrete material, it is surprising that the pH of the IS is only slightly alkaline, ranging from 8.0 to 9.4, while those of GW and DW are close to neutral. Highly discharging DW has a rather similar chemical composition compared with the GW, whereas the DW is enriched in alkalis resulting from concrete-GW interactions. Thus, the molar Na content of DW (and also

*Table 1. Mineralogical composition of damaged concrete material and the amount of water that was extracted by a hydraulic press. Mineral abbreviations are (Dol): dolomite, (Cal): calcite, (Gp): gypsum, (Tha): thaumasite, (Qz): quartz, (Ms): muscovite, (Bas): bassanite, (Arg): aragonite, (Fs): feldspar, (Mb) mirabilite, (Th): thenardite and (Hl): halite. Quantified contents are given in wt. %. The weighted profile R-factors ( $R_{wp}$ ) for Rietveld refinement are ranging between 6 and 9. \*Note that thenardite found in efflorescence is accounted to thermal decomposition of mirabilite induced by the X-ray beam during the measurement. (Ext IS): amount of extracted water after squeezing. (Ava IS): amount of available water after drying at 40 °C. (Ext Eff): extraction efficiency.*

Sample	Dol	Cal	Gp	Tha	Qz	Ms	Bas	Arg	Fsp	Mb	Th	Hl
<b>Highway tunnel</b>												
HW_IS01	28	36	2	33	< 1	-	-	-	-	-	-	-
HW_IS02	50	26	9	15	-	-	-	-	-	-	-	-
HW_IS03	50	20	22	3	1	-	-	4	-	-	< 1	< 1
HW_DW01	27	39	8	26	1	-	-	-	-	-	-	-
HW_Eff	-	-	-	-	-	-	-	-	-	> 95*	< 5*	-
<b>Railroad tunnel</b>												
RR_IS01	46	33	8	5	5	4	-	-	-	-	-	-
RR_IS02	51	18	14	9	4	4	-	-	-	-	-	-
RR_IS03	32	48	7	10	2	< 1	1	-	-	-	-	-
RR_IS04	36	13	21	17	< 1	-	5	8	-	-	-	-
RR_IS05	20	66	3	8	2	< 1	1	-	-	-	-	-
RR_IS06	-	9	-	-	53	1	-	7	30	-	-	-
RR_IS07	29	48	9	8	4	2	1	-	-	-	-	-
RR_Eff	-	-	-	-	-	-	-	-	-	> 95*	< 5*	-

Table 1. Continued

Sample	Ext IS [g]	Ava IS [wt. %]	Ext Eff [%]	Type
<b>Highway tunnel</b>				
HW_IS01	217	29	74	concrete
HW_IS02	136	29	78	concrete
HW_IS03	132	20	61	concrete + shotcrete
HW_DW01	na	na	na	drainage concrete
HW_Eff	na	na	na	efflorescence
<b>Railroad tunnel</b>				
RR_IS01	96	18	54	shotcrete
RR_IS02	120	19	57	shotcrete
RR_IS03	40	14	41	shotcrete
RR_IS04	48	14	36	shotcrete
RR_IS05	32	20	59	shotcrete
RR_IS06	32	18	55	joint filling
RR_IS07	56	20	59	shotcrete
RR_Eff	na	na	na	efflorescence

of IS) typically exceeds that of Cl. Stationary and slowly discharging DW are highly enriched in Na, Cl and  $\text{SO}_4$  which is expressed in up to  $8400 \text{ mg L}^{-1}$  of TDS. The IS are even more enriched in Na, Cl and  $\text{SO}_4$  compared to the DW. With regard to the local GW the IS show an extreme enrichment of especially monovalent cations and anions such as Na, K, Li, Rb, Cl,  $\text{NO}_3$  (Figure 4A). The dissolved components of the IS even yield up to  $62600 \text{ mg L}^{-1}$  of TDS, whereby the concentration of TDS is positively and linearly correlated with the  $\text{SO}_4$  concentration up to about  $30000 \text{ mg L}^{-1}$  (Figure 4B). In contrast, the Ca concentration is limited to about  $600 \text{ mg L}^{-1}$  and most of the solutions are supersaturated with respect to calcite. DW and IS containing  $\approx 600 \text{ mg L}^{-1}$  of Ca are nearly saturated or slightly supersaturated with respect to gypsum. In Figure 4C the relationship between the  $\text{SO}_4$  concentrations and the  $\text{SI}_{\text{Gypsum}}$  values indicates that, once the saturation with respect to gypsum is reached,  $\text{SO}_4$  is no longer exclusively balanced by Ca, but progressively by Na. Ongoing decrease of the Ca concentration by precipitation of calcium carbonate and thaumasite results in an overall Ca depletion versus  $\text{SO}_4$  in the residual solution (see equation (1)). Accordingly, Ca is kept almost constant during ongoing accumulation, whereas sulfate is accumulating until mirabilite saturation is reached as indicated in Figure 4C.

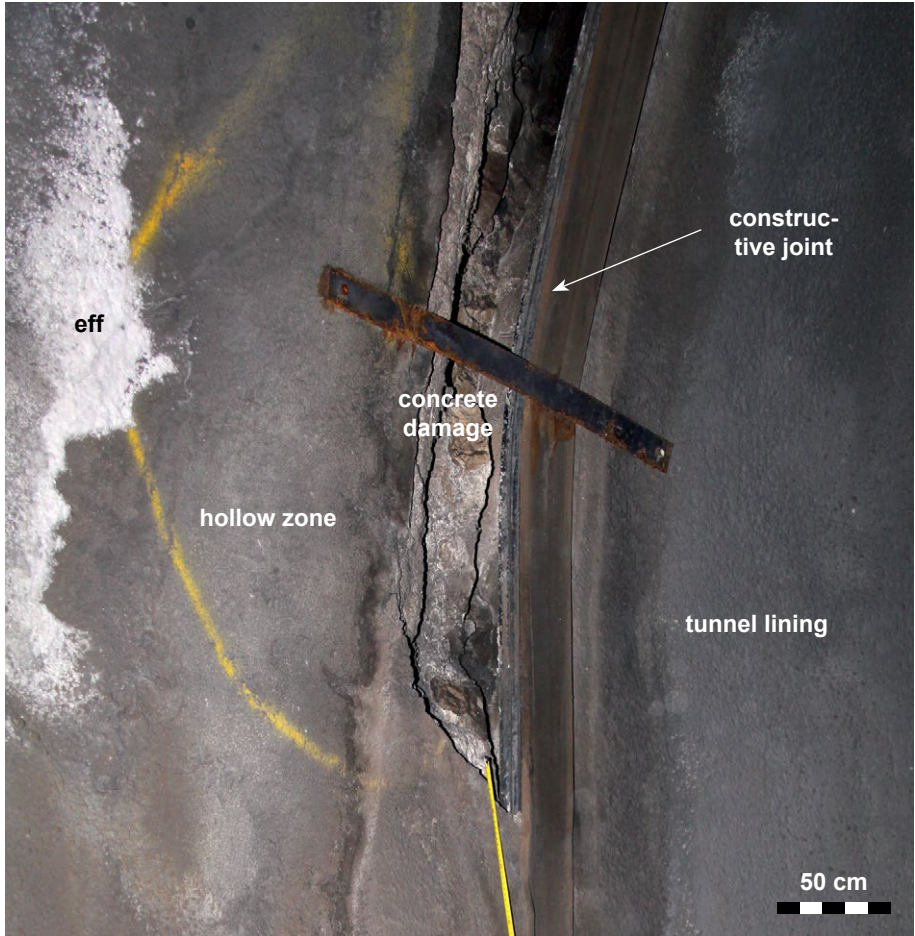


Figure 3. Intensive sulfate attack of the shotcrete from the tunnel lining in the rail-road tunnel. The damaged concrete area is located close to a constructive joint and has been completely disintegrated and broken out. At the hollow zone concrete damage at the border rock-concrete is developing. White efflorescence (eff), identified as mirabilite ( $\text{Na}_2\text{SO}_4 \cdot 10\text{H}_2\text{O}$ ), is located directly at the edge of this area. The concrete material and the expressed interstitial solution from this sample site are corresponding to sample RR\_IS04 in Tables 1, 2 and 3 in the appendix.

## Stable isotopes

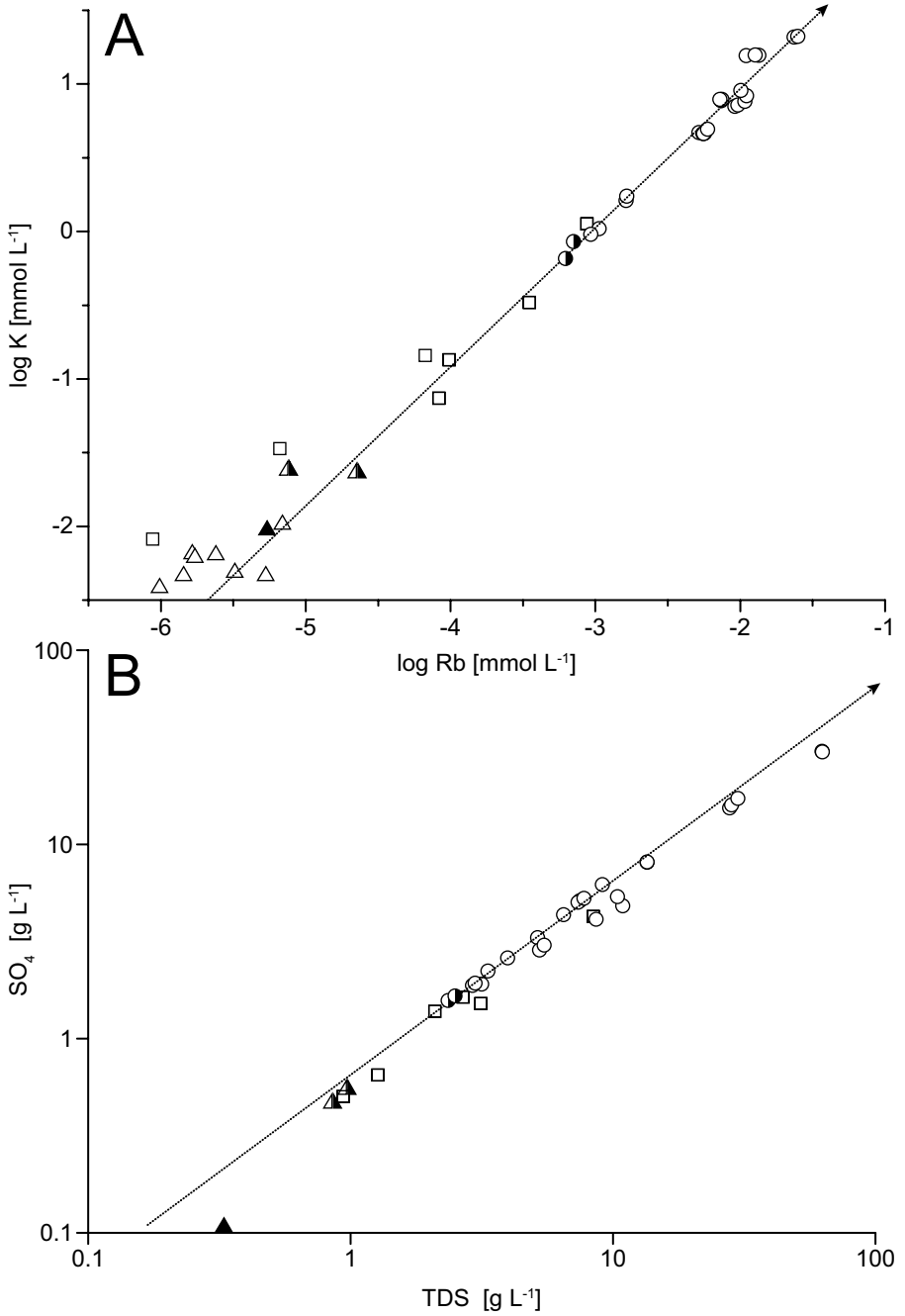
The results of the stable hydrogen and oxygen isotope measurements (see Table 2 and appendix) are given as  $\delta^2\text{H}$  and  $\delta^{18}\text{O}$  values and are shown in Figure 5. This figure indicates that the average precipitation recorded at the ANIP (Austrian Network of Isotopes in Precipitation and Surface Waters [33]) station N-36 Feuerkogel (located about 50 km northwest of the tunnels) as well as the GW and the fast discharging DW have similar isotopic signatures. The average precipitation yields  $\delta^2\text{H}$  and  $\delta^{18}\text{O}$  values of  $-82.8 \pm 22.4$  and  $-11.9 \pm 2.7$  ‰, respectively ( $n = 415$ ), while the average GW and the rapidly discharging DW have  $\delta^2\text{H}$  and  $\delta^{18}\text{O}$  values of  $-83.0 \pm 1.7$  and  $-12.0 \pm 0.2$  ‰, respectively ( $n = 14$ ). The local meteoritic water line (LMWL) was calculated using a regression derived from monthly observed isotope values of local precipitation which was recorded between the 1.01.1973 and 1.09.2011 [34]. Obviously, the GW and the fast discharging DW plot onto the LMWL (see Figure 5). This observation is in contrast to the  $\delta^2\text{H}$  and  $\delta^{18}\text{O}$  values of slowly flowing and stationary DW and those of the IS which show a significant trend to higher isotope values compared to the LMWL. This trend mirrors the typical behavior for evaporation of water and is caused by the isotope fractionation during the liberation of  $\text{H}_2\text{O}$  from the solution into the atmosphere [28]. In order to quantify the proportions of water liberated from the distinct solutions, the evolution of the isotopic compositions through ongoing evaporation was calculated according to the expression

$$F_e = 1 - e^{\frac{(\delta_e - \delta_i)}{\Delta}} \quad (2)$$

(adapted from Kendall and Caldwell [28]), where  $F_e$  is the mole fraction of liberated  $\text{H}_2\text{O}$  ( $0 < F_e < 1$ ).  $\delta_i$  and  $\delta_e$  denote the isotopic compositions of the initial solution and remaining solution throughout evaporation, respectively ( $\delta$  values are given in ‰).  $\Delta$  denotes the overall isotopic fractionation between aqueous and gaseous  $\text{H}_2\text{O}$  during evaporation. At a given temperature the value of  $\Delta$  depends largely on the relative humidity ( $0 < h < 1$ ) according to the equation

$$\Delta = (1 - \alpha_{\text{equ}}) \times 1000 + (1 - h) \times (1 - \alpha_{\text{kin}}) \times 1000 \quad (3)$$

(adapted from Kendall and Caldwell [28]). The individual equilibrium isotope fractionation factors between water and  $\text{H}_2\text{O}$  vapor ( $\alpha_{\text{equ}}$ ) are 1.10065 for  $^2\text{H}/\text{H}$  and 1.01091 for  $^{18}\text{O}/^{16}\text{O}$  at  $8^\circ\text{C}$  [35], whereas the respective kinetic isotope fractionation factors ( $\alpha_{\text{kin}}$ ) are 1.0251 for  $^2\text{H}/\text{H}$  and 1.0285 for  $^{18}\text{O}/^{16}\text{O}$  [28]. Considering the average composition of GW for the  $\delta_i$  value, the evolution of the isotopic values of the remaining water ( $\delta_e$ ) throughout evaporation is calculated for various humidities by using equations (2) and (3). The



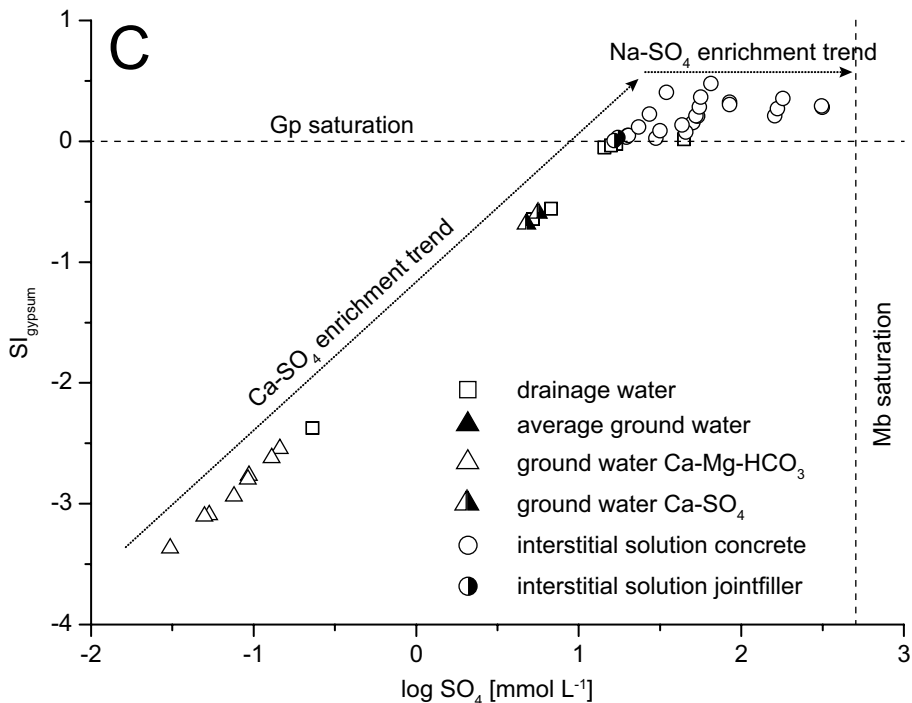


Figure 4. (A) Plotting the concentrations of  $K$  vs.  $Rb$  results in a slope close to 1 suggesting that both elements are incompatible for solid incorporation during evaporation (conservative behavior). Note that  $Rb$  is about 3 orders of magnitude lower in concentration compared to  $K$ . (B) Plot of  $SO_4$  versus TDS yields a linear relationship as dissolved ions are accumulated during evaporation. (C) GW, undersaturated with respect to gypsum (Gp), follows the theoretical Ca-SO<sub>4</sub> trend during evaporation. If saturation with respect to gypsum is reached further evaporation results in a Na-SO<sub>4</sub> type solutions. Ca is preferentially incorporated vs. sulfate in solid precipitates like thaumasite and calcite. Finally saturation with respect to mirabilite is reached if ongoing  $SO_4$  accumulation throughout evaporation occurs. The Mb saturation line was modeled from the evaporation of the solution HW\_IS03 by using PHREEQC.

obtained  $\delta_e$  evolutions are displayed in Figure 5 for relative humidities of 75, 85 and 95 % ( $h = 0.75, 0.85$  and  $0.95$ ) where up to about 40 % of the water is being evaporated ( $F_e = 0.4$ ). Noticeably, the evolution of the  $\delta_e$  values agrees well with the isotopic composition of the IS and DW. On the other way around the slopes of the regression lines for the isotope data derived from the average precipitation ( $\delta^2H = -83.0 \text{ ‰}$  and  $\delta^{18}O = -12.0 \text{ ‰}$ ) through the isotope values of both IS and DW yield an average relative humidity of about



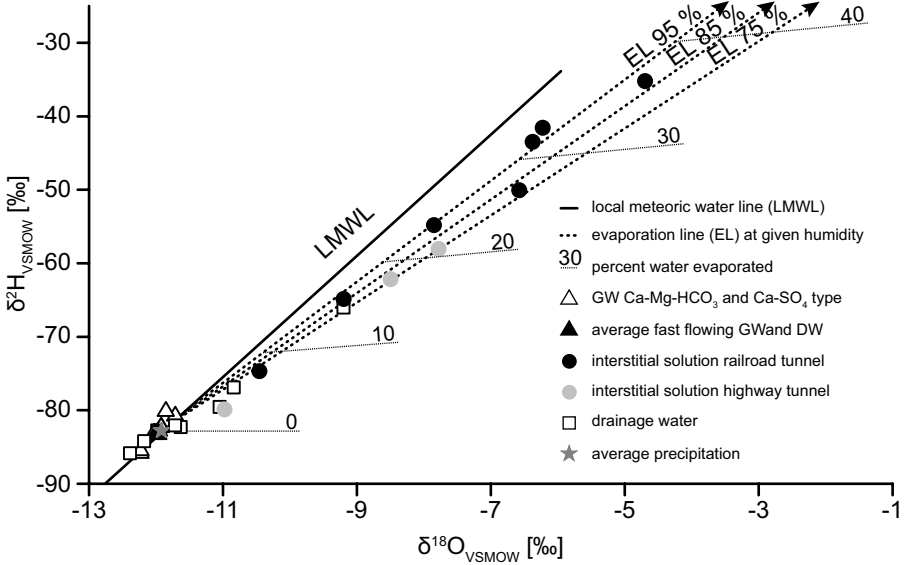


Figure 5.  $\delta^2\text{H}$  versus  $\delta^{18}\text{O}$  values of all aqueous solutions. Extracted IS, stationary and slowly discharging DW display the typical enrichment of heavy isotopes caused by isotope fractionation during the evaporation of water. The current degree of evaporation is calculated according to the equations (2) and (3) at a relative humidity of 85 and 79 % for the RR and HW tunnel, respectively ( $\Omega_e$  values are given in Table 2).

79 and 85 % for the site HW and RR, respectively. As the value of  $h$  is now reasonably defined for both case studies, the current degree of evaporation ( $\Omega_e = F_e \cdot 100$ , in %) for each IS as well as for stationary and slowly discharging DW can be estimated from equation (2) (see Table 2), whereby the values of  $\Omega_e$  reach a maximum current evaporation level of 38 %.

### 3.2.6. Impact of evaporation on solution-concrete interaction

#### Mineral formation and solution chemistry

The optical observations as well as the XRD results of the solids clearly indicate that concrete damage is accounted to intensive thaumasite form of sulfate attack (see Fig-

ures 1 and 2 and Table 1). Surprisingly, no ettringite was found within the damaged concrete which is a rather unusual observation as sulfate attack of concrete is mostly linked to its formation. Nevertheless the lack of ettringite in the studied samples is likely related to its solubility at the present pH values. It is well known from experiments that synthesized ettringite dissolves in the pH range from 9.5 to 10.7 [36]. The pH values of all IS are lower than 9.5 suggesting that ettringite is already dissolved while thaumasite

*Table 2. Isotopic composition and K, Rb and Li concentration of GW, DW and IS.  $\delta^2\text{H}$  and  $\delta^{18}\text{O}$  values of the solutions are given in ‰ (VSMOW) which obviously display an enrichment of the heavy isotopes ( $^2\text{H}$  and  $^{18}\text{O}$ ) of the IS and stationary DW versus the average rainfall (Pre\_Avg) and the average ground water (GW\_Avg). From the isotopic ratios the current degree of evaporation in percent ( $\Omega_c = F_c \cdot 100$ ) was calculated according to equation (2). The total degree of evaporation in percent ( $\Omega_t$ ) and the total amount in liters of water evaporated was estimated by comparing the contents of K, Rb and Li in the evaporated solutions to the elemental content of HW\_DW04. The latter solution is a slowly discharging drainage water with a very low evaporation impact in order to account for the influence from the concrete (see text for discussion). (na): not analyzed.*

Sample	$\delta^{18}\text{O}$ [‰]	$\delta^2\text{H}$ [‰]	$\Omega_c^{18}\text{O}$ [%]	$\Omega_c^2\text{H}$ [%]	K [ $\mu\text{g L}^{-1}$ ]	$\Omega_t\text{K}$ [%]	$\Omega_t\text{K}$ [L]	Rb [ $\mu\text{g L}^{-1}$ ]	$\Omega_t\text{Rb}$ [%]	$\Omega_t\text{Rb}$ [L]	Li [ $\mu\text{g L}^{-1}$ ]	$\Omega_t\text{Li}$ [%]	$\Omega_t\text{Li}$ [L]
<b>Highway tunnel</b>													
HW_DW01	-11.1	-79.5	5.3	3.2	12.9	77.5	3	29.9	76.2	3	53.5	66.3	2
HW_DW02	-9.2	-66.0	15.1	14.8	44.0	93.4	14	74.6	90.5	9	418	95.7	22
HW_DW04	-11.8	-82.1	1.1	0.8	2.9	0.0	0	7.11	0.0	0	18.0	0.0	0
HW_DW06	-10.8	-76.9	6.4	5.6	5.3	45.0	1	8.38	15.1	0.2	26.3	31.4	0.5
HW_IS01	-8.5	-62.1	18.5	17.9	63.4	95.4	21	140	94.9	19	145	87.6	7
HW_IS02	-11.0	-79.9	5.7	2.9	183	98.4	62	441	98.4	61	1062	98.3	58
HW_IS03	-7.8	-58.0	21.9	21.0	813	99.6	279	2127	99.7	298	3326	99.5	184
<b>Railroad tunnel</b>													
RR_IS01	-6.2	-41.5	31.5	32.8	180	98.4	61	507	98.6	70	385	95.3	20
RR_IS02	-7.9	-54.8	23.8	23.6	275	98.9	94	942	99.2	131	273	93.4	14
RR_IS03	-6.4	-43.5	30.8	31.5	611	99.5	210	1144	99.4	160	1434	98.7	79
RR_IS04	-6.6	-50.0	29.9	27.0	301	99.0	103	637	98.9	89	1020	98.2	56
RR_IS05	-10.5	-74.7	9.5	7.6	41.0	92.9	13	90.2	92.1	12	256	93.0	13
RR_IS06	-9.2	-64.8	16.7	16.0	25.8	88.8	8	60.1	88.2	7	38.5	53.2	1
RR_IS07	-4.7	-35.2	38.0	36.7	616	99.5	211	1264	99.4	177	415	95.7	22
Pre_Avg	-11.9	-82.8	-	-	na	-	-	na	-	-	na	-	-
GW_Avg	-12.0	-83.0	0.0	0.0	0.4	-	-	0.46	-	-	1.45	-	-

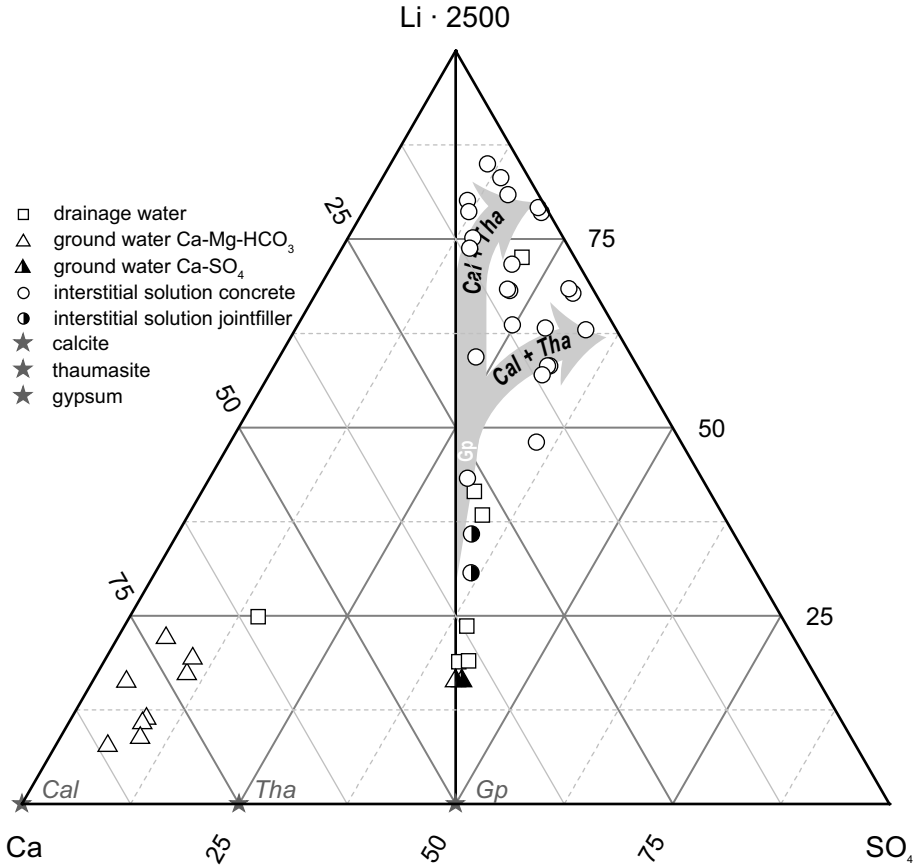


Figure 6. Ternary plot of aqueous solutions in molar ratios of Ca,  $SO_4$  and  $Li \cdot 2500$ . The triplot is displaying that the low mineralized Ca-Mg- $HCO_3$  type GW is not involved in the damage and well separated from the Ca- $SO_4$  type GW. The latter GW are stemming from gypsum dissolution in the local host rocks. In evaporated DW and IS the  $SO_4$  concentration is increasing due to the removal of Ca (e.g. by precipitation of thaumasite and calcite). The enrichment of incompatible elements such as Li is an indicator for the total evaporation degree (see discussion in the text).

is preserved. In the observed mushy damaged concrete material the OH<sup>-</sup> was leached out and/or was replaced by other anions. At the reaction front, however, the pH of the IS might still be elevated due to interactions with non-damaged concrete material leading to ettringite formation which can cause further damage to the microstructure of the concrete [37]. Concerns about the stability of thaumasite get approved by geochemical modeling. All GW and DW are undersaturated with respect to thaumasite, whereas some IS are supersaturated (e.g.  $SI_{\text{Thaumasite}} = 1.3$  for RR\_IS02d, Appendix). Interestingly, the only cementitious sample without thaumasite is the joint filling material (RR\_IS06) indicating that the mortar used more than a hundred of years ago did not contain any silica-based binding material, which is needed for thaumasite formation (see equation (1)).

The origin of secondary sulfates minerals such as thaumasite, gypsum and bassanite in the damaged concrete samples is known to be associated with the dissolution of marine calcium sulfates from the local host rock which can be followed by the Ca-SO<sub>4</sub> rich GW (type 2) [25]. The (trace) element characteristics of type 2 GW and of the IS are exhibiting distinct similarities in contrast to type 1 GW as shown in e.g. Figure 6 or in terms of an elevated Sr content (see appendix). The gypsum content in the damaged concrete may be significantly lower than that of thaumasite, although evaporation of GW with a 1:1 ratio of Ca to SO<sub>4</sub> concentrations should result in a massive formation of gypsum as soon as supersaturation is reached. Due to the fact that this is not the case and the non-flowing DW and IS are (super)saturated with respect to gypsum the presence of thaumasite and gypsum can be explained by the fast dissolution behavior of gypsum [38, 39]. Thus newly precipitated gypsum through ongoing evaporation can be easily re-dissolved at humid events. Moreover the formation and dissolution behavior of gypsum cannot explain the remarkable accumulation of SO<sub>4</sub> vs. Ca in the IS (Figure 4), because for a further increase of the SO<sub>4</sub> concentration related to evaporation, Ca ions have to be preferentially removed from the solution. This is indeed the case if secondary carbonates such as calcite and aragonite (CaCO<sub>3</sub>) are formed, which are present in both tunnels (see Table 1). Similar observations are reported in Hagelia and Sibbick[40], a feature that is referred to “popcorn calcite”. However, calcite is often used as concrete additive and or aggregate and it is impossible to distinguish between calcitic aggregates and secondary calcite solely by XRD. Previously, we have encountered electron microprobe analyses to determine the nature of the calcite mentioned and found that newly formed calcite is usually enriched in Sr in contrast to the calcite aggregates that were used as aggregates [41]. Sr rich GW - stemming from the dissolution of local marine anhydrite and gypsum horizons

- led to the formation of secondary Sr rich calcite (see appendix). The presence of aragonite also suggests a secondary formation of  $\text{CaCO}_3$ , because aragonitic aggregates are scarcely available for concrete production.

The formation of thaumasite additionally depletes Ca vs.  $\text{SO}_4$  at a molar ratio of 3 (see equation (1)), thus the occurrence of thaumasite is considered to be a further indication for sulfate accumulation and a relative depletion of Ca vs.  $\text{SO}_4$  in the IS. In contrast to gypsum and ettringite, the re-dissolution of thaumasite is slow and ineffective at the given conditions and thus thaumasite is preserved. This observation gives evidence of the slow dissolution kinetics of thaumasite as was already postulated by Schmidt et al. [42]. As soon as Ca is largely removed by quantitative incorporation in secondary sulfate and carbonate phases, Na accumulation through evaporation into the residual solution takes place and subsequent mirabilite formation starts at approximately  $50000 \text{ mg L}^{-1}$  of  $\text{SO}_4$ . Massive formation of hydrous and non-hydrous sodium sulfates such as mirabilite and thenardite has additional destructive effects on porous media such as concrete [13, 43, 44].

### Proxies for evaporation, humidity and drying-wetting cycles

Common evaporation indicators such as Na and Cl concentrations are not applicable in the given context as the local geological backgrounds are highly variable in the intercalated sequences of evaporitic rocks. The evidence of sodium sulfate hydrate efflorescences clearly indicates that Na can be removed from the solutions. In contrast, the molar Na vs. Cl ratio can even exceed 1 when Na originates from the concrete. The origin of Na in the concrete is most likely related to Na-containing solidification enhancers which were used for shotcrete fabrication in the present tunnel buildings. During evaporation all elements with a conservative behavior remain in the residual solution and are accumulated at constant element ratios. As was shown above, the K and Rb and Li concentrations can be used as proxies for the total evaporation degree ( $\Omega$ ), whereby especially the correlation between K and Rb concentration was successfully applied to detect evaporation conditions in natural systems [45]. However, in any case it has to be critically evaluated if the individual ions can be used as evaporation indicators or not. For instance, Rinder et al. [46] explicitly used K as an indicator of concrete interaction for high alkaline drainage solutions ( $\text{pH} > 10.5$ ). Keeping in mind that interaction of GW with the concrete will already yield an underlying concentration of K, Rb and Li without any evaporation, it seems realistic to choose a slowly recharging DW (HW\_DW04) as initial solution to model evaporation

as it is already slightly enriched in the elements named above vs. the average GW (see Table 2). All elemental proxies agree well in respect to the obtained  $\Omega_t$  values among themselves in most of the given cases. As is shown in Table 2, the degree of total evaporation derived from the elemental concentrations ( $\Omega_t$ ) is much higher than the current degree of evaporation ( $\Omega_c$ ) computed by the stable isotopes analyses.

The above described behavior of the stable hydrogen and oxygen isotopes of the extracted water can be used as a reliable proof for evaporation of  $H_2O$  that certainly took place in the damaged concrete material of our study. Water expressed from the concrete material typically shows a strong accumulation of the heavy isotopes ( $^2H$  and  $^{18}O$ ) vs. the light isotopes ( $H$  and  $^{16}O$ ) compared to the average local GW (Figure 5). The isotopic data of the IS and DW do not fit the LMWL due to kinetic isotope fractionation during evaporation, but indicate the degree of evaporation in respect to the relic water. However, complete evaporation of water related to drying within a drying-wetting cycle yields the isotope signal to be reset. The isotope proxy for evaporation is then reactivated by new moisturization during the following wetting period. Hence, the isotope signal we receive in our samples is a quasi-snap-shot of the current evaporation degree ( $\Omega_c$ ) in the respective drying-wetting cycle. Consequently, combining both elemental tracers and isotope ratios is suitable to claim proof for drying-wetting cycles. These changeable conditions, however, can trigger highly dynamic processes of dissolution and neof ormation of minerals and is in accordance with the literature to strongly accelerate concrete damage as outlined by e.g. Lothenbach et al. [47].

The relative humidity given in equation (3) by  $h \cdot 100$  in % is defined by the saturation in respect to  $H_2O$  of the atmosphere at the surface of the water. Both, relative humidity and temperature are the major factors controlling evaporation of water [28]. Considering tunnel surroundings, the average temperatures are known from ground water or can be monitored by air temperature measurements if aeration is valid e.g. by passing trains/cars or ventilation (in our case studies  $T = 8 \pm 2$  °C). As the temperature is given, the relative humidity during evaporation can be obtained from isotope data based on the fractionation of hydrogen and oxygen stable isotopes through  $H_2O$  liberation from the solution into the atmosphere according to equations (2) and (3). Note that in contrast to isotope discrimination the relative humidity cannot be followed by elemental accumulations such as Rb during evaporation. Interestingly, the estimated average relative humidity conditions from 75 to 95 % computed on the basis of the stable isotopes (Figure 5) match with the local occurrence and theoretical humidity range for the stability of mirabilite [48].

### 3.2.7 Summary and conclusions

In the present study, the reaction mechanisms and paths of concrete damage through TSA were characterized by combining mineralogical (XRD) and chemical analyses (IC and ICP-MS) of solids and aqueous solutions, hydrochemical modeling (PHREEQC) and stable hydrogen and oxygen isotope signals (WS-CRDS) within a multi proxy approach. The expression of interstitial solutions (IS) from concrete with TSA revealed elevated concentrations of dissolved ions which are highly beyond the guidelines of valid standard specifications (e.g. DIN EN 206-1). IS are (super)saturated with respect to typical concrete-damaging sulfate minerals such as thaumasite and gypsum. Elemental (e.g. K, Rb) and isotopic proxies ( $\delta^2\text{H}$ ,  $\delta^{18}\text{O}$ )

- verify the evaporation of water and
- indicate cyclic events of complete drying and wetting by giving
- the total and the current evaporation degree.

Such highly variable environmental conditions likely contribute to concrete damage at a high level of deterioration. The occurrence of mirabilite is in accordance with the estimated degree of humidity calculated by the  $\delta^2\text{H}$  and  $\delta^{18}\text{O}$  relationships. Accordingly, isotopic ratios of  $^2\text{H}/\text{H}$  and  $^{18}\text{O}/^{16}\text{O}$  are suitable to monitor changes of the relative humidity in underground structures.

In order to sustain concrete performance it is essential to diminish interactions of aqueous solutions such as local ground and drainage water with the concrete and to prevent evaporation of the IS. Low concrete porosities and the usage of low alkali cements and concrete are suitable to reduce capillary action and the potential for highly concentrated Na – SO<sub>4</sub> bearing pore solutions. Constructive joints and cracks should be sealed. In this aspect it is important to note that if evaporation is not prevented, in principal any ground water is capable of exceeding the concentration level of ions such as of SO<sub>4</sub> which is assigned in the valid standard specifications for concrete resistance by chemical attack.

### 3.2.8 Acknowledgements

The authors greatly acknowledge the funding of the present study by NAWI Graz (Graz Advanced School of Science, GASS) and the Österreichische Forschungsförderungsgesellschaft (FFG, 828476). Support by Daniel Höllen concerning sample preparation and elemental analytics as well as the helpful comments by Artur Deditius are highly appreciated.

## 3.3 Are environmental conditions during thaumasite and gypsum formation traced by crystal water?

### 3.3.1 Introduction

The initiative to start studying the isotopic composition of crystal water of minerals from deteriorated concrete and in specific that of thaumasite came up due to a discussion with Per Hagelia [49]. He remarked that evaporation does not necessarily have to be a driving force for thaumasite formation. Alternatively thaumasite formation might be a consequence of concrete being transformed to a mush which is obviously, but subsequently, highly active in respect to evaporation. In order to verify both theories the isotope ratios of the water molecules which are bound as crystal water in secondary hydrous sulfate phases such as thaumasite are investigated. So far crystal water from only one sample was successfully separated and measured in terms of distribution of stable hydrogen and oxygen isotopes.

### 3.3.2 Methodology

For the extraction of water the size fraction of  $< 1$  mm of a deteriorated concrete was sieved out, dried at  $40$  °C until weight was constant and analyzed by XRD. The separation of the crystal water from the dried solid material, which mostly consists of thaumasite, was done by a modified heating-cooling trap setup (Schlenk line). Experimental setup and techniques will be given in detail by [50] and are briefly described in the following: A heating mantle is tempering a glass tube containing the concrete material to about  $250$  °C. Under vacuum the liberated gaseous  $H_2O$  is transferred via glass tubes to a liquid nitrogen cooling trap. After 2 hours the accumulated ice in the cooling trap is carefully melted and stored in a container. Consequently stable isotope ratios of hydrogen and oxygen are measured in accordance to the methodology in section 3.2.3. The glassware with the dehydrated concrete material is stored in an oven at  $200$  °C over night to check weight constancy.



### 3.3.3 Preliminary Results and Outlook

The XRD pattern of the 40°C dried sample indicates thaumasite, gypsum, bassanite, dolomite, calcite and aragonite. The isotopic signal of the trapped crystal water is -60.2 and -2.57 ‰ for  $\delta^2\text{H}$  and  $\delta^{18}\text{O}$ , respectively. Obviously heavy stable isotopes are enriched in the separated crystal water compared to the ground water, but also in respect to the interstitial solutions from the studied area. These values do not plot within the field of evaporation (see Figure 5). Consequently an isotope fractionation between the crystal water and the aqueous solution during the formation of hydrous minerals is reasonably suggested. Since individual fractionation factors are not known for thaumasite and ettringite, in a first simplified approach the respective  $\alpha$ -values for gypsum with 0.985 for  $^2\text{H}$  and 1.0041 for  $^{18}\text{O}$  are used [51-53]. The latter values and the measured isotopic composition of the trapped crystal water results in a "formation solution" with  $\delta^2\text{H} = -45.2$  and  $\delta^{18}\text{O} = -6.7$  ‰. Surprisingly this value seems to be reasonable as extracted interstitial solution measured from two samples in the closest vicinity resembled similar values ( $\delta^2\text{H} = -43.5$ ,  $\delta^{18}\text{O} = -6.4$ , and  $\delta^2\text{H} = -50.0$ ,  $\delta^{18}\text{O} = -6.6$  ‰; Table. 2). By applying equation (2) from section 3.2.4 an average evaporation degree of  $\approx 30$  % can be calculated for the formation of the hydrous sulfates. This condition also seems to be reasonable and further measurements of deteriorated concrete material will be performed to verify this finding. In these aspects better knowledge on the fractionation of stable hydrogen and oxygen isotopes during of the formation of relevant hydrous phases is highly required. Thus self-made standard material of thaumasite, gypsum and ettringite will be implemented in this ongoing study [50]. To evaluate the methodology it is also planned to include an in-situ method similar to the setup described by Sharp et al. [54].

## 3.4 Conclusive Remarks

It was clearly shown in the present study that water evaporation is a driving force for concrete deterioration. From weak spots in the concrete structure e.g. constructive joints and cracks the interaction of interstitial solutions and the atmosphere can be initiated. Both physical and chemical sulfate attack may create ongoing micro structural damage to the concrete which allows further water ingress and consequently evaporation. Schmidt et al. [42] report from their lab experiments that thaumasite formation is preceding by expansion and cracking caused by ettringite formation. It

is suggested that thaumasite formation is facilitated by opening up of the concrete structure caused by ettringite induced cracking. This might certainly be the case, however for field performing concrete additional damaging mechanisms on the microstructure of concrete may be relevant:

- Cracking of concrete linings from rock mass load in tunnel buildings.
- Chloride ions induce steel corrosion which may cause cracking of the concrete structure.
- Thaw-freeze cycles may also cause microstructural damage of the concrete.

As the concrete had been pre-damaged and interstitial solutions were evaporating a critical degree of supersaturation with respect to minerals such as gypsum, ettringite and thaumasite is reached to form these hydrous mineral. Repeating evaporation events (wetting and drying cycles) have to be considered as documented by the (trace) elemental contents of e.g. K, Rb and Li of the interstitial solutions. Up to several hundreds of wetting-drying cycles are suggested from our results. Gaseous H<sub>2</sub>O is liberated into the tunnel atmosphere and the newly formed hydrous minerals are trapping the evaporated solutions in their crystal water. In the case of total loss of water by evaporation the isotopic composition of the water is reset by a subsequent wetting event. In contrast to Ett and Gp, Tha is suggested to remain by such wetting and drying cycles besides Cal and relicts of aggregates.

### 3.5 References

1. Bensted, J., Thaumasite - background and nature in deterioration of cements, mortars and concretes. *Cement and Concrete Composites*, 1999. 21(2): p. 117-121.
2. Mehta, P.K., Mechanism of sulfate attack on portland cement concrete — Another look. *Cement and Concrete Research*, 1983. 13(3): p. 401-406.
3. Stark, D.C., Occurrence of thaumasite in deteriorated concrete. *Cement and Concrete Composites*, 2003. 25(8): p. 1119-1121.
4. Leemann, A. and R. Loser, Analysis of concrete in a vertical ventilation shaft exposed to sulfate-containing groundwater for 45 years. *Cement and Concrete Composites*, 2011. 33(1): p. 74-83.
5. Ma, B.G., X.J. Gao, E.A. Byars, and Q.Z. Zhou, Thaumasite formation in a tunnel of bapaxia dam in Western China. *Cement and Concrete Research*, 2006. 36(4): p. 716-722.

6. Ma, J., Application of shotcrete linings under sulfate attack environments. *Advanced Materials Research*, 2011. 233-235: p. 2061-20672067.
7. Romer, M., L. Holzer, and M. Pfiffner, Swiss tunnel structures: concrete damage by formation of thaumasite. *Cement and Concrete Composites*, 2003. 25(8): p. 1111-1117.
8. Puppala, A.J., S. Saride, D. Dermatas, M. Al-Shamrani, and V. Chikyala, Forensic Investigations to Evaluate Sulfate-Induced Heave Attack on a Tunnel Shotcrete Liner. *Journal of Materials in Civil Engineering*, 2010. 22(9): p. 914-922.
9. Suput, J.S., A. Mladenovic, L. Cernilogar, and V. Olensek, Deterioration of mortar caused by the formation of thaumasite on the limestone cladding of some Slovenian railway tunnels. *Cement and Concrete Composites*, 2003. 25(8): p. 1141-1145.
10. Crammond, N., The occurrence of thaumasite in modern construction - a review. *Cement and Concrete Composites*, 2002. 24(3-4): p. 393-402.
11. Long, G.C., Y.J. Xie, D.H. Deng, and X.K. Li, Deterioration of concrete in railway tunnel suffering from sulfate attack. *Journal of Central South University of Technology*, 2011. 18(3): p. 881-888.
12. Romer, M. and P. Lienemann, Deterioration of shotcrete in the safety gallery of the Gotthard motorway tunnel by salt-containing water. *Chimia*, 1998. 52(5): p. 197-201.
13. John, D.A., St An unusual case of ground water sulphate attack on concrete. *Cement and Concrete Research*, 1982. 12(5): p. 633-639.
14. Hartell, J.A., A.J. Boyd, and C.C. Ferraro, Sulfate Attack on Concrete: Effect of Partial Immersion. *Journal of Materials in Civil Engineering*, 2011. 23(5): p. 572-579.
15. Neville, A., The confused world of sulfate attack on concrete. *Cement and Concrete Research*, 2004. 34(8): p. 1275-1296.
16. Bellmann, F., W. Erfurt, and H.M. Ludwig, Field performance of concrete exposed to sulphate and low pH conditions from natural and industrial sources. *Cement and Concrete Composites*, 2012. 34(1): p. 86-93.
17. Haynes, H., R. O'Neill, M. Neff, and P.K. Mehta, Salt weathering distress on concrete exposed to sodium sulfate environment. *Aci Materials Journal*, 2008. 105(1): p. 35-43.

18. Liu, Z., D. Deng, G.D. Schutter, and Z. Yu, Chemical sulfate attack performance of partially exposed cement and cement + fly ash paste. *Construction and Building Materials*, 2012. 28(1): p. 230-237.
19. Longuet, P., L. Burglen, and A. Zelwer, The liquid phase of hydrated cement. *Revue des matériaux de construction*, 1973. 676: p. 35-41.
20. Barneyback, R.S. and S. Diamond, Expression and analysis of pore fluids from hardened cement pastes and mortars. *Cement and Concrete Research*, 1981. 11(2): p. 279-285.
21. Cyr, M., P. Rivard, F. Labrecque, and A. Daidie, High-pressure device for fluid extraction from porous materials: Application to cement-based materials. *Journal of the American Ceramic Society*, 2008. 91(8): p. 2653-2658.
22. Schmidt, T., B. Lothenbach, M. Romer, K. Scrivener, D. Rentsch, and R. Figi, A thermodynamic and experimental study of the conditions of thaumasite formation. *Cement and Concrete Research*, 2008. 38(3): p. 337-349.
23. Iden, I.K. and P. Hagelia, C, O and S isotopic signatures in concrete which have suffered thaumasite formation and limited thaumasite form of sulfate attack. *Cement and Concrete Composites*, 2003. 25(8): p. 839-846.
24. Pye, K. and N. Schiavon, Cause of Sulfate Attack on Concrete, Render and Stone indicated by Sulfur Isotope Ratios. *Nature*, 1989. 342(6250): p. 663-664.
25. Mittermayr, F., C. Bauer, D. Klammer, M.E. Boettcher, A. Leis, P. Escher, and M. Dietzel, Concrete under sulfate attack: an isotope study on sulfur sources. *Isotopes in Environmental and Health Studies*, 2012. 48(1): p. 105-117.
26. Mittermayr, F., T. Rinder, D. Klammer, A. Leis, and M. Dietzel, A Carbon Isotope Study of Thaumasite and Calcite Sinter Formation in Underground Construction, in 1<sup>st</sup> International Congress on Durability of Concrete, H. Justnes and S. Jacobsen, Editors. 2012, NTNU: Trondheim. p. No. C6-1: 1-14.
27. Gat, J.R., Oxygen and hydrogen isotopes in the hydrologic cycle. *Annual Review of Earth and Planetary Sciences*, 1996. 24: p. 225-262.
28. Kendall, C. and E.A. Caldwell, Fundamentals of Isotope Geochemistry, in *Isotope Tracers in Catchment Hydrology*, C. Kendall and J.J. McDonnell Editors. 1998, Elsevier: Amsterdam. p. 51-86.

29. Parkhurst, D.L. and C.A.J. Apello, User's guide to PHREEQC (V2). U.S. Geol. Sur, 1999. 312.
30. Damidot, D., B. Lothenbach, D. Herfort, and F.P. Glasser, Thermodynamics and cement science. *Cement and Concrete Research*, 2011. 41(7): p. 679-695.
31. Gupta, P., D. Noone, J. Galewsky, C. Sweeney, and B.H. Vaughn, Demonstration of high-precision continuous measurements of water vapor isotopologues in laboratory and remote field deployments using wavelength-scanned cavity ring-down spectroscopy (WS-CRDS) technology. *Rapid Communications in Mass Spectrometry*, 2009. 23(16): p. 2534-2542.
32. Brand, W.A., H. Geilmann, E.R. Crosson, and C.W. Rella, Cavity ring-down spectroscopy versus high-temperature conversion isotope ratio mass spectrometry; a case study on  $\delta^2\text{H}$  and  $\delta^{18}\text{O}$  of pure water samples and alcohol/water mixtures. *Rapid Communications in Mass Spectrometry*, 2009. 23(12): p. 1879-1884.
33. Kralik, M., W. Papesch, and W. Stichler, Austrian Network of Isotopes in Precipitation (ANIP): Quality assurance and climatological phenomenon in one of the oldest and densest networks in the world, in *Intern. Symp. on Isotope Hydrology and Integrated Water Resources Management*. 2003, IAEA: Vienna. p. 146-149.
34. Umweltbundesamt, Austrian Network of Isotopes in Precipitation and Surface Waters (ANIP), WISA Lebensministerium VII/2, Editor. 2012, <http://wisa.lebensministerium.at> (date accessed 12.03.2012): Vienna.
35. Majoube, M.,  $^{18}\text{O}$  and  $^2\text{H}$  fractionation between water and steam. *Journal De Chimie Physique Et De Physico-Chimie Biologique*, 1971. 68(10): p. 1423-1436.
36. Myneni, S.C.B., S.J. Traina, and T.J. Logan, Ettringite solubility and geochemistry of the  $\text{Ca}(\text{OH})_2\text{-Al}_2(\text{SO}_4)_3\text{-H}_2\text{O}$  system at 1 atm pressure and 298 K. *Chemical Geology*, 1998. 148(1-2): p. 1-19.
37. Lorente, S., M.P. Yssorche-Cubaynes, and J. Auger, Sulfate transfer through concrete: Migration and diffusion results. *Cement and Concrete Composites*, 2011. 33(7): p. 735-741.
38. Jeschke, A.A., K. Vosbeck, and W. Dreybrodt, Surface controlled dissolution rates of gypsum in aqueous solutions exhibit nonlinear dissolution kinetics. *Geochimica Et Cosmochimica Acta*, 2001. 65(1): p. 27-34.

39. Liu, S.-T. and G.H. Nancollas, The kinetics of dissolution of calcium sulfate dihydrate. *Journal of Inorganic and Nuclear Chemistry*, 1971. 33(8): p. 2311-2316.
40. Hagelia, P. and R.G. Sibbick, Thaumassite Sulfate Attack, Popcorn Calcite Deposition and acid attack in concrete stored at the "Blindtarmen" test site Oslo, from 1952 to 1982. *Materials Characterization*, 2009. 60(7): p. 686-699.
41. Mittermayr, F., D. Klammer, D. Höllen, S. Köhler, M. Böttcher, A. Leis, and M. Dietzel, Deterioration of Concrete: Application of Stable Isotopes, in *Proceedings of the 10<sup>th</sup> International Congress for Applied Mineralogy (ICAM)*, M.A.T.M. Broekmans, Editor. 2012, Springer Berlin Heidelberg. p. 435-443.
42. Schmidt, T., B. Lothenbach, M. Romer, J. Neuenschwander, and K. Scrivener, Physical and microstructural aspects of sulfate attack on ordinary and limestone blended Portland cements. *Cement and Concrete Research*, 2009. 39(12): p. 1111-1121.
43. Scherer, G.W., Stress from crystallization of salt. *Cement and Concrete Research*, 2004. 34(9): p. 1613-1624.
44. Thaulow, N. and S. Sahu, Mechanism of concrete deterioration due to salt crystallization. *Materials Characterization*, 2004. 53(2-4): p. 123-127.
45. Schijf, J., Alkali elements (Na, K, Rb) and alkaline earth elements (Mg, Ca, Sr, Ba) in the anoxic brine of orca basin, northern gulf of Mexico. *Chemical Geology*, 2007. 243(3-4): p. 255-274.
46. Rinder, T., A. Leis, and M. Dietzel, Calcium Carbonate Scaling under Alkaline Conditions - Case Studies and Hydrochemical Modelling. *Applied Geochemistry*, submitted.
47. Lothenbach, B., B. Bary, P. Le Bescop, T. Schmidt, and N. Leterrier, Sulfate ingress in Portland cement. *Cement and Concrete Research*, 2010. 40(8): p. 1211-1225.
48. Steiger, M. and S. Asmussen, Crystallization of sodium sulfate phases in porous materials: The phase diagram  $\text{Na}_2\text{SO}_4\text{-H}_2\text{O}$  and the generation of stress. *Geochimica et Cosmochimica Acta*, 2008. 72(17): p. 4291-4306.
49. Hagelia, P. pers. comm.
50. Thaller, D., Information stored in crystal water of thaumasite. in prep., Graz University of Technology: Graz.
51. Hoefs, J., *Stable Isotope Geochemistry*. 6<sup>th</sup> ed. 2008, Berlin: Springer. 288.

52. Horita, J., Stable isotope fractionation factors of water in hydrated saline mineral-brine systems. *Earth and Planetary Science Letters*, 1989. 95(1–2): p. 173-179.
53. Sofer, Z., Isotopic composition of hydration water in gypsum. *Geochimica et Cosmochimica Acta*, 1978. 42(8): p. 1141-1149.
54. Sharp, Z.D., V. Atudorei, and T. Durakiewicz, A rapid method for determination of hydrogen and oxygen isotope ratios from water and hydrous minerals. *Chemical Geology*, 2001. 178(1–4): p. 197-210.

### 3.6 Appendix

*Table 3. Chemical composition of aqueous solutions from the distinct sampling sites. (TDS): Total dissolved solids; (na): not analyzed; (bld): below detection limit; (DIC): dissolved inorganic carbon; (SI): saturation indices. The average ground water (GW\_Avg; n=10) was calculated from all ground water samples. Note that for the average isotopic value of GW\_Avg the fast discharging drainage water samples are included (n=14). Ion charge balance errors are mostly  $\leq 3\%$ .*

Sample	pH	T	Na	K	Mg	Ca	Cl	NO <sub>3</sub>	SO <sub>4</sub>	DIC	TDS	Type
		[°C]	[mg L <sup>-1</sup> ]	[mg L <sup>-1</sup> ]	[mg L <sup>-1</sup> ]	[mg L <sup>-1</sup> ]	[mg L <sup>-1</sup> ]	[mg L <sup>-1</sup> ]	[mg L <sup>-1</sup> ]	[mmol L <sup>-1</sup> ]	[mg L <sup>-1</sup> ]	
<b>Highway tunnel</b>												
HW_DW01	7.72	11.2	50.6	12.9	110	558	31.5	1.2	1638	4.62	2684	non-flowing
HW_DW02	7.94	10.9	1328	44.0	604	502	1578	3.5	4256	1.44	8403	non-flowing
HW_DW03	8.18	10.3	48.6	5.6	57.8	234	60.7	1.3	650	3.51	1272	fast flowing
HW_DW04	8.10	11.7	11.4	2.9	42.5	534	8.1	0.1	1380	1.84	2092	slow-flowing
HW_DW05	na	na	na	na	na	na	na	na	na	na	na	fast flowing
HW_DW06	7.30	10.4	340	5.3	42.0	592	516	0.6	1516	1.98	3133	non-flowing
HW_GW01	8.35	6.7	0.4	0.4	7.6	25.0	0.4	3.3	2.9	1.83	152	CaMgHCO <sub>3</sub>
HW_GW02	8.31	6.9	0.2	0.3	7.9	27.6	0.3	2.3	5.1	1.94	162	CaMgHCO <sub>3</sub>
HW_GW03	8.30	6.8	0.2	0.2	8.9	27.9	0.4	1.8	7.3	1.92	164	CaMgHCO <sub>3</sub>
HW_GW04	8.32	6.5	0.2	0.2	7.1	28.4	0.3	2.0	4.8	1.89	158	CaMgHCO <sub>3</sub>
HW_IS01a	9.20	8.0	213	63.4	52.5	635	186	50.2	1914	0.61	3151	concrete
HW_IS01b	9.40	8.0	161	67.7	51.7	1262	171	68.2	3322	0.74	5149	concrete
HW_IS02	8.81	8.0	2438	183	268	700	2372	18.4	4831	1.14	10879	concrete
HW_IS03a	8.58	8.0	17153	813	1812	561	11386	288	30175	5.24	62508	concrete +
HW_IS03b	8.84	8.0	17314	823	1811	582	11582	287	29902	5.24	62621	shotcrete

Table 3. Continued

Sample	pH	T	Na	K	Mg	Ca	Cl	NO <sub>3</sub>	SO <sub>4</sub>	DIC	TDS	Type
		[°C]	[mg L <sup>-1</sup> ]	[mg L <sup>-1</sup> ]	[mg L <sup>-1</sup> ]	[mg L <sup>-1</sup> ]	[mg L <sup>-1</sup> ]	[mg L <sup>-1</sup> ]	[mg L <sup>-1</sup> ]	[mmol L <sup>-1</sup> ]	[mg L <sup>-1</sup> ]	
<b>Railroad tunnel</b>												
RR_DW01	8.34	6.3	6.7	0.3	10.0	37.6	7.4	3.0	22.1	2.28	226	fast flowing
RR_DW02	7.78	7.7	9.5	1.3	35.5	206	12.9	1.5	502	2.74	935	fast flowing
RR_GW01	7.67	8.8	4.0	0.9	34.2	219	5.9	blid	545	2.75	977	CaSO <sub>4</sub>
RR_GW02	8.32	8.5	0.8	0.3	10.6	40.2	1.0	3.7	13.9	2.46	221	CaMgHCO <sub>3</sub>
RR_GW03	8.17	7.7	0.4	0.2	9.4	35.5	0.7	3.3	9.0	2.23	195	CaMgHCO <sub>3</sub>
RR_GW04	7.54	7.8	3.5	0.9	31.6	193	3.8	1.9	464	2.65	861	CaSO <sub>4</sub>
RR_GW05	7.81	6.8	0.4	0.2	9.4	32.6	0.4	3.2	8.9	2.27	194	CaMgHCO <sub>3</sub>
RR_GW06	8.15	6.3	0.6	0.2	10.1	36.5	0.8	4.0	12.4	2.33	207	CaMgHCO <sub>3</sub>
RR_IS01a	8.49	8.0	74.0	180	47.6	597	20.2	14.6	1880	1.52	2906	shotcrete
RR_IS01b	8.49	8.0	74.3	181	51.4	612	21.4	16.0	1934	1.46	2980	shotcrete
RR_IS01c	8.52	8.0	74.4	180	59.6	680	25.1	14.3	2231	1.11	3333	shotcrete
RR_IS01d	8.52	8.0	83.2	193	78.4	857	54.4	21.0	2613	0.95	3958	shotcrete
RR_IS02a	8.93	8.0	688	275	498	684	39.0	50.8	5151	1.44	7474	shotcrete
RR_IS02b	8.94	8.0	674	281	482	692	38.5	50.0	5040	1.44	7344	shotcrete
RR_IS02c	8.79	8.0	707	298	451	809	39.4	50.8	5292	1.46	7737	shotcrete
RR_IS02d	8.79	8.0	748	325	400	1228	40.2	42.8	6230	1.32	9095	shotcrete
RR_IS02e	8.79	8.0	790	354	319	510	40.2	35.9	4357	0.87	6459	shotcrete
RR_IS03a	8.62	8.0	2425	611	467	819	722	143	8120	2.79	13478	shotcrete
RR_IS03b	8.73	8.0	2441	609	465	780	722	148	8124	2.81	13461	shotcrete
RR_IS04a	8.62	8.0	7299	301	868	560	3095	70.5	15371	3.07	27753	shotcrete
RR_IS04b	8.79	8.0	7239	307	942	636	2930	69.8	15953	3.08	28265	shotcrete
RR_IS04c	8.76	8.0	7367	307	1097	757	2832	67.6	17250	3.28	29877	shotcrete
RR_IS05a	8.61	8.0	1089	41.0	44.4	524	573	5.5	2861	1.71	5242	shotcrete
RR_IS05b	8.31	8.0	1086	37.5	43.0	597	579	5.6	3031	1.25	5456	shotcrete
RR_IS06a	8.14	8.0	31.6	25.8	29.4	596	7.1	16.0	1578	1.08	2350	joint filling
RR_IS06b	7.97	8.0	36.1	33.6	35.7	622	11.7	17.8	1666	1.16	2494	joint filling
RR_IS07a	8.03	8.0	1590	616	91.7	641	982	464	4128	1.70	8615	shotcrete
RR_IS07b	8.20	8.0	1700	676	106	1019	957	451	5390	1.54	10393	shotcrete
Pre_Avg	na	na	na	na	na	na	na	na	na	na	na	rainfall
GW_Avg	8.09	7.3	1.1	0.4	13.7	67	1.4	2.8	107	2.23	329	



Table 3. Continued

Sample	Li	Si	Rb	Sr	$\delta^{18}\text{O}$	$\delta^2\text{H}$	$\text{SI}_{\text{CaI}}$	$\text{SI}_{\text{Cp}}$	$\text{SI}_{\text{Tha}}$	$\text{SI}_{\text{Mb}}$
	[ $\mu\text{g L}^{-1}$ ]	[ $\mu\text{g L}^{-1}$ ]	[ $\mu\text{g L}^{-1}$ ]	[ $\mu\text{g L}^{-1}$ ]	[‰]	[‰]				
<b>Highway tunnel</b>										
HW_DW01	53.5	4945	29.9	8542	-11.1	-79.5	1.1	0.0	-5.7	-6.0
HW_DW02	418	2497	74.6	9426	-9.2	-66.0	0.6	0.0	-6.8	-3.0
HW_DW03	24.8	3343	5.72	3625	-11.6	-82.3	1.2	-0.6	-5.7	-6.2
HW_DW04	18.0	3036	7.11	6043	-11.8	-82.1	1.1	-0.1	-4.6	-7.4
HW_DW05	na	na	na	na	-12.0	-82.7	-	-	-	-
HW_DW06	26.3	1106	8.38	9443	-10.8	-76.9	0.3	0.0	-10.2	-4.4
HW_GW01	0.35	538	0.59	37.3	-12.0	-83.1	0.4	-3.4	-15.8	-12.2
HW_GW02	0.58	644	0.14	29.8	-11.9	-82.3	0.4	-3.1	-15.1	-12.6
HW_GW03	0.27	753	0.45	57.6	-12.2	-85.8	0.4	-2.9	-14.7	-12.4
HW_GW04	0.18	236	0.12	24.4	-11.7	-80.8	0.5	-3.1	-15.9	-12.6
HW_IS01a	145	4647	139	7640	-8.5	-62.1	1.5	0.1	0.7	-4.5
HW_IS01b	140	na	140	7304	na	na	1.8	0.4	-	-4.7
HW_IS02	1062	9695	441	13980	-11.0	-79.9	1.3	0.2	-0.5	-2.3
HW_IS03a	3326	na	2001	18177	-7.8	-58.0	1.4	0.3	-	-0.4
HW_IS03b	3443	13470	2127	20455	na	na	1.7	0.3	0.4	-0.3
<b>Railroad tunnel</b>										
RR_DW01	1.07	784	0.07	110	-12.2	-84.2	0.6	-2.4	-12.8	-8.9
RR_DW02	6.70	2335	0.57	2510	-12.4	-85.9	0.7	-0.6	-9.2	-7.6
RR_GW01	6.00	2141	1.96	2613	-12.0	-83.3	0.6	-0.6	-9.6	-8.3
RR_GW02	0.66	579	0.21	85.2	-12.0	-83.2	0.7	-2.5	-13.0	-11.1
RR_GW03	0.33	401	0.08	53.5	-12.2	-85.5	0.5	-2.8	-15.0	-11.8
RR_GW04	5.21	2067	0.66	2296	-12.0	-82.8	0.4	-0.7	-10.9	-8.5
RR_GW05	0.24	432	0.28	69.0	-11.9	-80.2	0.0	-2.8	-17.5	-11.7
RR_GW06	0.69	650	0.15	64.4	-11.9	-82.3	0.5	-2.6	-14.6	-11.2
RR_IS01a	385	25300	470	11994	-6.2	-41.5	1.4	0.1	-0.9	-5.4
RR_IS01b	362	24410	483	11060	na	na	1.3	0.1	-1.0	-5.4
RR_IS01c	337	26800	476	12210	na	na	1.3	0.1	-0.7	-5.4
RR_IS01d	379	25960	507	14870	na	na	1.3	0.3	-0.4	-5.3
RR_IS02a	273	5637	781	7656	-7.9	-54.8	1.5	0.2	0.0	-3.3
RR_IS02b	270	6875	821	8065	na	na	1.5	0.2	0.2	-3.3
RR_IS02c	277	11150	914	10527	na	na	1.5	0.3	0.3	-3.3
RR_IS02d	245	13690	942	9601	na	na	1.6	0.5	1.3	-3.2
RR_IS02e	278	5684	860	10978	na	na	1.1	0.1	-1.9	-3.2
RR_IS03a	1434	14400	1144	14760	-6.4	-43.5	1.6	0.4	-0.1	-2.1

Table 3. Continued

Sample	Li	Si	Rb	Sr	$\delta^{18}\text{O}$	$\delta^2\text{H}$	SI <sub>Cal</sub>	SI <sub>Cp</sub>	SI <sub>Tha</sub>	SI <sub>Mb</sub>
	[ $\mu\text{g L}^{-1}$ ]	[ $\mu\text{g L}^{-1}$ ]	[ $\mu\text{g L}^{-1}$ ]	[ $\mu\text{g L}^{-1}$ ]	[‰]	[‰]				
RR_IS03b	1221	10930	935	6465	na	na	1.6	0.3	0.2	-2.1
RR_IS04a	1020	5099	628	3818	-6.6	-50.0	1.3	0.2	-2.2	-1.1
RR_IS04b	1096	5340	637	4799	na	na	1.5	0.3	-0.9	-1.1
RR_IS04c	939	8448	616	4209	na	na	1.6	0.4	-0.2	-1.1
RR_IS05a	256	23200	90.2	7469	-10.5	-74.7	1.4	0.1	-0.8	-3.0
RR_IS05b	226	27770	79.4	7505	na	na	1.0	0.1	-2.3	-3.0
RR_IS06a	38.5	2092	53.0	4804	-9.2	-64.8	0.9	0.0	-5.4	-6.2
RR_IS06b	51.1	1750	60.1	5355	na	na	0.8	0.1	-6.4	-6.1
RR_IS07a	415	34820	1083	2190	-4.7	-35.2	0.8	0.2	-3.5	-2.7
RR_IS07b	490	34950	1264	3134	na	na	1.1	0.4	-1.5	-2.5
Pre_Avg	na	na	na	na	-11.9	-82.8	-	-	-	-
GW_Avg	1.45	844	0.46	533	-12.0	-83.0	-	-	-	-

## CHAPTER 4

# The Sources of Carbon for Thaumasite

### 4.1 Introduction

This chapter raises the question “Where does the carbon in thaumasite come from?” This topic is not unambiguously resolved and still debated for several decades. Three primary sources that are frequently suggested as carbon (carbonate) source for thaumasite are

- dissolved inorganic carbon (DIC) of interstitial solution gained from ground water,
- absorption of atmospheric  $\text{CO}_2$  at alkaline conditions and
- carbon from aggregates such as limestones or dolostones.

It is quite obvious from many experimental studies that adding limestone filler to the cement has a negative effect concerning TSA [1]. This is believed to be related to the formation of the AFm phase calcium aluminate monocarbonate hydrate ( $\text{C}_3\text{A}\cdot\text{CaCO}_3\cdot 11\text{H}_2\text{O}$ ) or changes in the capillary porosity when limestone filler is used to replace cement clinker [2-5]. However the detailed reaction mechanisms and causes for thaumasite formation involving carbonate fillers or aggregates are not known. It is also shown in the present study that dolomite aggregates can be affected by sulfate attack and might have an impact on thaumasite formation (see Chapter 5). A method that is capable of bringing more clarity in this hotly debated topic is the application of stable carbon isotopes. Iden and Hagelia [6] and French [7] have successfully introduced this technique to investigate thaumasite in deteriorated concrete. In the following section we present the first systematic study on carbon isotope ratios ( $^{13}\text{C}/^{12}\text{C}$ ) performed on thaumasite that has damaged concrete field structures. In our field study the isotopic composition indicates that carbon is getting infiltrated as DIC of the local ground water for thaumasite formation. Further aspects of thaumasite formation and promising future projects are given in section 4.3.

## 4.2 A Carbon Isotope Study of Thaumasite and Calcite Sinter Formation in Underground Constructions

Florian Mittermayr<sup>1</sup>, Thomas Rinder<sup>1</sup>, Dietmar Klammer<sup>1</sup>, Albrecht Leis<sup>2</sup>, and Martin Dietzel<sup>1</sup>

<sup>1</sup>*Institute of Applied Geosciences, Graz University of Technology, Graz, Austria*

<sup>2</sup>*RESOURCES – Institute for Water, Energy and Sustainability, Joanneum Research, Graz, Austria*

### 4.2.1 Abstract

Secondary formation of sulfate and carbonate minerals (e.g. thaumasite, ettringite, gypsum, and calcite) may cause serious problems concerning the durability of concrete and the overall lifespan of man-made constructions. Thereby high costs for servicing and renovation are incurring. A key to understand the reactions involving deterioration of concrete constructions is to decipher the causes for its appearance by identifying the individual sources. The occurrence of sulfate attack on concrete and drainage clogging is well known and documented from field and laboratory studies. However reactions that lead to the formation of secondary minerals as well as the origin of the involved ions such as carbonate ( $\text{CO}_3$ ) and sulfate ( $\text{SO}_4$ ) are poorly understood and still hotly debated. In the presented study we highlight the application of stable carbon isotopes ( $^{13}\text{C}/^{12}\text{C}$ ) to get further insights about potential sources for carbonate minerals. The study comprises results from calcite sinters ( $\text{CaCO}_3$ ) which cause drainage clogging and from concrete that suffered severe sulfate attack leading to the formation of thaumasite ( $\text{Ca}_3\text{Si}(\text{OH})_6(\text{CO}_3)(\text{SO}_4)\cdot 12\text{H}_2\text{O}$ ). Carbon for  $\text{CaCO}_3$  sinter formation is either originating from the absorption of atmospheric  $\text{CO}_2$  into high alkaline drainage solutions or stemming from dissolved inorganic carbon (DIC) mainly present as bicarbonate ( $\text{HCO}_3$ ) in the ground water. This results in typical  $\delta^{13}\text{C}$  values (VPDB) of  $-25\text{‰} \pm 3$  and  $-11\text{‰} \pm 3$ , respectively. Isotope data from 3 tunnel case studies indicate DIC of the local ground water to be the main source of  $\text{CO}_3$  for thaumasite formation with  $\delta^{13}\text{C}$  values of about  $-8\text{‰}$ . In contrary to calcite sinter formation no clear evidence for absorption of atmospheric  $\text{CO}_2$  is found and the dissolution of carbonate fillers/aggregates could not be verified as the proper  $\text{CO}_3$  source for thaumasite formation.

## 4.2.2 Introduction

Concrete has become the most important building material resulting in a fast increasing cement production. In 2006 the cement production was about 2.5 Gt and almost double of this amount is predicted for 2050 [8]. As this trend is continuing less space will be available e.g. in agglomerations leading to taller buildings. The increasing demand will also shift more and more construction into the underground. Furthermore traffic routes are subject for future optimization of infrastructures especially in regions difficult to pass and with little space available like in mountainous areas. Thus traffic routes for rail road and highways are also built in the underground. For instance many trans-alpine projects are in construction and some are close to finishing. Prior to these mega underground projects long lasting intensive planning is needed to meet the requirements of subsurface conditions and to assure the intended lifespan.

A crucial aspect for the initiative of the present study is how to deal with undesired and negative effects concerning the interaction of concrete used in underground construction with the adjacent natural environment. This comprises chemical interaction in the system concrete – ground water – underground atmosphere which leads to leaching of certain

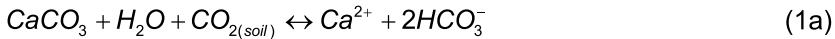


Figure 1. Calcite sinter formation in a drainage tube.

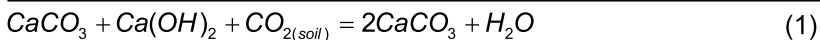
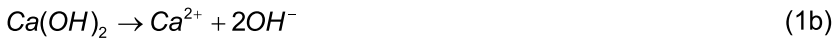
elements and precipitation elsewhere such as in drainage systems (Figure 1). Thus it is highly challenging to understand the processes that cause potential problems. Promising studies on this task are investigations on existing underground buildings where chemical interaction provokes serious alterations of concrete itself or performance limitations of the whole construction. An advanced approach to gain further knowledge on how certain elements react under the apparent conditions is the application of stable isotopes, which was pointed out in several former studies [9-16]. In the present study we focus on the use of stable carbon isotopes which already have a wide field of applications in the aspect of environmental, biological and geological tasks [17-20].

### CaCO<sub>3</sub> sinter formation in drainage systems

Calcium carbonate scaling in tunnel drainage systems may be caused by different reaction mechanisms. In a first approach calcium and bicarbonate from ground water has to be considered as a potential source for CaCO<sub>3</sub> formation. Following the overall reaction

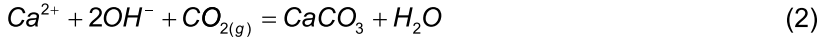


Limestone within the catchment area of ground water (GW) is dissolved which is stimulated by the uptake of CO<sub>2</sub> from soil horizons. Ongoing limestone dissolution results in Ca and HCO<sub>3</sub> rich ground water. Subsequently dissolved Ca and HCO<sub>3</sub> may precipitate causing scaling in drainage systems by CaCO<sub>3</sub> precipitates when entering the tunnel atmosphere [21-25]. This can be induced by CO<sub>2</sub> degassing from the solution which results in an increase of pH and a redistribution of dissolved inorganic carbon (DIC). As a critical supersaturation with respect to CaI is reached, precipitation of calcite is triggered comparable to natural speleothem formation in karst systems. Moreover, the reaction of GW with shotcrete of the tunnel wall has to be considered as a crucial mechanism for CaCO<sub>3</sub> formation. Dissolution of the highly soluble mineral portlandite (equation 1b) from the shotcrete results in alkaline solutions with elevated CO<sub>3</sub> / DIC ratios (equation 1c) and consequently calcite can be precipitated in the drainage system (equation 1d).



In this case the carbonate ion for the formation of calcite according to the overall

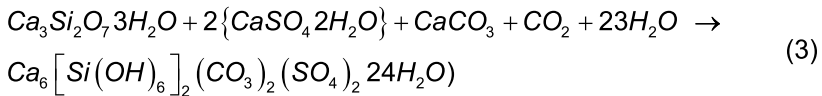
reaction (1) is gained from the ground water as a mixture of soil  $\text{CO}_2$  and carbonate from the dissolved limestone. A third mechanism for  $\text{CaCO}_3$  formation in drainage solutions is valid for high alkaline solutions with low internal  $\text{CO}_2$  partial pressures, where absorption of atmospheric  $\text{CO}_2$  occurs. According to the overall reaction



the absorbed  $\text{CO}_2$  reacts with  $\text{OH}^-$  to form  $\text{HCO}_3^-$  which is mostly converted to  $\text{CO}_3$  in strong alkaline solutions. If Ca ions are present from dissolution of e.g. primary limestone or portlandite from the concrete,  $\text{CaCO}_3$  can precipitate. Such precipitates contain carbon from atmospheric  $\text{CO}_2$ .

### Sulfate attack and thaumasite formation

A well-known “concrete disease” is accounted to sulfate attack and the formation of thaumasite according to the overall reaction



besides that of ettringite and gypsum [26, 27]. Neoformation of such minerals in concretes is accompanied with softening, cracking and in extreme cases with a complete loss of stability and failure of the concrete construction [28, 29]. The sulfate for mineral formation can be gained from internal and external sources stemming from the cement, aggregates, additives, atmosphere or ground water generated from catchment areas with sulfate and sulfide bearing host rocks and soils [30-33]. For the identification of individual sources the application of stable sulfur isotopes has revealed confirming results [6, 34, 35]. However the origin of the carbonate ( $\text{CO}_3$ ) in thaumasite is still debated by absorption of atmospheric  $\text{CO}_2$ , DIC of the ground water, carbonate from aggregates and cement fillers [36-38]. For instance Bensted [39] suggests both calcite and atmospheric  $\text{CO}_2$  as carbonate source for thaumasite formation in accordance to equations (3).

### 4.2.3 Case Studies

Sampling of solids comprises drainage sinter, deteriorated shotcrete and concrete from the tunnel linings as well as local host rocks. Aqueous solutions were collected

from drainage water (DW), ground water (GW) and drip water (DrW). Compositions of typical solids and aqueous solutions from the case studies are given in Tables 1 and 2, respectively (see appendix). For drainage sinter formation 5 solids were collected from the drainage system of an Austrian tunnel. Additionally 4 speleothem-like sinters from the concrete wall were sampled. Moreover, 6 solutions from the drainage system have been taken, as well as one ground water sample and a drip water from a speleothem, formed on the shotcrete lining. Sampling of damaged concrete was conducted at 3 Austrian railroad and highway tunnels running through the eastern Alps, where it is possible to investigate concrete that has suffered intensive deterioration due to sulfate attack in distinct areas (Figure 2).

#### 4.2.4 Materials and Methods

Solid samples were dried at 40 °C and grounded for phase identification by X-ray powder diffraction (XRD). XRD patterns were recorded with a PANalytical X'Pert PRO diffractometer with an X'Celerator detector (CoK $\alpha$  radiation, 45 kV and 40



Figure 2. Concrete heavily damaged by thaumasite form of sulfate attack (TSA).



mA). Secondary electron images (SEI) were obtained using a Zeiss DSM 982 Gemini scanning electron microscope (SEM) and in situ chemical analyses were acquired by electron microprobe analyzer (EPMA) Jeol JXA-8200 at 10 kV and 5 nA with wavelength dispersive X-ray spectroscopy measurements (WDX). In order to remove aggregates or consolidated concrete from damaged concrete material, samples were treated by ultrasonic and sedimentation techniques to increase the content of thaumasite for carbon isotope analyses in analogy to [34]. During sampling of aqueous solutions in the field temperature and pH of ground and drainage waters were measured. Potentiometric titration was used to determine the alkalinity with 0.005 M HCl. Concentrations of major dissolved cations and anions (Na, K, Mg, Ca, Cl, NO<sub>3</sub> and SO<sub>4</sub>) were quantified by ion chromatography with a Dionex ICS-3000. The computer code PHREEQC (Version 2.17.01) was used to calculate the saturation indices with respect to calcite and gypsum as well as internal CO<sub>2</sub> partial pressures (P<sub>CO<sub>2</sub></sub>) and DIC speciations [40]. Ion charge balance was checked by deviations from electric charge neutrality being generally < ±3 %.

Results from stable carbon isotope measurements (<sup>13</sup>C/<sup>12</sup>C) are given in the δ-notation as δ<sup>13</sup>C<sub>VPDB</sub> values in ‰ relative to the Vienna Pee Dee Belemnite standard. Isotopic compositions of DIC and solid carbonates were analyzed using a fully automated peripheral continuous-flow gas preparation device (Gasbench II), which was connected to a Finnigan DELTA<sup>plus</sup> XP Mass Spectrometer. The analytical setup is comparable to previous studies and reproducibility of measurements is better than ±0.03 ‰ [41].

## 4.2.5 Results and Discussion

### CaCO<sub>3</sub> sinter formation in drainage systems

XRD pattern and SEM images of drainage sinters indicate almost pure calcite with small quantities of detritus like quartz or mica. On the macroscopic scale sinters mostly precipitate as white dense or brownish-white layered hard crusts. Figure 3 images a typical sinter under the SEM. Besides hard crusts speleothem-like tubes hanging from the concrete linings or soft mushy or sometimes egg-shaped accumulations can be found in the studied tunnel. In principle, the macroscopic sinter shape and microscopic crystal shape is related to the solution properties [42].

Solution KAT\_8-GW resembles the chemical composition of local ground water with Na

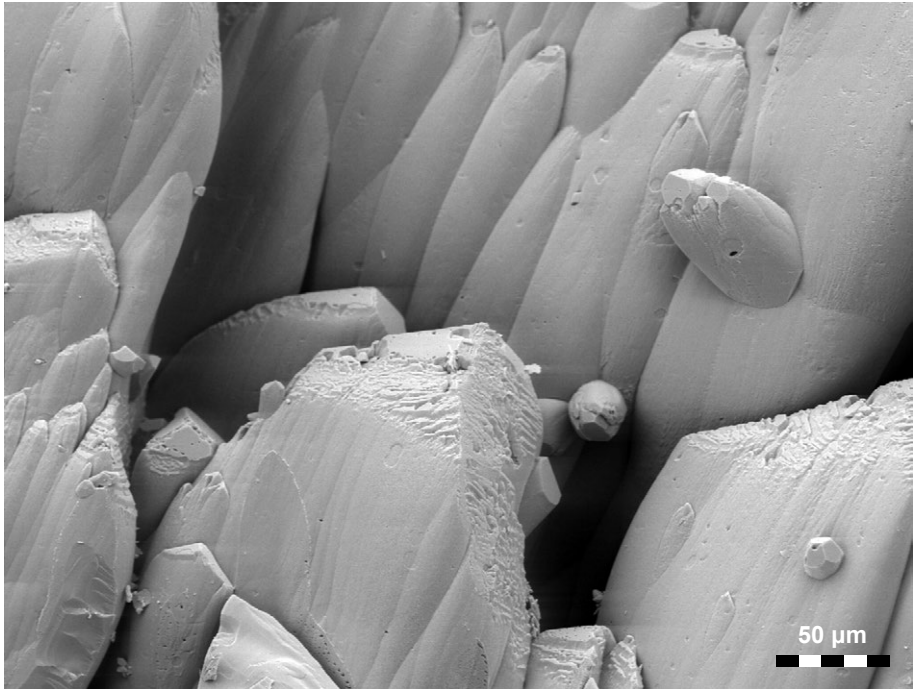


Figure 3. Secondary electron image of calcite crystals from a drainage scaling.

and K concentrations of 4.9 and 1.7 mg L<sup>-1</sup>, respectively. In contrast solution KAT\_7-DrW presents the opposite end-member, a highly alkaline solution derived from intensive water – shotcrete interaction. At the high pH of the solution KAT\_7-DrW typically elevated concentrations of Na (19.1 mg L<sup>-1</sup>) and K (30.1 mg L<sup>-1</sup>) and a strong depletion of magnesium ions due to brucite (Mg(OH)<sub>2</sub>) formation are obtained [43-45]. Drainage solutions KAT\_1-DW to KAT\_6-DW are collected along the flow path of the tunnel drainage. Generally these solutions can be considered as mixtures between end member solutions GW and DrW. The evolution of K and Na concentrations from KAT\_1-DW to KAT\_6-DW suggests only minor inflow of GW into the drainage along the given flow path with values ranging from 11.6 to 15.8 mg L<sup>-1</sup> and 9.3 to 11.0 mg L<sup>-1</sup>, respectively (see Table 2 in the appendix). Thus, CaCO<sub>3</sub> formation and CO<sub>2</sub> exchange between solution and atmosphere has to be considered as the main reasons for continuous change of physicochemical parameters. Obviously, the decrease in concentration of dissolved Ca (Figure 4a) and the evolution of saturation index with respect to calcite (SI<sub>Cal</sub> Figure 4b) give evidence of ongoing calcite formation. The decrease of CO<sub>3</sub> along the

flow path is to some extent due to the pH decrease and the accompanied shift of the DIC species toward bicarbonate and to the consumption of  $\text{CO}_3$  by  $\text{CaCO}_3$  formation. Accordingly almost constant DIC concentrations reflect nearly zero net C-balance for  $\text{CO}_2$  uptake from the atmosphere and precipitation of  $\text{CaCO}_3$ .

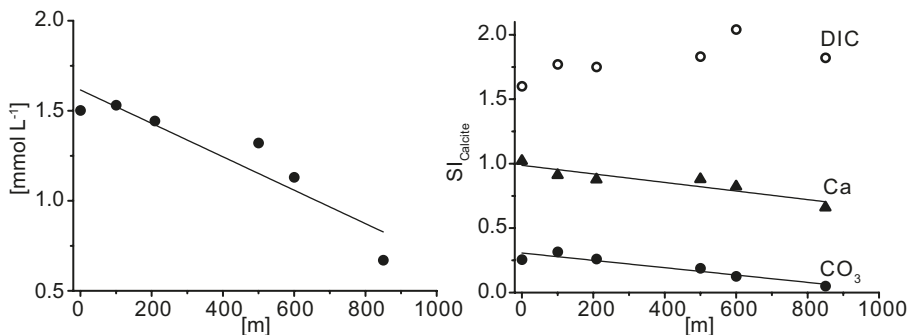


Figure 4. Evolution of Ca,  $\text{CO}_3$  and DIC - content of solutions KAT\_1-DW to KAT\_6-DW along the flow path of the drainage system (4a) and  $SI_{\text{Calcite}}$  (4b).

### Sulfate attack and thaumasite formation

Petrological investigations (XRD, SEM and EPMA) indicate concrete damage from sulfate attack which is mainly due to the formation of thaumasite (Figure 5). However the presence of ettringite could not be clearly distinguished from thaumasite by XRD pattern due to the dominance of thaumasite and structural similarities. Quantitative chemical analyses by WDX indicate a solid solution between ettringite and thaumasite with a maximum molar Si/Al ratio from 8 to 1. Higher Al contents were particularly found in areas of damaged concrete with less intensive damage or transition horizons to non-altered concrete. However in intensively damaged mushy materials the composition of thaumasite was mostly very pure and almost free of Al. As described in a former study on the present altered concretes, incongruent dissolution of dolomite aggregates and partial replacement by calcite and brucite was found in most of the samples [44].

The compositions of typical local ground (GW) and drainage water (DW) inside the tunnels are given in Table 2 (see appendix). In general GW and DW are enriched in  $\text{SO}_4$  (500-1500  $\text{mg L}^{-1}$ ) due to the local geological units containing sulfate minerals. However ground water with a high discharge ( $>10 \text{ L s}^{-1}$ ) within limestone and dolomite horizons displays very low  $\text{SO}_4$  contents of less than 10  $\text{mg L}^{-1}$ . In contrast DW with less discharge and drip waters are nearly saturated with respect to gypsum

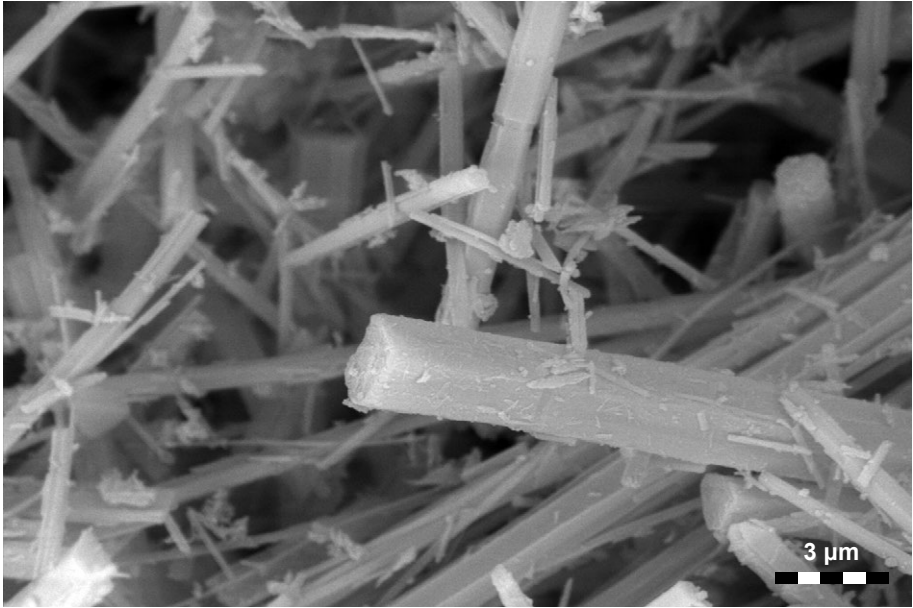


Figure 5. Secondary electron image showing thaumasite needles (separated sample).

with  $\text{SO}_4$  concentration up to about  $4000 \text{ mg L}^{-1}$ . Latter solutions is therefore being a potential threat for sulfate attack. Na and Cl are partly to be accounted to rock salt dissolution but also to intensive concrete and shotcrete interaction when molar Na/Cl ratios exceed 1 as for solution TT\_2-DrW. Ca concentrations reach up to  $600 \text{ mg L}^{-1}$ , but are limited to the solubility of gypsum. Mixing of Ca and  $\text{SO}_4$  rich GW or DrW with high alkaline DW from the interaction with concrete has a high potential for drainage clogging due to  $\text{CaCO}_3$  sinter formation at a high supersaturation degree.

### Stable carbon isotopes

As conventional chemical analyses are not suitable to decipher the individual source of  $\text{CO}_3$  in the precipitated solids, stable carbon isotopes are introduced for both calcite and thaumasite formation issues. The mechanisms responsible for precipitation of calcite can be identified by the use of stable carbon isotope analysis ( $^{13}\text{C}/^{12}\text{C}$ ) of the DIC and solids. Hydroxylation of  $\text{CO}_2$  at high pH conditions leads to a depletion of  $^{13}\text{C}$  vs.  $^{12}\text{C}$  with a kinetic isotope fractionation of about  $-18 \text{ ‰}$  [46, 47]. This results in  $\delta^{13}\text{C}_{\text{CaCO}_3} \approx -26 \text{ ‰}$  for the fixation of atmospheric  $\text{CO}_2$  ( $\delta^{13}\text{C}_{\text{atm CO}_2} \approx -8 \text{ ‰}$ ). The  $^{13}\text{C}/^{12}\text{C}$  isotope values in precipitated calcite gained from

ground water bicarbonate is indicated by a 1:1 mixture of soil  $\text{CO}_2$  ( $\delta^{13}\text{C}_{\text{soil CO}_2} \approx -25 \text{‰}$ ) and dissolved local marine limestone ( $\delta^{13}\text{C} \approx 0 \text{‰}$ ) leading to  $\delta^{13}\text{C}_{\text{CaCO}_3} \approx -13 \text{‰}$  [47]. In our case (KAT samples) the  $\delta^{13}\text{C}_{\text{DIC}}$  value of the local ground water is  $-11.1 \text{‰}$ , whereas analysis of highly alkaline drip water from the tunnel wall shows a value of  $-19.8 \text{‰}$  (dominated by absorption of atmospheric  $\text{CO}_2$ ) giving the range of carbon isotope values in the present system (Table 2 see appendix). The solutions from the drainage system show a continuous uptake of  $\text{CO}_2$  from the Earth's atmosphere by means of decreasing  $\delta^{13}\text{C}_{\text{DIC}}$  values from  $-12.6$  to  $-14.1 \text{‰}$  (Figure 6). Apparent stable carbon isotope fractionation between  $\delta^{13}\text{C}_{\text{DIC}}$  and  $\delta^{13}\text{C}_{\text{CaCO}_3}$  is close to the known equilibrium fractionation [48] as  $\text{CaCO}_3$  solids in the drainage are between  $2.0$  and  $3.2 \text{‰}$  isotopically heavier than the associated DIC. For KAT\_6-DW at the end of the tunnel, the analyzed solid results in a  $\delta^{13}\text{C}_{\text{CaCO}_3}$  value which is  $2.7 \text{‰}$  isotopically lighter than the corresponding DIC. In the latter case the solution KAT\_6-DW was sampled from the outlet of the main drainage into a storage basin. The basin itself receives drainage solutions from various origins. Thus precipitated  $\text{CaCO}_3$  in the storage basin cannot be directly related to the drainage solution KAT\_6-DW.

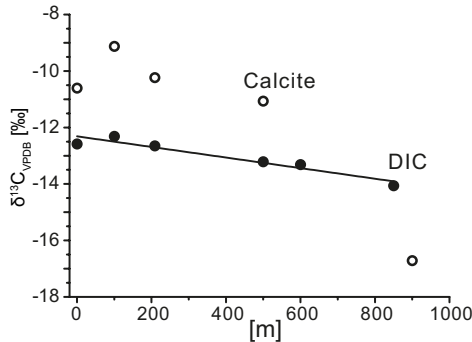


Figure 6. Evolution of stable carbon isotopes of the solution and the corresponding calcite along the flow path of the drainage.

Although fractionation mechanisms of stable carbon isotope in the system  $\text{CO}_2\text{-H}_2\text{O-CaCO}_3$  are mostly well understood, knowledge of such aspects is very limited for thaumasite formation [6, 7]. Iden and Hagelia [6] reported a high overall variability with respect to the isotopic composition on a micro scale basis due to fine grained materials. Our presented approach is in accordance with results from Iden and Hagelia to use small sample volumes of solids and if possible monomineralic material to exclude variation due to inhomogeneities. By purifying damaged concrete material with ultrasonic treatment the final

material consists of almost pure thaumasite (> 95 wt.%) with less than 3 wt. % calcite or dolomite, which may slightly disrupt  $\delta^{13}\text{C}$  results. Tables 1 and 2 (see appendix) comprise  $\delta^{13}\text{C}$  values of solid carbonate samples and of the DIC, respectively. Obviously given ranges of isotope data in Figure 7 indicate DIC of the local ground water as carbon source accounted to thaumasite formation. However other carbon sources like atmospheric  $\text{CO}_2$  or carbon from dissolution of carbonate filler and aggregates may also be likely carbon source as postulated by [1, 36, 37, 49]. In our study carbon isotope results show that the impact of atmospheric  $\text{CO}_2$  can be almost ruled out as a shift of  $\delta^{13}\text{C}$  values to -25 ‰ was not detected in any case. Dissolution of carbonate aggregates and fillers in the concrete due to  $\text{CO}_2$  from interacting ground water is also very unlikely. The local ground water is already close to saturation with respect to calcite and dolomite with  $P_{\text{CO}_2}$  values near the Earth's atmosphere level at slightly alkaline conditions. Thus  $\text{CO}_2$  from soil uptake cannot be assumed for potential aggregate dissolution. Nevertheless for dolomite aggregates, de-dolomitization has to be considered, resulting in precipitation of brucite and calcite. This would lead to lower  $\delta^{13}\text{C}$  isotopic signals in DIC and thaumasite as  $\delta^{13}\text{C}$  of dolomite aggregates is close to 0 ‰ (see carbonate aggregates in Figure 7). However a shift of  $\delta^{13}\text{C}$  of thaumasite to 0 ‰ is not shown in Figure 7. Therefore within a first approach we believe that bicarbonate of the ground water is the major source for thaumasite formation. Interestingly, an analogous behavior was obtained for  $\text{SO}_4$  in thaumasite from the same tunnels by using stable sulfur isotope signals where  $\text{SO}_4$  from ground water was identified for thaumasite formation [34, 50].

## 4.2.6 Conclusive Remarks

The application of stable carbon isotope distribution has shown to be a very useful tool to gain an advanced understanding of the formation of carbonate containing minerals like  $\text{CaCO}_3$  and thaumasite induced by cement-water reactions.  $\text{CaCO}_3$  sinter formation is referred to both the bicarbonate of the ground water and the absorption of atmospheric  $\text{CO}_2$ . Absorption phenomena were studied by  $\text{CaCO}_3$  sinter formation in the drainage along a flow path via isotopic  $^{13}\text{C}/^{12}\text{C}$  evolution in the DIC and in the  $\text{CaCO}_3$  precipitates. In the case of thaumasite the  $\text{CO}_3$  is mainly derived from DIC of the ground water. Ongoing experiments for thaumasite formation are carried out to verify the latter findings by involving stable carbon isotope distribution.

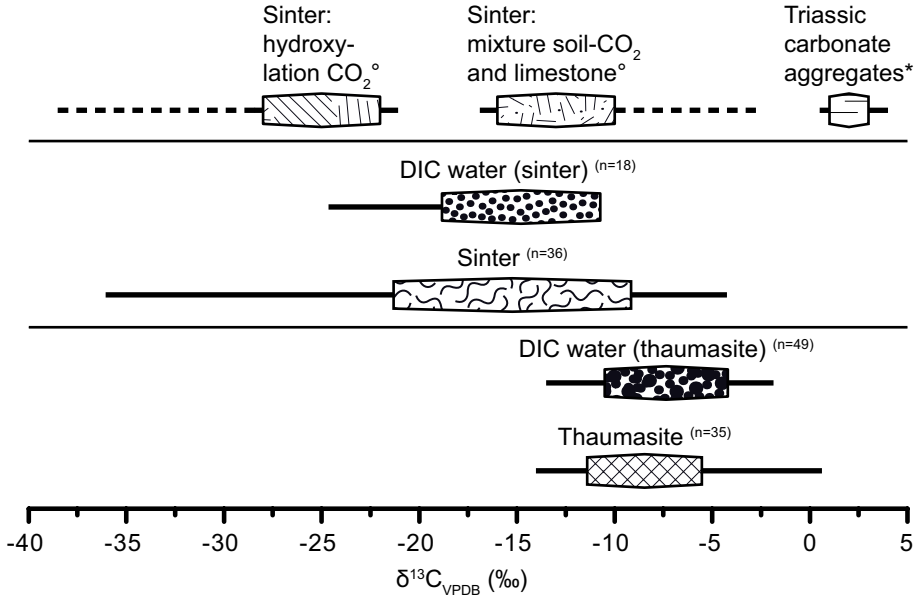


Figure 7. Range of  $\delta^{13}\text{C}_{\text{VPDB}}$  values from studies of drainage sinter formation and thaumasite formation.  $^\circ$ denotes  $\delta^{13}\text{C}_{\text{VPDB}}$  values of  $\text{CaCO}_3$  sinter from the literature [42, 47, 51]. \*denotes  $\delta^{13}\text{C}_{\text{VPDB}}$  values from this study and the literature[52].

#### 4.2.7 Acknowledgement

The authors greatly appreciate financial support of the present study by NAWI Graz (Graz Advanced School of Science, GASS) and Österreichische Forschungsförderungsgesellschaft (FFG, 828476). The authors also want thank Josef Tritthart for the helpful comments and discussions.

### 4.3. Remarks and Outlook

As thaumasite ( $\text{Ca}_6[\text{Si}(\text{OH})_6]_2(\text{CO}_3)_2(\text{SO}_4)_2 \cdot 24\text{H}_2\text{O}$ ) is a carbonate containing mineral analogous mechanisms in terms of isotope fractionation should apply as for calcite. The results from our study clearly show that the carbonate is mainly stemming from the ground water. This finding is supported by the paper on sulfur sources given in Chapter 2 as the sulfate is coming from the ground water as well. However, experiments to synthesize thaumasite and isotope analyses lead to a better understanding of pos-

sible fractionation mechanisms. Additionally the interpretation of  $\delta^{18}\text{O}$  values should be implemented for the carbonate ion in future studies.

For both sulfur and carbon isotope measurements small bulk samples of separated thaumasite (0.001 – 0.002 g) are required. Providing of monomineralic thaumasite is even more relevant for analyzing carbon isotope ratios compared to sulfur isotopes because carbonate aggregates or fillers and further secondary carbonates may disturb the isotope signal of thaumasite. With an alternating sequence of ultrasonic treatment and decanting, thaumasite can be well separated from the other material of damaged concrete (mostly better than 90 wt. %; see Chapter 2). An even better result could be achieved by enhancing this technique by the use of sodium polytungstate solutions with a known density (e.g.  $\rho \approx 2.2 \text{ kg m}^{-3}$ ) and centrifugation. The density of thaumasite ( $\rho \approx 1.9 \text{ kg m}^{-3}$ ) is much lower than those of calcite and dolomite ( $\rho \geq 2.7 \text{ kg m}^{-3}$ ).

French [7] considers calcite as an intermediate phase that may re-dissolve for the formation of thaumasite. In our study this theory could not be verified. Secondary calcite is forming during sulfate attack but will not re-dissolve at the preferred thaumasite formation pH conditions of  $>10.5$  [53]. The influence of calcite dissolution on thaumasite formation that was primarily used as filler is more likely. During cement hardening (before sulfate attack is taking place) monocarbonate gets preferentially formed as stable AFm phase when calcite fillers are used as described by Schmidt et al. [4] and citations herein. Additionally results of our study contradict the finding of French [7] that the source of the carbonate ions for thaumasite in the described samples is mostly related to the combustion of hydrocarbons from traffic. It seems more likely that thaumasite formation is also related to carbonate containing ground water comparable to the present study (see chapter 4.2). However the two given  $\delta^{13}\text{C}$  values of thaumasite of about  $-20 \text{ ‰}$  in the study of French [7] are most likely linked to the absorption of atmospheric  $\text{CO}_2$ . In our studies no indication of atmospheric  $\text{CO}_2$  absorption leading to discriminated carbon isotopic values of thaumasite could be observed. However some calcite sinter yield  $\delta^{13}\text{C}$  values of down to  $-40 \text{ ‰}$  which is generated by the hydroxylation of atmospheric  $\text{CO}_2$  that has been strongly influenced by combustion fumes.

Possible influences of organic matter on Tha formation are not validated in the present study [54]. Hence bacterial activity related to sulfate attack was described by Hagelia [55]. Mg ions and organic molecules slow down or inhibit Cal formation [56]. Thus Tha might be more likely formed instead of  $\text{CaCO}_3$ . Interestingly in sucrose solutions thaumasite was well synthesized [57]. A further step in thaumasite research will be to increase the existing data set of  $\delta^{13}\text{C}$  and  $\delta^{18}\text{O}$  for field concrete structures and subsequently include thaumasite from fully immersed experimental studies of mortar specimens.



## 4.4 References

1. Justnes, H., Thaumassite formed by sulfate attack on mortar with limestone filler. *Cement and Concrete Composites*, 2003. 25(8): p. 955-959.
2. Bonavetti, V., H. Donza, G. Menéndez, O. Cabrera, and E.F. Irassar, Limestone filler cement in low w/c concrete: A rational use of energy. *Cement and Concrete Research*, 2003. 33(6): p. 865-871.
3. Cyr, M., P. Lawrence, and E. Ringot, Efficiency of mineral admixtures in mortars: Quantification of the physical and chemical effects of fine admixtures in relation with compressive strength. *Cement and Concrete Research*, 2006. 36(2): p. 264-277.
4. Schmidt, T., B. Lothenbach, M. Romer, K. Scrivener, D. Rentsch, and R. Figi, A thermodynamic and experimental study of the conditions of thaumasite formation. *Cement and Concrete Research*, 2008. 38(3): p. 337-349.
5. Berman, H.A. and E.S. Newman, Heat of formation of calcium aluminate monocarbonate at 25 °C. *Journal of Research of the National Bureau of Standards*, 1961. A 65(3): p. 197-207.
6. Iden, I.K. and P. Hagelia, C, O and S isotopic signatures in concrete which have suffered thaumasite formation and limited thaumasite form of sulfate attack. *Cement and Concrete Composites*, 2003. 25(8): p. 839-846.
7. French, W.J., Presidential Address 2003: Why concrete cracks - geological factors in concrete failure. *Proceedings of the Geologists Association*, 2005. 116: p. 89-105.
8. Schneider, M., M. Romer, M. Tschudin, and H. Bolio, Sustainable cement production—present and future. *Cement and Concrete Research*, 2011. 41(7): p. 642-650.
9. Rafai, N., R. Letolle, P. Blanc, P. Gégout, and E. Revertegat, Carbonation-decarbonation of concretes studied by the way of carbon and oxygen stable isotopes. *Cement and Concrete Research*, 1992. 22(5): p. 882-890.
10. Rafai, N., R. Letolle, P. Blanc, A. Person, and P. Gegout, Isotope geochemistry ( $^{13}\text{C}$ ,  $^{18}\text{O}$ ) of carbonation processes in concretes. *Cement and Concrete Research*, 1991. 21(2-3): p. 368-377.
11. Kosednar-Legenstein, B., M. Dietzel, A. Leis, and K. Stingl, Stable carbon and oxygen isotope investigation in historical lime mortar and plaster - Results from

- field and experimental study. *Applied Geochemistry*, 2008. 23(8): p. 2425-2437.
12. Létolle, R., P. Gégout, N. Rafai, and E. Revertegat, Stable isotopes of carbon and oxygen for the study of carbonation/decarbonation processes in concretes. *Cement and Concrete Research*, 1992. 22(2-3): p. 235-240.
  13. Graham, I.J., R.L. Goguel, and D.A. St John, Use of strontium isotopes to determine the origin of cement in concretes: Case examples from New Zealand. *Cement and Concrete Research*, 2000. 30(7): p. 1105-1111.
  14. Kloppmann, W., P. Bromblet, J.M. Vallet, V. Vergès-Belmin, O. Rolland, C. Guerrot, and C. Gosselin, Building materials as intrinsic sources of sulfate: A hidden face of salt weathering of historical monuments investigated through multi-isotope tracing (B, O, S). *Science of The Total Environment*, 2011. 409(9): p. 1658-1669.
  15. Clark, I.D., R. Dayal, and H.N. Khoury, The Maqarin (Jordan) natural analogue for  $^{14}\text{C}$  attenuation in cementitious barriers. *Waste Management*, 1994. 14(5): p. 467-477.
  16. Dotsika, E., D. Psomiadis, D. Poutoukis, B. Raco, and P. Gamaletsos, Isotopic analysis for degradation diagnosis of calcite matrix in mortar. *Analytical and Bioanalytical Chemistry*, 2009. 395(7): p. 2227-2234.
  17. Górka, M., P.E. Sauer, D. Lewicka-Szczebak, and M.-O. Jedrysek, Carbon isotope signature of dissolved inorganic carbon (DIC) in precipitation and atmospheric  $\text{CO}_2$ . *Environmental Pollution*, 2011. 159(1): p. 294-301.
  18. Hoefs, J., *Stable Isotope Geochemistry*. 6<sup>th</sup> ed. 2008, Berlin: Springer. 288.
  19. O'Neil, J.R. and I. Barnes,  $^{13}\text{C}$  and  $^{18}\text{O}$  compositions in some fresh-water carbonates associated with ultramafic rocks and serpentinites: western United States. *Geochimica et Cosmochimica Acta*, 1971. 35(7): p. 687-697.
  20. Wilson, S.A., S.L.L. Barker, G.M. Dipple, and V. Atudorei, Isotopic Disequilibrium during Uptake of Atmospheric  $\text{CO}_2$  into Mine Process Waters: Implications for  $\text{CO}_2$  Sequestration. *Environmental Science & Technology*, 2010. 44(24): p. 9522-9529.
  21. Dietzel, M.,  $^{13}\text{C}/^{12}\text{C}$ -signatures and  $^{18}\text{O}/^{16}\text{O}$ -signatures of calcite precipitations in drainage systems. *Acta Hydrochimica Et Hydrobiologica*, 1995. 23(4): p. 180-184.
  22. Dietzel, M., Measurement of the stable carbon isotopes in calcite sinters on concrete. *ZKG International*, 2000. 53(9): p. 544-548.

23. Dietzel, M.,  $^{13}\text{C}/^{12}\text{C}$ -signatures of calcite-sinter onto concrete. *Applied Mineralogy*, Vols 1 and 2, 2000: p. 747-748.
24. Girmscheid, G., T. Gamisch, T. Klein, and A. Meinlschmidt, Scale sintering in tunnel drainages - Mechanisms of scale formation. *Bauingenieur*, 2003. 78: p. 292-300.
25. Girmscheid, G., T. Gamisch, and A. Meinlschmidt, Scale sintering in tunnel drainages – Recommendations for maintenance of tunnels. *Bauingenieur*, 2003. 78: p. 562-570.
26. Bensted, J., Thaumassite - background and nature in deterioration of cements, mortars and concretes. *Cement and Concrete Composites*, 1999. 21(2): p. 117-121.
27. Jallad, K.N., M. Santhanam, and M.D. Cohen, Stability and reactivity of thaumasite at different pH levels. *Cement and Concrete Research*, 2003. 33(3): p. 433-437.
28. Romer, M., Steam locomotive soot and the formation of thaumasite in shotcrete. *Cement and Concrete Composites*, 2003. 25(8): p. 1173-1176.
29. Schlegel, M.C., U. Mueller, U. Panne, and F. Emmerling, Deciphering the sulfate attack of cementitious materials by high-resolution micro-X-ray diffraction. *Analytical Chemistry*, 2011. 83(10): p. 3744-3749.
30. Glasser, F.P., J. Marchand, and E. Samson, Durability of concrete — Degradation phenomena involving detrimental chemical reactions. *Cement and Concrete Research*, 2008. 38(2): p. 226-246.
31. Tritthart, J., D. Klammer, F. Mittermayr, and A. Brunnsteiner, A Casestudy of Thaumassite Formation in an Austrian Tunnel, in *13<sup>th</sup> International Congress on the Chemistry of Cement*. 2011: Madrid. p. 431.
32. Bellmann, F., W. Erfurt, and H.M. Ludwig, Field performance of concrete exposed to sulphate and low pH conditions from natural and industrial sources. *Cement and Concrete Composites*, 2012. 34(1): p. 86-93
33. Blanco-Varela, M.T., J. Aguilera, S. Martinez-Ramirez, F. Puertas, A. Palomo, C. Sabbioni, G. Zappia, C. Riontino, K. Van Balen, and E.E. Toumbakari, Thaumassite formation due to atmospheric  $\text{SO}_2$ -hydraulic mortar interaction. *Cement and Concrete Composites*, 2003. 25(8): p. 983-990.
34. Mittermayr, F., C. Bauer, D. Klammer, M.E. Böttcher, A. Leis, P. Escher, and M. Dietzel, Concrete under Sulfate Attack: An Isotope Study on Sulfur Sources Isotopes in *Environmental & Health Studies*, 2012. 48(1): p. 105-117.

35. Pye, K. and N. Schiavon, Cause of Sulfate Attack on Concrete, Render and Stone indicated by Sulfur Isotope Ratios. *Nature*, 1989. 342(6250): p. 663-664.
36. Collett, G., N.J. Crammond, R.N. Swamy, and J.H. Sharp, The role of carbon dioxide in the formation of thaumasite. *Cement and Concrete Research*, 2004. 34(9): p. 1599-1612.
37. Thomas, M.D.A., C.A. Rogers, and R.F. Bleszynski, Occurrences of thaumasite in laboratory and field concrete. *Cement and Concrete Composites*, 2003. 25(8): p. 1045-1050.
38. Hagelia, P. and R.G. Sibbick, Thaumasite Sulfate Attack, Popcorn Calcite Deposition and acid attack in concrete stored at the "Blindtarmen" test site Oslo, from 1952 to 1982. *Materials Characterization*, 2009. 60(7): p. 686-699.
39. Bensted, J., Thaumasite—direct, woodfordite and other possible formation routes. *Cement and Concrete Composites*, 2003. 25(8): p. 873-877.
40. Parkhurst, D.L. and C.A.J. Apello, User's guide to PHREEQC (V2). U.S. Geol. Sur, 1999. 312.
41. Spötl, C., A robust and fast method of sampling and analysis of  $\delta^{13}\text{C}$  of dissolved inorganic carbon in ground waters. *Isotopes in Environmental and Health Studies*, 2005. 41(3): p. 217-221.
42. Dietzel, M., T. Rinder, A. Niedermayr, F. Mittermayr, A. Leis, D. Klammer, S. Köhler, and P. Reichl, Mechanisms of Sinter Formation in Drainage Systems. *BHM Berg- und Hüttenmännische Monatshefte*, 2008. 153(10): p. 369-372.
43. Chen, W. and H.J.H. Brouwers, Alkali binding in hydrated Portland cement paste. *Cement and Concrete Research*, 2010. 40(5): p. 716-722.
44. Mittermayr, F., D. Klammer, S. Köhler, A. Leis, D. Höllen, and M. Dietzel, Dissolution of Dolomite in alkaline cementitious media, in 13<sup>th</sup> International Congress on the Chemistry of Cement. 2011: Madrid. p. 445.
45. Pokrovsky, O.S. and J. Schott, Experimental study of brucite dissolution and precipitation in aqueous solutions: surface speciation and chemical affinity control. *Geochimica et Cosmochimica Acta*, 2004. 68(1): p. 31-45.
46. Usdowski, E. and J. Hoefs,  $^{13}\text{C}/^{12}\text{C}$  partitioning and kinetics of  $\text{CO}_2$  absorption by hydroxide buffer solutions. *Earth and Planetary Science Letters*, 1986. 80(1-2): p. 130-134.
47. Dietzel, M., E. Usdowski, and J. Hoefs, Chemical and  $^{13}\text{C}/^{12}\text{C}$ - and  $^{18}\text{O}/^{16}\text{O}$ -isotope evolution of alkaline drainage waters and the precipitation of calcite. *Applied*

- Geochemistry, 1992. 7(2): p. 177-184.
48. Dandurand, J.L., R. Gout, J. Hoefs, G. Menschel, J. Schott, and E. Usdowski, Kinetically controlled variations of major components and carbon and oxygen isotopes in a calcite-precipitating spring. *Chemical Geology*, 1982. 36(3-4): p. 299-315.
  49. Torres, S.M., C.J. Lynsdale, R.N. Swamy, and J.H. Sharp, Microstructure of 5-year-old mortars containing limestone filler damaged by thaumasite. *Cement and Concrete Research*, 2006. 36(2): p. 384-394.
  50. Mittermayr, F., D. Klammer, D. Höllen, S. Köhler, M.E. Böttcher, A. Leis, and M. Dietzel, Deterioration of concrete – application of stable isotopes, in 10<sup>th</sup> International Congress for Applied Mineralogy, M.A.T.M. Broekmans, Editor. 2011: Trondheim. p. 435-445.
  51. Clark, I. and P. Fritz, *Environmental Isotopes in Hydrogeology*. 1997, Boca Raton: Lewis Publishers. 328.
  52. Schroll, E., V. Geochemische und geochronologische Daten und Erläuterungen, in *Archiv für Lagerstätten Forschung*, L. Weber, Editor. 1997, Geologische Bundesanstalt: Wien. p. 395-537.
  53. Zhou, Q., J. Hill, E.A. Byars, J.C. Cripps, C.J. Lynsdale, and J.H. Sharp, The role of pH in thaumasite sulfate attack. *Cement and Concrete Research*, 2006. 36(1): p. 160-170.
  54. Blanco-Varela, M.T., P.M. Carmona-Quiroga, I.F. Sáez del Bosque, and S. Martínez-Ramírez, Role of organic admixtures on thaumasite precipitation. *Cement and Concrete Research*, 2012. 42(7): p. 994-1000.
  55. Hagelia, P., Deterioration Mechanisms and Durability of Sprayed Concrete for Rock Support in Tunnels, in *Materials Characterization*. 2011, TU Delft: Delft. p. 320.
  56. Niedermayr, A., Effekte von Magnesium, Polyasparaginsäure und Karbonatakkumulationsrate auf die Kristallisation, Morphologie, Elementeinbau und Isotopenfraktionierung von Kalziumkarbonatphasen. 2012, TU Graz: Graz. p. 168.
  57. Martínez-Ramírez, S., M.T. Blanco-Varela, and J. Rapazote, Thaumasite formation in sugary solutions: Effect of temperature and sucrose concentration. *Construction and Building Materials*, 2011. 25(1): p. 21-29.

## 4.5 Appendix

Table 1. Typical  $\delta^{13}\text{C}$  values of carbonate minerals; Cal: calcite; Dol: dolomite; Tha: thaumasite.

Sample	Position [m]	$\delta^{13}\text{C}$ [‰]	Type
KAT_1-DW	0	-10.6	Cal sinter
KAT_2-DW	100	-9.1	Cal sinter
KAT_3-DW	209	-10.2	Cal sinter
KAT_4-DW	500	-11.1	Cal sinter
KAT_6-DW	850	-16.7	Cal sinter
KAT_7-DrW	-	-18.2	Cal sinter
KAT_9-DrW	-	-13.8	Cal sinter
KAT_10-DrW	-	-35.0	Cal sinter
KAT_11-DrW	-	-20.7	Cal sinter
Bos_Tha1	211	-8.7	Tha
Bos_Tha2	3269	-4.5	Tha
Bos_Tha3	4206	-6.0	Tha
TT_Tha1	0	-8.8	Tha
TT_Tha2	1860	-9.3	Tha
TT_Tha3	3316	-6.7	Tha
TT_Cal	3541	-3.2	Cal host rock
TT_Agg	-	1.0	Dol aggregate
TT_DolGp	1754	3.9	Dol host rock
TT_GpDol	5921	0.3	Dol host rock

Table 2. Chemical composition of aqueous solutions from various sampling sites; ion contents are given in  $\text{mg L}^{-1}$ ; DW: drainage water; GW: ground water; DrW drip water; TDS: total dissolved solids; n.d.: not detectable; DIC: dissolved inorganic carbon - values given in  $\text{mmol L}^{-1}$ ;  $P_{\text{CO}_2}$ , internal partial pressure of  $\text{CO}_2$  ( $P_{\text{CO}_2}$ ) and saturation indices (SI) were calculated with PHREEQC [40].

Sample	Na	K	Mg	Ca	Cl	$\text{NO}_3$	$\text{SO}_4$	DIC
KAT_1-DW	11.0	15.8	14.7	40.9	8.96	23.8	22.2	1.60
KAT_2-DW	10.4	15.1	14.8	36.5	9.08	20.9	24.1	1.77
KAT_3-DW	10.4	14.6	14.5	35.2	8.65	19.4	25.9	1.75
KAT_4-DW	10.1	13.2	13.8	35.3	8.58	18.1	26.7	1.83
KAT_5-DW	9.84	12.7	13.6	33.0	8.66	17.9	26.9	2.04
KAT_6-DW	9.27	11.6	11.3	26.5	9.05	15.8	36.6	1.82

Table 2. Continued

Sample	Na	K	Mg	Ca	Cl	NO <sub>3</sub>	SO <sub>4</sub>	DIC
KAT_7-DrW	19.8	30.1	0.24	112.5	11.5	55.8	14.7	0.36
KAT_8-GW	4.93	1.68	20.4	54.0	7.32	0.08	48.5	3.89
Bos_S1-DrW	1328	44.0	604	502	1578	3.54	4256	1.44
Bos_S2-GW	0.18	0.25	7.88	27.6	0.25	2.32	5.13	1.93
Bos_S3-DW	48.6	5.63	57.8	234	60.7	1.33	650	3.47
Bos_R1-DW	6.70	0.32	10.0	38.0	7.37	3.00	22.1	2.27
Bos_R2-GW	0.89	0.32	10.8	40.3	0.85	3.98	18.1	2.46
Bos_R3-GW	3.77	0.92	32.9	206	4.85	0.96	505	2.8
TT_1-DW	650	34.3	18.9	144	656	12.0	820	2.03
TT_2-DrW	1227	10.2	126	428	46.1	3.37	4072	1.37
TT_3-GW	2.03	0.79	35.4	554	0.82	n.d.	1298	2.65

Sample	Position [m]	T [°C]	pH	TDS	$\delta^{13}\text{C}_{\text{DIC}}$ [‰]	P <sub>CO2</sub> [atm]	SI <sub>Gp</sub>	SI <sub>Cal</sub>
KAT_1-DW	0	13.3	9.71	264	-12.6	-5.0	-2.0	1.5
KAT_2-DW	100	13.1	9.77	274	-12.3	-5.0	-2.0	1.5
KAT_3-DW	209	13.2	9.66	264	-12.7	-4.9	-2.0	1.4
KAT_4-DW	500	12.9	9.46	258	-13.2	-4.6	-2.0	1.3
KAT_5-DW	600	13.0	9.20	260	-13.3	-4.2	-2.0	1.1
KAT_6-DW	850	14.3	8.83	236	-14.1	-3.9	-2.1	0.7
KAT_7-DrW	-	17.0	12.06	602	-19.8	-9.9	-2.0	1.7
KAT_8-GW	-	14.7	8.23	380	-11.1	-3.0	-1.7	0.7
Bos_S1-DrW	750	10.9	7.94	8403	-7.0	-3.3	0.3	0.3
Bos_S2-GW	1600	6.9	8.31	162	-2.0	-3.4	-2.8	0.2
Bos_S3-DW	5425	10.3	8.18	1272	-8.8	-3.0	-0.3	1.0
Bos_R1-DW	0	6.3	8.34	226	-5.5	-3.4	-2.1	0.4
Bos_R2-GW	1196	8.5	8.32	226	-7.1	-3.3	-2.2	0.4
Bos_R3-GW	4766	7.2	7.60	919	-5.6	-2.6	-0.4	0.2
TT_1-DW	0	11.4	8.28	2460	-11.6	-3.4	-0.5	0.6
TT_2-DrW	1950	14.7	7.49	5993	-9.2	-2.8	0.3	-0.1
TT_3-GW	3117	5.6	7.60	2048	-7.0	-2.6	0.2	0.5





## CHAPTER 5

# Is Dolomite in Concrete affected by Sulfate Attack?

### 5.1 Introduction

In this chapter the performance of dolomite aggregates in concrete that has been deteriorated by sulfate attack is discussed. Surprisingly incongruent dolomite dissolution was found in all samples that contain thaumasite and where dolomite was used as aggregate. The reaction products of the incongruent dissolution of dolomite are brucite, calcite, (aragonite) and (thaumasite). Calcite and aragonite formation associated with sulfate attack can be clearly distinguished from primarily used carbonate aggregates as secondary formation of  $\text{CaCO}_3$  are enriched in strontium. The Sr is delivered from Ca and  $\text{SO}_4$  rich ground water found in the catchment areas of marine evaporites [1]. Thus the question that has been raised in the title is answered with yes! However with the restriction that it is not clearly solved whether the decomposition of dolomite is contributing carbonate to the formation of thaumasite at the micro scale and if de-dolomitization is a primary mechanism related to sulfate attack or only a consequence of intensive deterioration. Interestingly, the state of the art report on “Deleterious Reactions of Aggregate with Alkalis in Concrete” by Broekmans [2] does not discuss possible connections between de-dolomitization and sulfate attack. In this sense it is necessary to gain a better understanding of de-dolomitization reactions that negatively affect the performance of concrete which is subjected to sulfate environments. Even though this aspect is not a primary focus of this thesis the sustainability of dolomite is a highly relevant and interesting topic for further research.

## 5.2 Dissolution of Dolomite in Alkaline Cementitious Media

Florian Mittermayr<sup>1</sup>, Dietmar Klammer<sup>1</sup>, Stephan Köhler<sup>1,2</sup>, Albrecht Leis<sup>3</sup>, Daniel Höllen<sup>1</sup>, and Martin Dietzel<sup>1</sup>

<sup>1</sup>*Institute of Applied Geosciences, Graz University of Technology, Graz, Austria*

<sup>2</sup>*Swedish University of Agricultural Sciences, Uppsala, Sweden*

<sup>3</sup>*RESOURCES – Institute for Water, Energy and Sustainability, Joanneum Research, Graz, Austria*

### 5.2.1 Abstract

In this study we are gaining new insights into the conditions that can lead to the dissolution of dolomite in concrete. We investigated concrete samples from Austrian tunnels that show partially dissolved dolomite aggregates. Petrological analyses such as microprobe, SEM and Raman spectroscopy, hydrochemical analyses of interstitial solutions and ground water as well as modelling with PHREEQC were carried out. In addition a series of batch experiments was set up. Dolomite aggregates in concrete showed incongruent dissolution and newly formed calcite ( $\text{CaCO}_3$ ) and brucite ( $\text{Mg}(\text{OH})_2$ ) replacement. Phases were characterized in situ by EMPA and Raman spectroscopy. Modelling using PHREEQC indicates a possibility for incongruent dissolution of dolomite in the alkaline range when Ca is added to the solution. In this case dolomite starts to be getting more and more unstable versus calcite. In ground water Ca can be highly enriched by e.g. the dissolution of calcium sulfates (gypsum and anhydrite) in the catchment areas. Additional Ca can be gained from dissolution of portlandite ( $\text{Ca}(\text{OH})_2$ ) from concrete. Furthermore high ionic strength is influencing the dissolution behavior of dolomite. Extracted interstitial solutions are dominated by Na and  $\text{SO}_4$  and reach concentrations up to  $65 \text{ g L}^{-1}$  TDS. High pH values further accelerate the process of de-dolomitization as Mg is precipitated as brucite. Analogous de-dolomitization mechanisms are evident from the experimental results, where fine-grained dolomite crystals are incongruently dissolved by precipitation of calcite and brucite in alkaline solutions within 60 - 120 days. Dolomite dissolution under alkaline conditions is a dynamic process of dissolution and precipitation stimulated by high Ca concentration, high ionic strength, low temperature and high pH due to low Mg concentration.

## 5.2.2 Originality

In this contribution we present new approaches to understanding complex reactions in the field of the alkali aggregate reactions (AAR) that lead to the deterioration of concrete. We want to highlight our research of the so called Alkali Carbonate Reaction (ACR). From concrete samples - initially investigated for the thaumasite form of sulfate attack (TSA) - it became evident that partial dissolution of dolomite aggregates occurred. Thermodynamic modelling of water-rock-cement-aggregate-interstitial solution interactions, petrological analyses, and experimental approaches show that more parameters have to be considered as previously assumed. This topic is related to further studies of our group presented at this conference [3, 4].

## 5.2.3 Chief contributions

The main contribution of our research is to demonstrate the complexity and the mechanisms responsible for the de-dolomitization of aggregates used in concrete. Acquiring data from affected concretes found in different structures, knowledge about interacting ground water, interstitial solutions, data from experiments and thermodynamic modelling lead to a better understanding of AAR.

## 5.2.4 Introduction

Chemical alteration of concrete has gained much attention over the past decades as many cases of deterioration due to sulfate attack, thaumasite formation (TSA) or alkali silica reactions (ASR) have been reported in various constructions [5-10]. Much less is known about the so called alkali carbonate reaction (ACR). In general it is believed that dolomite aggregates can react with the alkalis from the cement, dissolve and form calcite and brucite [11-17]. Due to the very low solubility of dolomite in alkaline solutions this reaction seems doubtful and further mechanisms have to be taken into account [18-21].

Initially, concretes that were found to show incongruent dolomite dissolution were collected in Austrian tunnels to study the Thaumasite Form of Sulfate Attack (TSA) [3, 4, 22]. Application of the electron microprobe (EMPA) revealed partial dissolution of the dolomite aggregates and the crystallization of new phases (Figure 1). The major

questions that arise with this finding are: Why are dolomite aggregates dissolving under alkaline conditions and is this connected with the thaumasite formation? In this study we gained new insights into the conditions and reactions that lead to the incongruent dissolution of dolomite in concrete using various petrological and hydro-chemical methods combined with experimental and modelling approaches.

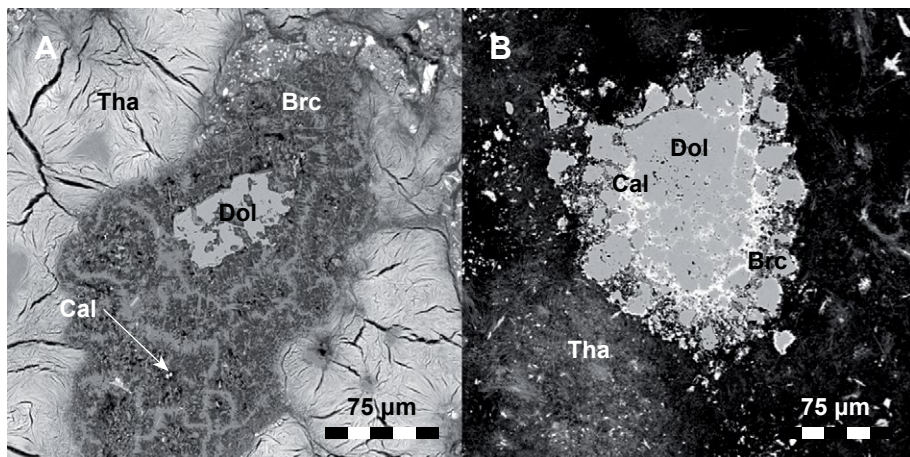


*Figure 1 (A) (B): Back scattered electron images (BSE) of different concrete samples from Austrian tunnels which show partially dissolved dolomite grains. The reaction products of the incongruent dolomite (Dol) dissolution are calcite (Cal) and brucite (Brc). The cement matrix is completely altered and mainly consists of thaumasite (Tha).*

## 5.2.5 Samples and Methods

### Case Studies

Solid and aqueous samples were taken from Austrian tunnels where the concrete was significantly damaged at several places. Solid samples include deteriorated and non-altered concrete. Petrological analyses comprise EMPA, scanning electron microscopy (SEM), X-ray diffractometry (XRD) with phase quantification by Rietveld refinement, Fourier transform infrared spectroscopy (FTIR) and Raman spectroscopy. Aqueous samples are local ground water, drainage water and extracted interstitial solutions from damaged concretes [22]. The pH, electric conductivity (EC) and temperature of drainage solution and ground water were measured on-site. Alkalinity was determined by titration with 0.005 M HCl. Major and trace ion concentrations

were analyzed by ion chromatography (IC) and inductively coupled plasma optical emission (ICP-OES) and inductively coupled plasma mass spectroscopy (ICP-MS).

## Experimental

For all experiments pure dolomite in gemstone quality from Eugui, Spain, was taken. Idiomorphic dolomite crystals were crushed in an agate mortar to a fine powder ( $< 63 \mu\text{m}$ ). About 0.25 g of dolomite powder were placed in gas-tight glass reactors with a volume of 300 ml. Experimental solutions were prepared using Titrisol for NaOH and  $\text{CaCl}_2$ ,  $\text{Na}_2\text{SO}_4 \cdot 10\text{H}_2\text{O}$ , NaCl (pro analysi) chemicals and MQ water. For  $\text{Ca}(\text{OH})_2$  solutions portlandite (pro analysi) was dissolved in MQ water under an Argon atmosphere and filtered through  $0.45 \mu\text{m}$  membrane filter to remove calcite impurities. After adding the experimental solutions to the dolomite, the reactors were kept gas-tight at temperature of 5, 20 and  $75 \text{ }^\circ\text{C}$  up to 4 months. At the end of the experiment the pH was measured and solids were filtered through  $0.45 \mu\text{m}$  membrane filter, rinsed with ethanol and dried at  $40 \text{ }^\circ\text{C}$ . Samples of all initial and final solutions were collected and acidified to 2 %  $\text{HNO}_3$  for inductively coupled plasma optical emission spectroscopy (ICP-OES) analyses.

## Modelling

For modelling approaches of the specific solution properties and designing the experiments the computer code PHREEQC was used, which is based on the thermodynamic and kinetic databases published by Parkhurst and Apello [23].

### 5.2.6 Results and Discussion

Samples from both case studies and experiments indicate incongruent dolomite dissolution at various alkaline conditions. This result is in contrast to the general concept that carbonates including dolomite are less soluble with increasing pH [18]. Thus further factors besides already known mechanisms in concrete have to be considered [15, 24]. Thermodynamic modelling approaches using PHREEQC show a possibility for de-dolomitization in the alkaline range when additional Ca ions in solution cause dolomite to become more and more undersaturated as calcite supersaturates. Associated local ground water is enriched in Ca and saturated with respect to gypsum as marine evaporites are found in the catchment area. Portlandite ( $\text{Ca}(\text{OH})_2$ ) from the concrete

can act as an additional Ca source. Similar mechanisms are described for geological settings when Ca rich ground water is reacting with dolomite. E.g. rocks that have formed by the replacement of dolomite by calcite which is driven by the infiltration of Ca-rich water are described as dedolomites [19]. A further incongruent dolomite dissolution reaction is given by Appelo and Postma [20] where the interacting  $\text{SO}_4$  and Ca bearing ground water dissolves dolomite. Local ground water is usually much more abundant in Ca versus Na and K.

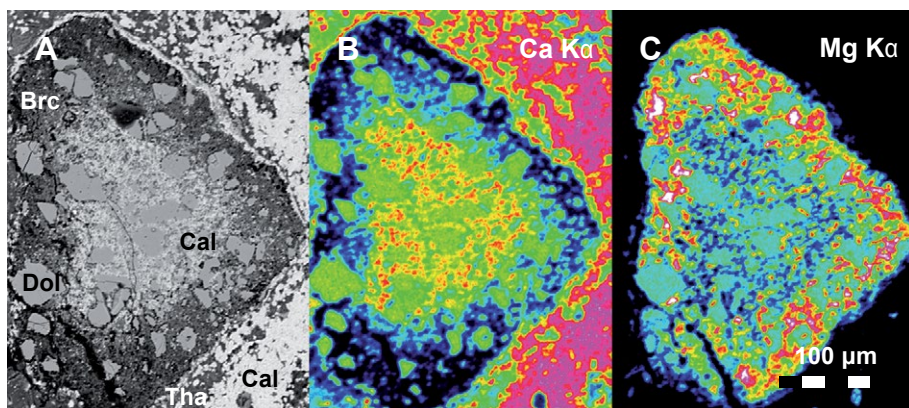


*Figure 2 (A): BSE image of an incongruently dissolved dolomite aggregate grain surrounded by calcite and brucite. (B): Elemental mapping of the Ca  $K\alpha$  line. Ca concentrations range from 0 to 40 wt. %. Light colors indicate high and black low concentration. (C) Elemental mapping of the Mg  $K\alpha$  line. Mg concentrations range from 0 - 42 wt. %. White indicates the highest and black low concentration. The dissolution of dolomite aggregates is caused by the reaction with Ca and  $\text{SO}_4$  rich ground water at  $\text{pH} > 10$ . The existence of brucite ( $\text{Mg}(\text{OH})_2$ ) provides evidence of high pH.*

However, some interstitial solutions, extracted from concrete which has suffered TSA, are dominated by Na and  $\text{SO}_4$  and reach concentrations up to  $65 \text{ g L}^{-1}$  TDS [3, 4]. It is believed that solutions can even reach saturation with respect to mirabilite ( $\text{Na}_2\text{SO}_4 \cdot 10\text{H}_2\text{O}$ ) as respective efflorescences are found on the tunnel walls. Dolomite solubility increases with increasing ionic strength and the solubility in the system calcite - dolomite depends also on temperature. Dolomite has a solubility maximum at around  $6^\circ\text{C}$ , where calcite has a minimum at this temperature [21]. This effect is highly relevant in underground constructions especially at low temperatures. At  $\text{pH} > 10$  the removal of Mg by brucite ( $\text{Mg}(\text{OH})_2$ ) precipitation further accelerates the de-dolomitization process. Accordingly, brucite and calcite were detected by EMPA

and Raman spectroscopy surrounding partially dissolved dolomite grains (Figure 2). Similar dissolution products were described as magnesium-rich residue, but could not clearly be identified as brucite [25]. Magnesium silicate hydrate gels, which had been discussed as products of ASR, have not been found in our samples as the accumulation of silicon is not detected by elemental mapping within the area of the dissolved dolomite aggregates [26]. Analogous de-dolomitization mechanisms are evident from the experimental results, where dolomite grains are incongruently dissolved by precipitation of calcite, aragonite and brucite in alkaline solutions within 60 to 120 days. These minerals were identified by XRD and quantified using Rietveld refinement. Brucite or  $\text{Mg-OH-CO}_3$ -phases were not detected by XRD analyses in all experiments. However, apparently poorly crystalline or gel-like brucite was detected by FTIR and Raman spectroscopy.

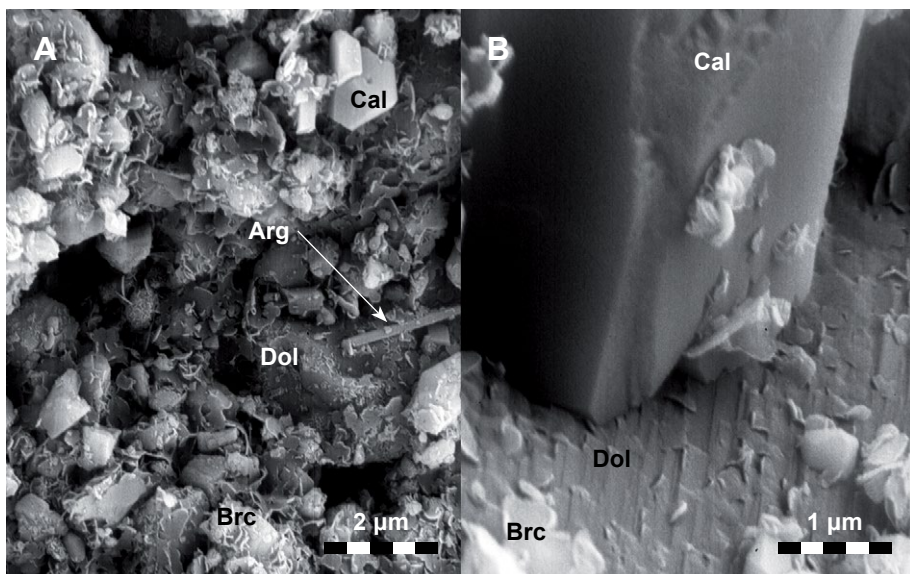


Figure 3 (A) Secondary electron image (SEI) of a dolomite from a dissolution experiment, where crushed pure dolomite reacted with 0.02 M NaOH (120 days, 5 °C). Calcite (Cal), Aragonite (Arg) and Brucite (Brc) were detected. (B) SEI of a dolomite from a dissolution experiment, where crushed pure dolomite reacted with 0.02 M  $\text{Ca(OH)}_2$  (120 days, 5 °C). Etching of the dolomite surface and new crystal growth of calcite and brucite on the dolomite surface has been detected.

### 5.2.7 Conclusions

- Dolomite dissolution can be associated with thaumasite formation as the cement matrix becomes unstable and the interstitial solutions can penetrate more easily. Both processes are favoured at low temperature.
- Calcite is more stable than dolomite at the given physicochemical conditions. Thus calcite should be favorable when used as aggregate.
- Dolomite aggregates in concrete dissolve preferentially with interacting ground waters at high Ca/Mg ratio.
- At pH >10 the amount of dolomite that can be dissolved per time increases as Mg is removed from the solution by brucite precipitation.
- The so called "Alkali-Carbonate Reaction" can take place in absence of Na and K.

### 5.2.8 Acknowledgement

The authors wish to thank FFG, NAWI Graz and the involved companies for funding and permission of sampling. Josef Tritthart for the helpful comments and Patrick Grunert for providing SEM imaging.

## 5.3 Remarks and Outlook

Limestone fillers as replacement for clinker may cause a higher risk of TSA when the concrete is subjected to sulfate attack (see Chapter 4). However, producing more ecological concretes by reducing the amount of clinker is gaining popularity. Thus alternative additives such as dolomite have to be tested and used [27, 28]. Authors are describing similar performance of concrete produced with dolomite filler versus concrete where calcite is used. However no results on sulfate attack performance are mentioned in the studies named above. Some studies, dealing with sulfate attack, are describing the occurrence of thaumasite in the presence of dolomitic aggregates [29-31]. In spite this finding the authors did not point out a potential connection of the occurrence of both minerals. But Veniale et al. [32] already found that dolomite is more reactive than calcite and dolomite content is reciprocally decreasing with increasing thaumasite content. Additionally Hobbs [33] identified dolomite to play a major role in increasing the risk of thaumasite attack. To the author's knowledge there are no lab tests for sulfate attack comparing concrete with dolomite and concrete with calcite fillers or aggregates. The lack is calling for more research on this topic.



## 5.4 References

1. Mittermayr, F., D. Klammer, D. Höllen, S. Köhler, M. Böttcher, A. Leis, and M. Dietzel, Deterioration of Concrete: Application of Stable Isotopes, in Proceedings of the 10<sup>th</sup> International Congress for Applied Mineralogy (ICAM), M.A.T.M. Broekmans, Editor. 2012, Springer Berlin Heidelberg. p. 435-443.
2. Broekmans, M.A.T.M., Deleterious Reactions of Aggregate With Alkalis in Concrete. Reviews in Mineralogy and Geochemistry, 2012. 74(1): p. 279-364.
3. Dietzel, M., F. Mittermayr, D. Klammer, D. Höllen, S. Köhler, and A. Leis, What do Stable Isotopes tell us about Deterioration of Concrete, in Cementing a sustainable future 13<sup>th</sup> International Congress on the Chemistry of Cement, Á. Palomo, A. Zaragoza, and J. C. López Agüí, Editors. 2011, CSIC: Madrid. p. No. 274: 1-6
4. Tritthart, J., D. Klammer, F. Mittermayr, and A. Brunnsteiner, A Casestudy of Thaumassite Formation in an Austrian Tunnel, in Cementing a sustainable future 13<sup>th</sup> International Congress on the Chemistry of Cement, Á. Palomo, A. Zaragoza, and J. C. López Agüí, Editors. 2011, CSIC: Madrid. p. No. 126: 1-6
5. Tong, L. and M. Tang, A case study of two airport runways affected by alkali-carbonate reaction part two: Microstructural investigations. Cement and Concrete Research, 1997. 27(3): p. 329-336.
6. Romer, M., L. Holzer, and M. Pfiffner, Swiss tunnel structures: concrete damage by formation of thaumasite. Cement and Concrete Composites, 2003. 25(8): p. 1111-1117.
7. Lee, H., R.D. Cody, A.M. Cody, and P.G. Spry, The formation and role of ettringite in Iowa highway concrete deterioration. Cement and Concrete Research, 2005. 35(2): p. 332-343.
8. Ma, B., X. Gao, E.A. Byars, and Q. Zhou, Thaumassite formation in a tunnel of Bapanxia Dam in Western China. Cement and Concrete Research, 2006. 36(4): p. 716-722.
9. Lee, S.T., D.H. Lee, D.K. Kim, H.S. Jung, K.P. Park, S.S. Kim, and C.S. Lee, Occurrence of thaumasite in lining concrete of old-tunnel structure, in Geotechnical Engineering for Disaster Mitigation and Rehabilitation, H. Liu, A. Deng, and J. Chu, Editors. 2008, Science Press Beijing: Beijing. p. 860-865.
10. Shayan, A., A. Xu, G. Chirgwin, and H. Morris, Effects of seawater on AAR expansion of concrete. Cement and Concrete Research, 2010. 40(4): p. 563-568.

11. Galí, S., C. Ayora, P. Alfonso, E. Tauler, and M. Labrador, Kinetics of dolomite-portlandite reaction: Application to portland cement concrete. *Cement and Concrete Research*, 2001. 31(6): p. 933-939.
12. García, E., P. Alfonso, M. Labrador, and S. Galí, Dedolomitization in different alkaline media: Application to Portland cement paste. *Cement and Concrete Research*, 2003. 33(9): p. 1443-1448.
13. García, E., P. Alfonso, E. Tauler, and S. Galí, Surface alteration of dolomite in dedolomitization reaction in alkaline media. *Cement and Concrete Research*, 2003. 33(9): p. 1449-1456.
14. Katayama, T., How to identify carbonate rock reactions in concrete. *Materials Characterization*, 2004. 53(2-4): p. 85-104.
15. Katayama, T., The so-called alkali-carbonate reaction (ACR) -- Its mineralogical and geochemical details, with special reference to ASR. *Cement and Concrete Research*, 2010. 40(4): p. 643-675.
16. López-Buendía, A.M., V. Climent, and P. Verdú, Lithological influence of aggregate in the alkali-carbonate reaction. *Cement and Concrete Research*, 2006. 36(8): p. 1490-1500.
17. Xu, Z., X. Lan, M. Deng, and M. Tang, A new accelerated method for determining the potential alkali-carbonate reactivity. *Cement and Concrete Research*, 2002. 32(6): p. 851-857.
18. Pokrovsky, O.S. and J. Schott, Kinetics and mechanism of dolomite dissolution in neutral to alkaline solutions revisited. *American Journal of Science*, 2001. 301(7): p. 597-626.
19. Ayora, C., C. Taberner, M.W. Saaltink, and J. Carrera, The genesis of dedolomites: a discussion based on reactive transport modeling. *Journal of Hydrology*, 1998. 209(1-4): p. 346-365.
20. Appelo, C.A.J. and D. Postma, *Geochemistry, groundwater and pollution*. 2<sup>nd</sup> ed. 2007, Amsterdam: A.A.Balkema Publishers. 649.
21. Merkel, B. and B. Planer-Friedrich, *Grundwasserchemie: Praxisorientierter Leitfaden zur numerischen Modellierung von Beschaffenheit, Kontamination und Sanierung aquatischer Systeme*. 2<sup>nd</sup> ed. 2008, Berlin: Springer. 244.

22. Mittermayr, F., D. Klammer, M. Dietzel, C. Bauer, M.E. Böttcher, M. Koch, S. Köhler, A. Mayer, and A. Leis, Thaumasilbildungen in Tunnelbauten - Hydrogeochemie und stabile Isotope. *Geotechnik*, 2008: p. 115-132.
23. Parkhurst, D.L. and C.A.J. Apello, User's guide to PHREEQC (V2). U.S. Geol. Sur, 1999. 312.
24. Glasser, F.P., J. Marchand, and E. Samson, Durability of concrete - Degradation phenomena involving detrimental chemical reactions. *Cement and Concrete Research*, 2008. 38(2): p. 226-246.
25. Leemann, A. and R. Loser, Analysis of concrete in a vertical ventilation shaft exposed to sulfate-containing groundwater for 45 years. *Cement and Concrete Composites*, 2011. 33(1): p. 74-83.
26. Brew, D.R.M. and F.P. Glasser, Synthesis and characterisation of magnesium silicate hydrate gels. *Cement and Concrete Research*, 2005. 35(1): p. 85-98.
27. Schöne, S., W. Dienemann, and E. Wagner. Portland dolomite cement as alternative to portland limestone cement. in 13<sup>th</sup> International Congress on the Chemistry of Cement. 2011. Madrid: CSIC.
28. Zajac, M., W. Dienemann, and G. Bolte. Comparative experimental and virtual investigations of the influence of calcium and magnesium carbonates on replacing cement. in 13<sup>th</sup> International Congress on the Chemistry of Cement. 2011. Madrid: CSIC.
29. Thomas, M.D.A., C.A. Rogers, and R.F. Bleszynski, Occurrences of thaumasite in laboratory and field concrete. *Cement and Concrete Composites*, 2003. 25(8): p. 1045-1050.
30. Crammond, N.J., G.W. Collett, and T.I. Longworth, Thaumasilite field trial at Shipston on Stour: three-year preliminary assessment of buried concretes. *Cement and Concrete Composites*, 2003. 25(8): p. 1035-1043.
31. Irassar, E.F., V.L. Bonavetti, and M. González, Microstructural study of sulfate attack on ordinary and limestone Portland cements at ambient temperature. *Cement and Concrete Research*, 2003. 33(1): p. 31-41.
32. Veniale, F., M. Setti, C. Rodriguez-Navarro, S. Lodola, W. Palestra, and A. Busetto, Thaumasilite as decay product of cement mortar in brick masonry of a church near Venice. *Cement and Concrete Composites*, 2003. 25(8): p. 1123-1129.
33. Hobbs, D.W., Thaumasilite sulfate attack in field and laboratory concretes: implications for specifications. *Cement and Concrete Composites*, 2003. 25(8): p. 1195-1202.



# CHAPTER 6

## Perspectives

### 6.1 Introduction

In this chapter perspectives for future research on thaumasite formation are developed in order to decipher the

- details of reaction mechanisms of its formation and the
- impact of its formation on concrete deterioration.

### 6.2 Thaumasite Dissolution and Syntheses

A crucial parameter for any theoretical thermodynamic calculation within the thaumasite-water system is a reliable value of the solubility constant of thaumasite. The available constant in the literature is not experimentally determined, but calculated from a unit cell based approach [1, 2]. Even though the postulated  $K_{\text{Thaumasite}}$  value has recently been verified and calculations for the interstitial solutions (Chapter 3) seem to be reasonable, further studies using monomineralic thaumasite - formed in field concrete structures - are feasible [3]. This approach is highly promising to provide an advanced understanding, to simulate and evaluate individual reaction paths by thermodynamic modeling involving concrete and for syntheses approaches.

In contrast to thaumasite the synthesis of ettringite is a rather spontaneous process which can be induced by mixing of the aqueous solutions [4]. In a preliminary attempt to synthesize thaumasite, several experiments were already performed where the ettringite procedure was taken and Al was stepwise stoichiometrically replaced by Si. The reaction kinetics to form thaumasite is suggested to be slow and it may take years to form thaumasite. However, an important factor could be the reaction kinetics of competing reactions [5]. Competing fast mineral formation (e.g. calcite) or dissolved components may inhibit or kinetically slowdown or even accelerate thaumasite formation. Interestingly the few successful thaumasite syntheses were carried out with sucrose solutions [6, 7].

Introducing the element germanium as substitute for silicon in thaumasite might be a promising approach for investigating the origin of Si in thaumasite and other Si bearing phases related to concrete [8].

### 6.3 Studies on Natural Thaumasite

Another perspective for future investigations on thaumasite formation in concrete structures is to focus on natural thaumasite material and to setup a comparative study with thaumasite formed in concrete. From individual natural localities many details on the environmental conditions during thaumasite formation are already known. However a systematic combined study on thaumasite from variable origins has not been conducted yet [9-13]and references therein. Preliminary electron microprobe results have shown that natural thaumasite from several localities contains significant amounts of Al. In contrast thaumasite found in tunnels may be very “pure” with basically no Al content. Furthermore microprobe results from thaumasite formed in concrete indicate significant chloride contents. Cl might be trapped in fluid inclusions, but this finding has to be verified. Micro Raman spectroscopy is known for an unambiguous identification of thaumasite [14, 15]. Some preliminary results of natural thaumasite and deteriorated concrete samples containing thaumasite have revealed the same characteristic peaks at 123, 147 and 660  $\text{cm}^{-1}$ . Raman can also be applied to investigate fluid inclusions in thaumasite if present. If this is the case the composition of the fluid inclusions can be identified and additional heating-cooling table investigations could give valuable insights in order to determine the formation conditions from natural thaumasite.

So far hardly any isotope data of natural thaumasite exists, except for very few  $\delta^{34}\text{S}$  values [13, 16]. Most interestingly, authors of the studies named above, have also analyzed expressed interstitial solutions which contain high contents of Cl similar to this study (see Chapter 3). Finally, remarkable but preliminary  $\delta^{13}\text{C}$  and  $\delta^{18}\text{O}$  data of ettringite and thaumasite from South Africa and Austria indicate different formation conditions.

### 6.4 Critical Level of Sulfate in Concrete

One main part of our FFG supported project “The Critical Level of sulfate in concrete” is based on field investigation of deteriorated concrete that has suffered from sulfate attack. This part is elaborated in the present thesis. The other main part of the above overall project is focused on the exposure of mortar specimens

to environmental conditions with a high potential for sulfate attack (city sewage, industrial sewage, and wastewater treatment plant) and under lab conditions from 200 to 6000 mg L<sup>-1</sup> of SO<sub>4</sub> between 5 and 20 °C. As the project is still running, the following outlines only a few highlights.

Mortar test specimens were fabricated by using ordinary Portland cement clinker, advanced admixtures with different additives as well as various water-binder ratios and different aggregates. Compressive strength, flexural tension, total sulfate and pore fluid composition of the pristine and altered samples are measured. Optical microscopy, XRD, SEM and EMPA are applied to investigate the mineralogical composition and to get insights about microstructure properties (e.g. Figure 1). Preliminary results are summarized in the yearly work reports so far [17, 18]. It is planned to investigate the 3-dimensional microstructure on some selected samples by micro-computer tomography.

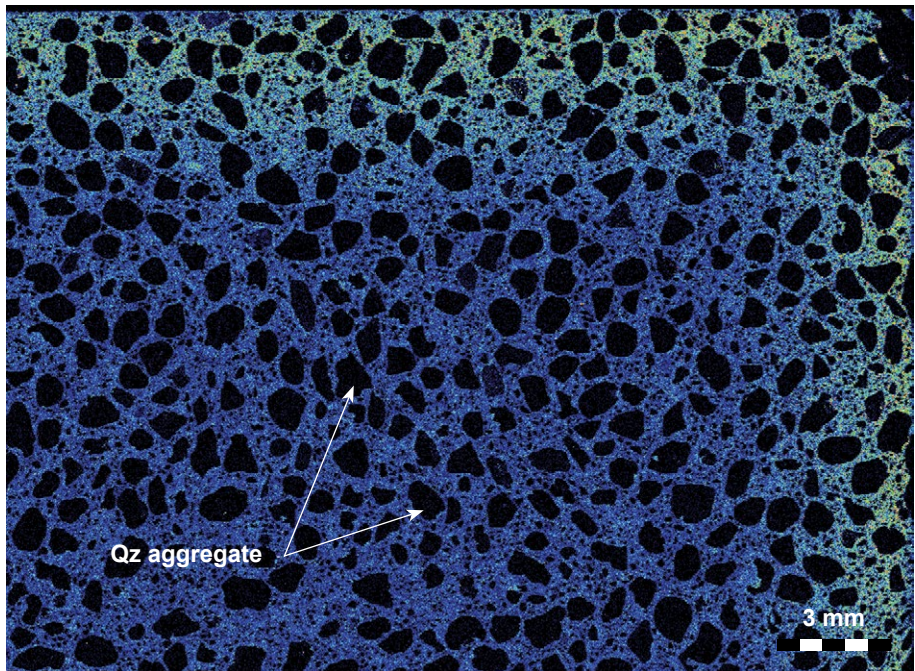


Figure 1: Distribution of sulfur in a CEM I W/Z 0.70 specimen exposed at 6000 mg L<sup>-1</sup> SO<sub>4</sub> and 20 °C. Obviously, the sulfate (light color) has penetrated about 3 - 6 mm after 6 months.

## 6.5 Accelerated Sulfate Attack Test

The current situation for testing sulfate resistance of concrete and mortar samples is rather confusing. In fact samples of different sizes are used which are mostly completely submerged in solutions with various sulfate concentrations. The vast majority is using either solely Na or solely Mg sulfate solutions (e.g. Breitenbücher et al. [19] and references therein). Most challenging issues with respect to testing procedure are that results cannot be compared between different studies and are far from the individual environmental conditions in the field. For instance

- solely Na or Mg sulfate solutions hardly ever occur in the field,
- the evolution of the solution itself is of no concern. Consequently phases formed at an initial stage may dissolve at a later stage (e.g. ettringite).
- Reaction times in the lab cannot resolve field conditions at decades of years.

This situation is calling for a more advanced testing approach of an accelerated sulfate attack (ASAT) within a reasonable time span. The realization of a suitable ASAT is certainly a very ambitious and challenging project which needs further evaluations.

## 6.6 References

1. Schmidt, T., B. Lothenbach, M. Romer, K. Scrivener, D. Rentsch, and R. Figi, A thermodynamic and experimental study of the conditions of thaumasite formation. *Cement and Concrete Research*, 2008. 38(3): p. 337-349.
2. Jacobsen, S.D., J.R. Smyth, and R.J. Swope, Thermal expansion of hydrated six-coordinate silicon in thaumasite,  $\text{Ca}_3\text{Si}(\text{OH})_6(\text{CO}_3)(\text{SO}_4)\cdot 12\text{H}_2\text{O}$ . *Physics and Chemistry of Minerals*, 2003. 30(6): p. 321-329.
3. Damidot, D., B. Lothenbach, D. Herfort, and F.P. Glasser, Thermodynamics and cement science. *Cement and Concrete Research*, 2011. 41(7): p. 679-695.
4. Perkins, R.B. and C.D. Palmer, Solubility of ettringite ( $\text{Ca}_6[\text{Al}(\text{OH})_6]_2(\text{SO}_4)_3\cdot 26\text{H}_2\text{O}$ ) at 5 – 75 °C. *Geochimica et Cosmochimica Acta*, 1999. 63(13–14): p. 1969-1980.
5. Aldred, J. pers. comm.
6. Martinez-Ramirez, S., M.T. Blanco-Varela, and J. Rapazote, Thaumasite formation in sugary solutions: Effect of temperature and sucrose concentration. *Construction and Building Materials*, 2011. 25(1): p. 21-29.



7. Aguilera, J., M.T.B. Varela, and T. Vázquez, Procedure of synthesis of thaumasite. *Cement and Concrete Research*, 2001. 31(8): p. 1163-1168.
8. Merlino, S. and P. Orlandi, Carraraite and zaccagnaite, two new minerals from the Carrara marble quarries: their chemical compositions, physical properties, and structural features. *American Mineralogist*, 2001. 86(10): p. 1293-1301.
9. Foshag, W.F., Thaumasite (and spurrite) from Crestmore, California. *American Mineralogist*, 1920. 5(4): p. 80-81.
10. Noack, Y., Occurrence interaction, of thaumasite in a seawater-basalt Mururoa atoll (French Polynesia, South Pacific). *Mineralogical Magazine*, 1983. 47(342): p. 47-50.
11. Grubessi, O., A. Mottana, and E. Paris, Thaumasite from the Tschwinning mine, South Africa *Tschermaks Mineralogische Und Petrographische Mitteilungen*, 1986. 35(3): p. 149-156.
12. Gatta, G.D., G.J. McIntyre, J.G. Swanson, and S.D. Jacobsen, Minerals in cement chemistry: A single-crystal neutron diffraction and Raman spectroscopic study of thaumasite,  $\text{Ca}_3\text{Si}(\text{OH})_6(\text{CO}_3)(\text{SO}_4)\cdot 12\text{H}_2\text{O}$ . *American Mineralogist*, 2012. 97(7): p. 1060-1069.
13. Schöps, D. and P.M. Herzig, Thaumasite in Lau Basin basaltic andesite, Hole 841B. in *Ocean Drilling Program, Scientific Results*. 1994. College Station, TX: Ocean Drilling Program.
14. Brough, A.R. and A. Atkinson, Micro-Raman spectroscopy of thaumasite. *Cement and Concrete Research*, 2001. 31(3): p. 421-424.
15. Sahu, S., D.L. Exline, and M.P. Nelson, Identification of thaumasite in concrete by Raman chemical imaging. *Cement and Concrete Composites*, 2002. 24(3-4): p. 347-350.
16. Alt, J.C. and J.W. Burdett, Sulfur in Pacific deep-sea sediments (Leg 129) and implications for cycling of sediment in subduction zones. in *Ocean Drilling Program, Scientific Results*. 1992. College Station, TX: Ocean Drilling Program.
17. Tritthart, J. and D. Klammer, Bericht: Ermittlung des kritischen Sulfatgehaltes von Beton. 2012: Graz. p. 28.
18. Tritthart, J. and D. Klammer, Bericht: Ermittlung des kritischen Sulfatgehaltes von Beton. 2011: Graz. p. 8.
19. Breitenbücher, R., D. Heinz, K. Lipus, J. Paschke, G. Thielen, L. Urbonas, and F. Wisotzky, Sachstandbericht - Sulfatangriff auf Beton. Vol. 554. 2006, Berlin: Deutscher Ausschuss für Stahlbeton. 172.



# CHAPTER 7

## Afterword

### 7.1 Acknowledgement

First of all I would like to greatly thank my supervisors who have encouraged and supported me throughout my entire thesis. I appreciate the countless scientific discussions and the trust you have given me during my work. It has been a great pleasure to work with my colleagues at the Institute of Applied Geosciences, other institutes from the Graz University of Technology and from other universities and companies. Thank you for all the help and support. I appreciate the work of peers, some of which I unfortunately still have not met personally, for the critical and helpful comments and bringing new perspectives into my thesis. The present research was financially supported by NAWI Graz, Graz Advanced School of Science (GASS), Österreichische Forschungsförderungsgesellschaft (FFG, 828476) and various companies involved in the project. Finally my biggest thanks go to all members of my family and my friends. Thank you for being there for me.

### 7.2 Curriculum Vitae

Florian Mittermayr was born on October 9<sup>th</sup> 1980 in Rum, Austria. He attended the Akademische Gymnasium Innsbruck (AGI), Austria, from 1991 until 1997. In 1998 he received a diploma from Blake School Minneapolis (USA) for completing an international program. After graduating from AGI in 1999 he enrolled for studying Earth Sciences at the Leopold Franzens University in Innsbruck. During his study he was employed as scientific project assistant from 2002 to 2005 at the Institute of Mineralogy and Petrography. There he finished his diploma thesis entitled “Solubility and Chemistry of Synthetic and Natural Corundum” in 2006. In 2007 Mittermayr started working at Institute of Applied Geosciences at Graz University of Technology as university project assistant in the project entitled “Carbonate and Sulfate Mineral Formation

in Hydraulic-setting Cements” which is part of the doctorate program Graz Advanced School of Science (GASS). From 2010 until present he is participating in the project “Critical Level of Sulfate in Concrete” financed by the Österreichische Forschungsförderungsgesellschaft (FFG). From 2012 until present he is on paternity leave with marginal employment at the Institute of Applied Geosciences. Florian Mittermayr is a member of the Austrian Mineralogical Society (ÖMG).

## 7.3 References

Reviewed journal and conference papers

### Related to Sulfate Attack on Concrete

1. Dietzel, M., F. Mittermayr, D. Klammer, D. Höllen, S. Köhler, and A. Leis, What do Stable Isotopes tell us about Deterioration of Concrete, in *Cementing a sustainable future 13<sup>th</sup> International Congress on the Chemistry of Cement*, Á. Palomo, A. Zaragoza, and J. C. López Agüí, Editors. 2011, CSIC: Madrid. p. No. 274: 1-6
2. Mittermayr, F., D. Klammer, D. Höllen, M. Dietzel, C. Kurta, A. Leis, and M.E. Böttcher, Concrete damage in underground structures, in *Concrete Repair, Rehabilitation and Retrofitting III*, M.G. Alexander, et al., Editors. 2012, Taylor & Francis Group: London,UK. p. 580-584.
3. Mittermayr, F., D. Klammer, D. Höllen, S. Köhler, M. Böttcher, A. Leis, and M. Dietzel, Deterioration of Concrete: Application of Stable Isotopes, in *Proceedings of the 10<sup>th</sup> International Congress for Applied Mineralogy (ICAM)*, M.A.T.M. Broekmans, Editor. 2012, Springer Berlin Heidelberg. p. 435-443.
4. Mittermayr, F., D. Klammer, S. Köhler, A. Leis, D. Höllen, and M. Dietzel, Dissolution of Dolomite in alkaline cementitious media, in *Cementing a sustainable future 13<sup>th</sup> International Congress on the Chemistry of Cement*, Á. Palomo, A. Zaragoza, and J. C. López Agüí, Editors. 2011, CSIC: Madrid. p. No. 278: 1-6
5. Dietzel, M., D. Klammer, and F. Mittermayr, Alteration von historischen und modernen Baustoffen – Mineralogie und stabile Isotope, in *Bauphysiktagung 2012*. 2012, Graz University of Technology: Graz. p. 1-11.

6. Tritthart, J., D. Klammer, F. Mittermayr, and A. Brunnsteiner, A Casestudy of Thaumasite Formation in an Austrian Tunnel, in *Cementing a sustainable future 13<sup>th</sup> International Congress on the Chemistry of Cement*, Á. Palomo, A. Zaragoza, and J. C. López Agüf, Editors. 2011, CSIC: Madrid. p. No. 126: 1-6
7. Klammer, D., J. Tritthart, F. Mittermayr, and A. Brunnsteiner, Deterioration of concrete caused by the thaumasite form of sulfate attack (TSA) - A case study, in *8<sup>th</sup> International Conference: Concrete in the Low Carbon Era*, M.R. Jones, Editor. 2012, University of Dundee – Concrete Technology Unit: Dundee, UK. p. 1572-1580.
8. Mittermayr, F., D. Klammer, S. Köhler, M.E. Böttcher, A. Leis, and M. Dietzel, Sulfatangriff: Die Bildung von Thaumasit und die Auflösung von dolomitischen Zuschlagstoffen, in *Ibausil. 2009*, F.A. Finger-Institut für Baustoffkunde: Weimar. p. 323 - 328
9. Mittermayr, F., T. Rinder, D. Klammer, A. Leis, and M. Dietzel, A Carbon Isotope Study of Thaumasite and Calcite Sinter Formation in Underground Construction, in *1<sup>st</sup> International Congress on Durability of Concrete*, H. Justnes and S. Jacobsen, Editors. 2012, NTNU: Trondheim. p. No. C6-1: 1-14.
10. Tritthart, J., F. Mittermayr, D. Klammer, and A. Brunnsteiner, Schädigung von Beton durch Thaumasit, in *Spritzbeton - Tagung 2012*, W. Kusterle, Editor. 2012: Alpach. p. 77 - 83.
11. Dietzel, M., G. Harer, D. Klammer, S. Köhler, A. Leis, F. Mittermayr, A. Niedermayr, R. Peter, and T. Rinder, Karbonatabscheidungen in Drainagesystemen von Tunnelbauten. *Beiträge zur Hydrogeologie 2010*. 57: p. 143 - 153.
12. Dietzel, M., T. Rinder, A. Niedermayr, F. Mittermayr, A. Leis, D. Klammer, S. Köhler, and R. Peter, Ursachen und Mechanismen der Versinterung von Tunneldrainagen. *BHM Berg- und Hüttenmännische Monatshefte 2008*. 153(10): p. 369 - 372
13. Mittermayr, F., C. Bauer, D. Klammer, M.E. Böttcher, A. Leis, P. Escher, and M. Dietzel, Concrete under Sulfate Attack: An Isotope Study on Sulfur Sources Isotopes in *Environmental & Health Studies*, 2012. 48(1): p. 105-117.
14. Mittermayr, F., D. Klammer, M. Dietzel, C. Bauer, M.E. Böttcher, M. Koch, S. Köhler, A. Mayer, and A. Leis, Thaumasitbildungen in Tunnelbauten - Hydrogeochemie und stabile Isotope. *Geotechnik*, 2008: p. 115-132.
15. Dietzel, M., D. Klammer, and F. Mittermayr, Concrete Attack – Evidence from Stable Isotopes in TU Graz Research. 2010, Graz University of Technology: Graz. p. 22 - 24.

16. Mittermayr, F., A. Baldermann, C. Kurta, T. Rinder, D. Klammer, A. Leis, J. Tritthart, and M. Dietzel, Evaporation – A Key Mechanism for the Thaumassite Form of Sulfate Attack. *Cement and Concrete Research*, submitted.
17. Klammer, D., J. Tritthart, F. Mittermayr, and A. Brunnsteiner, Sulfatbeständigkeit - aktuelle Forschungsergebnisse, in 1.Grazer Betonkolloquium : Die Vielseitigkeit eines Baustoffes, P. Maydl and B. Freytag, Editors. 2012, Verlag der Technischen Universität Graz: Graz, Austria. p. 57-68.

## Related to Topics of Material Science and Applied Mineralogy

18. Pudar, M., L. Malik, F. Mittermayr, and R. Vallant. Dissimilar Joining of Magnesium in body construction. in JOIN-EX. 2012. Vienna: Schweißtechnische Zentralanstalt (SZA). p. 1 - 9.
19. Kurta, C., L. Dorta, K. Prattes, F. Mittermayr, G. Günther, B. Hattendorf, and W. Goessler, Rapid screening of boron isotope ratios in nuclear shielding materials by LA-ICPMS – a comparison of standard and high-end equipment. *Journal of Analytical Atomic Spectrometry*, submitted.
20. Mittermayr, F., C. Hauzenberger, E. Dachs, J. Konzett, and P. Tropper, Corundum solubility and crack healing in (K,Na)OH solution at hydrothermal conditions. in prep.
21. Naderer, M., D. Schütz, T. Kainz, K. Reichmann, and F. Mittermayr, The formation of secondary phases in  $\text{Bi}_{0.5}\text{Na}_{0.375}\text{K}_{0.125}\text{TiO}_3$  ceramics. *Journal of the European Ceramic Society*, 2012. 32(10): p. 2399-2404.
22. Reich, M., A.P. Deditius, S.L. Chryssoulis, J. Li, C. Ma, M.A. Parada, F. Barra, and F. Mittermayr, Precious metals, metalloids and heavy metals in pyrite from a porphyry copper system. *Geochimica Et Cosmochimica Acta*, in press.
23. Schütz, D., C. Kurta, M. Arar, F. Mittermayr, and K. Reichmann, High temperature transport phenomena at metal/ceramic interfaces revealed by LA-ICPMS. *Journal of the European Ceramic Society*, in prep.



